WADC TECHNICAL REPORT NO. 53-50

UNCLASSIFIED

MECHANICAL-PROPERTY TESTS ON CERAMIC BODIES

O. K. SALMASSY, W. H. DUCKWORTH,
and A. D. SCHWOPE

22 MARCH 1953

Statement A
Approved for Public Release

BATTELLE MEMORIAL INSTITUTE

WADC TECHNICAL REPORT NO. 53-50

THIRD ANNUAL REPORT

on

MECHANICAL-PROPERTY TESTS ON CERAMIC BODIES

to

Wright-Patterson Air Force Base
Ohio

22 March 1953

Attention: Materials Laboratory
Engineering Division
MCREXM-3

Contract No. AF 33(038)-8682
Expenditure Order No. R605-23?SR-3A

by

O. K. Salmassy, W. H. Duckworth,
and A. D. Schwope

Report for the Period of
21 February 1952 to 21 February 1953

BATTELLE MEMORIAL INSTITUTE
505 King Avenue
Columbus 1, Ohio

FOREWORD

This report was prepared by Battelle Memorial Institute, Columbus, Ohio, on Contract No. AF 33(038)-8682. Research at Battelle Memorial Institute was initiated as a project of the Materials Laboratory, Research Division, Wright-Patterson Air Force Base, with Mr. L. D. Richardson as Project Engineer.

This report is the Third Annual Report covering the period 21 February 1952 to 21 February 1953. Research conducted during previous periods appears in Air Force Technical Reports No. 6512 and No. 52-67.

The authors wish to thank M. C. Brockway for his aid in the mathematical treatment of the data and F. J. Buffington for his help in designing and carrying out the experiments.

ABSTRACT

The factors influencing the fracture of brittle ceramic materials were studied: the effects of size and stress state were given primary consideration. In addition, initial consideration was given to the effects of strain rate and temperature.

The strength of plaster of Paris was found to decrease with an increase of size in the simple stress states of tension, compression, bending, and torsion. Initial analyses indicated that Weibull's statistical theory of strength could be used to predict the observed effects of size and stress state on the strength of plaster.

The effects of combined stresses on the fracture strength were studied by means of tests conducted on cylinders of plaster subjected to internal pressure and axial loading. Initial analyses of data from these combined-stress tests indicated that fracture data could be analyzed using the elastic theory of thick-walled cylinders.

The effect of superposed bending stresses on tension-test data was analyzed using Weibull's theory. This analysis indicated that superposed bending stresses should increase the observed tensile strength of a brittle material. Tension data on plaster agreed qualitatively with this prediction.

Analysis of the standard compression test indicated that fracture data from this type of test were unreliable and that the standard compression test could not be used in a research program where precise quantitative fracture data were required.

Exploratory studies were made of the effect of varying the strain rate or the stress rate on the fracture of plaster of Paris. These studies indicated a decrease of fracture stress with increased rates of loading, an effect opposite to that reported in the literature for other brittle materials. The relation between the effects of rate of loading and stress duration (static fatigue) was considered.

TABLE OF CONTENTS

TABLE OF CONTENTS
(Continued)

LIST OF TABLES

LIST OF TABLES
(Continued)

LIST OF ILLUSTRATIONS

TABLE OF CONTENTS
(Continued)

WADC TECHNICAL REPORT NO. 53-50

THIRD ANNUAL REPORT

on

MECHANICAL-PROPERTY TESTS ON CERAMIC BODIES

to

WRIGHT-PATTERSON AIR FORCE BASE
OHIO

ATTENTION: MATERIALS LABORATORY
ENGINEERING DIVISION
MCREXM-3

CONTRACT NO. AF 33(038)-8682
EXPENDITURE ORDER NO. R605-233SR-3A

from

BATTELLE MEMORIAL INSTITUTE

by

O. K. Salmassy, W. H. Duckworth,
and A. D. Schwope

22 March 1953

INTRODUCTION

In this age of gas turbines and jet engines, the ceramic component offers the solution to many of the problems of the aircraft designer. However, the technical and economic benefits indicated often cannot be realized because the ceramic materials are brittle. Corrective measures are frustrated by the absence of any accepted theory of brittle fracture, or even working equations for designing parts of brittle materials.

The ultimate aim of this investigation is to furnish a clear understanding of the fracture of ceramic bodies, and, if possible, to determine quantitative definitions of the resistance to fracture in terms of external variables. Among the fracture phenomena to be considered are the following:

1. The effect of stress state on fracture strength
2. The effect of size on fracture strength
3. The effect of the rate of stressing on fracture strength
4. The effect of temperature on fracture strength

The knowledge of the mechanical behavior of ceramics is not sufficiently advanced to permit considering this list as complete. As the research progresses, the effects of other fracture variables probably will require consideration.

Classically, there are two approaches to the problem of the strength of materials. The older, the phenomenological approach, attempts to describe the reaction of a solid to its external environment. All of the phenomenological theories assume homogeneity and isotropy of the material, and the criteria which these theories set up are based on relations of stress and strain evolved from the classical theory of elasticity. All of these phenomenological theories take into consideration only one variable, stress state. In general, these theories place no restrictions on the nature of the material to which they are to be applied. As a result, no single phenomenological theory has been found to be applicable to all materials or to all conditions of failure.

The second approach to the problem of the strength of materials is mechanistic in nature. Here, strength properties are analyzed from the point of view of what makes the material fail. These theories are concerned with the fact that materials may fracture at stresses 100 to 1000 times less than their theoretical fracture strength. As a result, all of these theories assume, tacitly or otherwise, the presence in a material of "flaws" of such a nature as to cause this reduction in strength. Although the mechanistic theories postulate a mechanism of fracture, they still require an assumption of a criterion for fracture, as do the phenomenological theories. Fracture still is considered to occur at some condition of stress or strain; nevertheless, the mechanistic theories have the advantage of providing a qualitative picture of fracture phenomena.

In this investigation, the approach to the problem of the strength of ceramics has been to analyze fracture data in the light of all existing theories, phenomenological and mechanistic. It is possible, however, that no existing theory can be found which satisfactorily predicts the strength of a ceramic body under varying conditions. Then a new and unified theory of strength would be in order; however, the development of such a broad theory, if it were to be worth while, probably would require exhaustive effort. As an alternative, empirical expressions might be developed which would furnish design data for particular materials under specific conditions. In any event, when all these factors have been considered, an effort will be made to establish a method by which aircraft designers can determine reliably the design strength of ceramic components under operating conditions.

In this investigation, the approach has been to study the fracture properties of ceramics as a class of materials; that is, to study the phenomena of brittle fracture. No attempt has been made to study the fracture properties of any one ceramic material with the view of obtaining practical design data. Far too little is known at this time about the effects of external variables on the brittle fracture of ceramics to warrant such a study.

Of primary concern in selecting materials for this investigation have been the factors:

1. Reproducibility from body to body
2. Homogeneity and isotropy
3. Ease of fabrication
4. Lack of plastic flow prior to fracture

The objectives of this investigation require maximum control of all possible variables at all times. Although control is of paramount interest in the selection of materials, potential utility in aircraft is also of interest. However, such utility becomes secondary in this fundamental study to the problems of determining the effects of external variables on fracture.

During the period covered by this report, the approach has been to determine the individual effects of certain external variables on the fracture strength of plaster of Paris, and to determine how each observed effect correlates with existing theory. Plaster was used in accordance with the above discussion, as an experimental material from which to gain insight into the fracture phenomena of brittle ceramics. Also, the use of plaster in the early stages of each experimental phase will result in an appreciable saving of time and money.

By its very nature, this problem is a very complex one; yet, the solution will provide the key to the utilization of ceramic materials in modern aircraft. The margin of error between the operating strength of a ceramic body and its predicted design strength must be reduced if ceramics are to be considered safe for practical application in aircraft.

Research on this problem was initiated at Battelle Memorial Institute in October, 1948, on a subcontract under Contract No. W 33-038 ac 14105 between the Air Force and the RAND Corporation. The research was assumed by Battelle under direct Air Force sponsorship during November, 1949.

The research conducted for the RAND Corporation is covered in RAND Report R-209, "Mechanical Properties of Ceramic Bodies", dated 31 August 1950. The bulk of this research was with porous and nonporous specimens of of a silicate porcelain. A correlation was obtained between elastic properties from room-temperature compression, torsion, and bend tests. The

effect of porosity upon elastic-moduli data was studied. Observed fracture phenomena could be explained qualitstively to some extent on the basis of a flaw-type mechanism of fracture.

Research for the first year of direct Air Force sponsorship, from 18 November 1949 to 18 November 1950 is covered by AF Technical Report No. 6512, April 1951. This work was limited to K151A, a nickel-bonded titanium carbide product of Kennametal, Incorporated. Although this material exhibited slight plastic flow in compression, bending, and torsion at room temperature, the mode of fracture was that normally found in brittle ceramics. However, research revealed the reproducibility and the homogeneity of K151A to be so poor that any attempt at quantitative correlation of fracture data was futile. Nevertheless, the data of this period, as in the previous period, indicated that a flaw-type mechanism offered the most likely basis for developing correlations.

Research for the second year of direct Air Force sponsorship from 18 November 1950 to 22 March 1952 is covered in WADC Technical Report No. 52-67, dated 22 March 1952. During this period, particular attention was given to the effect of size on fracture strength, using bend tests on plaster of Paris. Such work was considered essential to evaluating and developing theories from a flaw-type mechanism of fracture. As an important concurrent effort, a critical survey was undertaken of the principal phenomenological and mechanistic theories of strength.

The present report covers the research conducted during the third year of direct Air Force sponsorship from 21 February 1952 to 21 February 1953. During this period, research was conducted on the effects of size, stress state, strain rate, and temperature on fracture phenomena, utilizing data obtained principally from tests conducted on plaster of Paris.

SUMMARY

The results of the research of this period have indicated that certain statistical theories of strength, particularly Weibull's theory, may be used to correlate fracture data from brittle ceramic materials. If these indications are valid, then it may now be possible to design, with confidence, ceramic parts for aircraft. A most important consequence of the year's work is the conclusion that ceramic materials should not be selected for design on the basis of the highest mean fracture strength. A more realistic and safe criterion for selection is a "safe" strength, a strength below which there is no chance that ceramic parts will fail.

The results of this period have not confirmed the validity of Weibull's theory or of any other statistical theory, but the results of the research have shown conclusively the importance of the statistical analysis of test data.

The results of the research into the effect of stress state on fracture have shown that such an effect exists in ceramic materials. In essence, this means that the ceramic engineer must use care in designing with test data. Strengths determined from the bend test cannot be used to design a ceramic part to be loaded in tension, and vice versa, unless the relation is known between the tension and bend strengths for the ceramic in question. For example, if the material was a typical ceramic, similar to plaster, the mean strength in tension is about 3/4 of that in bending and 0.83 of that in torsion.

In addition, this research has indicated that the size of a structure influences its design. Specifically, it was found that the larger a ceramic structure, the lower must be its design strength. This research indicates that the testing of ceramic models to determine the design strength of ceramic prototypes may not be reliable where there are large variations between the size of the model and the prototype unless the quantitative effects of size are known.

The research of this period has also produced indications that the rate at which a load is applied to a ceramic structure may affect the magnitude of the load it can withstand before fracture. This means that the ceramic designer must consider the effects of shock, thermal and mechanical, and of dynamic loading.

It is felt that a new era in the design of ceramic structures has been entered during the past year, an era in which the ceramic engineer no longer will follow the classical theories of strength so useful in metal design, but will be guided by design criteria applicable to brittle materials.

EXPERIMENTAL MATERIALS

The selection of materials suitable for investigation has been one of the more difficult problems of this research. As pointed out earlier, reproducibility from specimen to specimen is essential to proper control of the tests. Specimens must be relatively free of macroscopic flaws, such as cracks, voids, or inclusions, for these have been found to render fracture data so unreliable as to be of little value. Also, the material must be representative of ceramic materials. The ease of fabrication and the cost of a material are also of importance, since the research, of necessity, demands the testing of large numbers of specimens of widely varying design.

An ideal material has not been found; however, a number of materials can be utilized successfully to carry out various phases of the research. During this year, the greater portion of the research was conducted on plaster of Paris. Additional experiments have been conducted on specimens of porcelain and on specimens of nickel-bonded titanium carbide.

Plaster

Plaster specimens tested during this period were fabricated from Hydrostone plaster, a product of the United States Gypsum Company. Hydrostone specimens were prepared by adding 1500 grams of the powder to 550 grams of distilled water. The resulting slurry was placed in an evacuating system and mixed for five minutes at a pressure of 1 inch of mercury absolute. Mixing in a vacuum helped to insure a uniform air-free mixture. Then the slurry was poured into polished Lucite molds, and the plaster was allowed to harden. After the plaster had set (about 30 minutes), the specimens were removed from the mold and were placed in a dryer at 110 F until the 14th day after casting. All Hydrostone plaster specimens were tested on the 14th day after casting.

Plaster has proved to be a very useful material in this research, as plaster specimens are inexpensive and easily fabricated. Although the properties of plaster are sensitive to changes in conditions of preparation and curing, specimens with uniform properties can be produced if proper control is exercised.

A chemical analysis of plaster taken from specimens used in this investigation showed the following approximate composition:

Constituent	Per Cent of Composition
$CaSO_4$	50.7
SiO_2	0.5
Al_2O_3	0.2
CaO	28.5
MgO	0.5
H_2O	19.5
MnO, SrO, Fe, Cu	Trace

Specimens of this composition have been used in this investigation to study the effects of size and stress state on fracture phenomena. Specimens of plaster cannot be used to study the effects of temperature on brittle fracture, since the properties of plaster, as a hydrated material, are affected adversely by temperature.

Porcelain

A high-alumina porcelain, a spark plug porcelain manufactured by the Champion Spark Plug Company of Detroit, Michigan, also was used to study the effects of size and stress state on fracture phenomena. This porcelain is a very carefully controlled ceramic product, and initial tests of specimens fabricated from this material have indicated a high degree of homogeneity and uniformity. All the porcelain specimens used in this investigation were fabricated by the manufacturer, who exercised the utmost care in fabrication.

These specimens are prepared from powders which are ground and spray dried. Then the dry powders are poured into rubber molds and cold pressed into blanks. The resulting blanks are ground to shape and then fired in a hanging position at a temperature of about 3000 F. The specimens shrink to their final form in the firing process. The specimens used in this investigation were not ground after firing, but were tested as fired.

Nickel-Bonded Titanium Carbide

During this period, a few tests were conducted on torsion specimens of a nickel-bonded titanium carbide body to study the effect of temperature on fracture strength. This material is a product of Kennametal, Incorporated, and is known as K151A. K151A has a nickel content of 20 per cent and a specific gravity of 5.8. The specimens used during this period were fabricated by Kennametal, and had been finish ground.

This material, which was used in the earlier stages of this investigation, has been discussed in detail in AF Technical Report No. 6512 and WADC Technical Report No. 52-67. K151A is of immediate practical value to the aircraft designer, because it possesses the physical and mechanical properties which are desirable for high-temperature engine parts. However, during previous states of this investigation, it was found that K151A has two undesirable characteristics which reduce its value for the investigation of fracture phenomena. It exhibits significant plastic flow prior to fracture, even at room temperature, so that it is not an ideally brittle material, and it has been found to contain objectionable defects or flaws, which have tended to invalidate the fracture data. In addition, specimens of this material are quite expensive; therefore, until such time as the undesirable qualities of this material are corrected, K151A is not considered a profitable material for use in this investigation.

THE EFFECT OF SIZE ON MECHANICAL PROPERTIES

For many years, the failure of materials has been studied from the point of view of the classical theory of elasticity. The resulting theories for the failure of materials were all based on the assumption that materials are perfectly homogeneous; i.e., that the intrinsic properties of an elemental volume of a body are identical to the properties of every other element in the body. This assumption leads to the conclusion that the gross properties of a body are the same as those of its elements, regardless of the size of the body. As a result, these classical theories of failure predict that the strength of a body is that of its elements and, hence, that all bodies of a material should have the same strength. This prediction of uniqueness of strength is not supported by experimental data. Not only do experiments conducted on nominally identical specimens reveal a variation in fracture strength, but tests conducted on specimens of different sizes reveal a variation of fracture strength. This apparent effect of size on fracture strength has been observed in a large number of tests on specimens of brittle materials such as glass[1, 2, 3], plaster of Paris[4, 5], rock salt[6], crystalline minerals[2, 7], cast iron[8, 9, 10], porcelain[11], and steel at low temperatures[12].*

The phenomenological theories mentioned earlier belong to the classical group of theories that predict a unique fracture strength of a material. As a result, these phenomenological theories fail to predict the effect of size on fracture strength observed in brittle materials.

The mechanistic theories which are based on the flaw concept of fracture do predict that the strength of a body may vary with its physical size. The statistical theories of strength, in particular, predict an effect of size on the fracture strength of a material. The fundamental hypothesis of these theories is that materials are weakened by the presence of very small "flaws" or localized stress concentrations in their structure. According to this concept, there will be a certain probability that fracture will take place in a stressed unit of material containing these flaws. This probability is expected to be a function of the average level of the stress in the unit and of the physical size of the unit. Consequently, this concept has led to the prediction that the observed fracture stress of a material should decrease with size, and that the standard deviation of the strength of a number of specimens should decrease with an increase in size. Since the strengths of certain ceramic materials have been observed to vary with size, it would be profitable to initiate the study of the fracture of such materials by a study of size effects. Such an effort was undertaken during the period of this report.

Although determining the nature of the effect of size on strength should be the ultimate goal of any size-effect study, the first requirement is to

*References are listed at the end of the report.

establish the existence of a size effect. Therefore, a program was set up during this period to determine the existence of a size effect in the various stress states — tension, compression, bending, and torsion.

Briefly, it was proposed that elastic and fracture data be obtained from tests on different sizes of geometrically similar specimens, and that these data be compared. If the fracture strengths of the various sizes showed no significant scatter or trend, it could be concluded that there was no significant effect of size on fracture strength at that particular temperature and strain rate. Conversely, if analyses of the fracture data showed a significant variation in behavior with size, the existence of an effect of size on fracture strength could be postulated.

Once the existence of an effect of size on strength was established, a study of the nature of this effect could be undertaken and an attempt made to analyze the data by means of existing theory.

Size-Effect Experiments on Plaster

Hydrostone plaster was chosen as a material on which to study the effect of size on strength. Tension, torsion, bending, and compression specimens were designed for carrying out the size-effect program. Two sizes, a large and a small, of each specimen were designed, and these sizes were geometrically similar in all cases except one. (The two tension specimens were not similar in their end regions, but were similar in their gage sections; Figure 4.) The large torsion, bending, and compression specimens were 5 times the size (125 times the volume) of the small specimens. The large tension specimen was 4 times the size (64 times the volume) of the small tension specimen. A series of tests was conducted on each size of these specimens, and the resulting data were compiled and analyzed. The experiments on plaster were so designed that, if they proved successful, the techniques and analyses developed could be used to extend the size-effect program to other ceramic materials.

Compression Tests

Compression tests were run to fracture, but no quantitative analysis of apparent fracture strengths was attempted owing to the invalidating effect of end restraints upon data on fracture in compression. (See section of report entitled "Effect of Friction on Compression Strength".) Elastic data in compression were compared, however, for the purpose of establishing the relation between the moduli of elasticity in tension and in compression.

Specimens. The sizes of compression specimens used in this size-effect program are shown in Figure 1. A ratio of length to diameter of

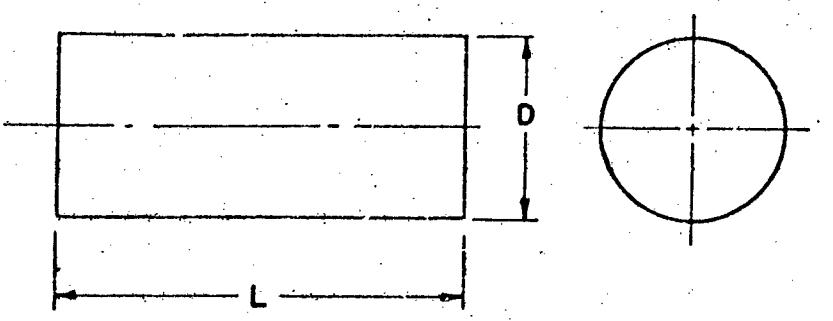

$\frac{L}{D} = 2.25$

Specimen Size	D	L
1	0.500	1.125
5	2.500	5.625

Dimensions in inches

FIGURE 1. SIZE-EFFECT COMPRESSION SPECIMENS

A-4699

2.25 was chosen in order to insure more uniform stress distribution in the gage section.(13, 14) Figure 2 is a photograph of the Hydrostone plaster specimens of the largest, No. 5, and the smallest, No. 1, sizes upon which compression tests were conducted. The volume of the No. 5 specimen is 125 times that of the No. 1 specimen. In the casting and curing of these specimens, the standard technique for casting and curing Hydrostone plaster was employed (see AF Technical Report No. 52-67).

The methods used in testing these specimens are described in a later section of this report. In addition, the procedure used in calculating the various data from the size-effect compression tests is discussed in detail in Appendix I. It should be pointed out here that all strain data were calculated taking into consideration the effect of the transverse sensitivity of the strain gages.(16)

Results. The data obtained from the size-effect tests on Hydrostone compression specimens are given in Table 1. The stress reported in Table 1 as the "compression strength" is the axial stress at fracture obtained by dividing the load at fracture by the cross-sectional area. This was not reported as a fracture stress, because it was not the stress in the region where fracture initiated. The significance of this interpretation is discussed in detail in another section of this report.

The data in Table 1 indicate that small specimens of Hydrostone have higher compression strengths than large specimens and that, for the size variation studied, this difference in strength was of the order of 8 per cent. It is important to note that these data indicate an increase in strength with a decrease in size. This is precisely the effect predicted by the mechanistic theories of strength.

The compression size-effect specimens of Hydrostone failed with the typical "cone type" fracture observed in other brittle materials. In most cases, this "cone of fracture" was observed only at the top end of the specimen. The apparent reason for the consistent appearance of the cone at the top of the specimen was that the top surface was rougher than the bottom surface. The resultant effect upon the compression test was the creation of a higher frictional resistance to lateral expansion at the top than at the bottom of the specimen.

At this point, the question of whether or not the reported compression strength could have any value in the investigation of fracture phenomena arose. The compression test was studied in an attempt to appraise its value in a study of size effects. As a result of this evaluation, it was decided to forego any attempt to analyze fracture data from the conventional compression test. The reason and significance of this decision have been discussed in detail in a later section entitled "The Effect of Friction on Compression

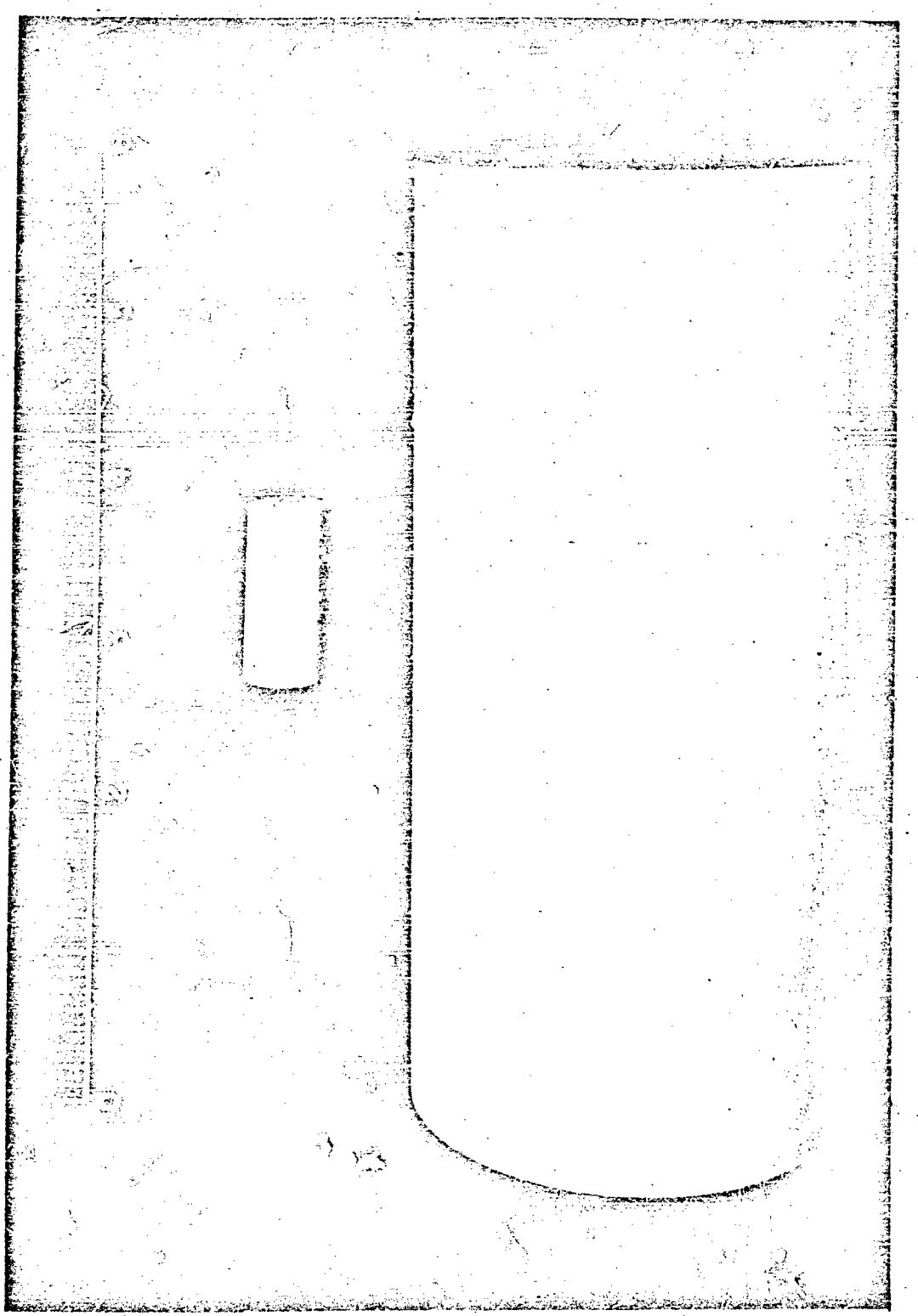

91633

FIGURE 2. SIZE-EFFECT COMPRESSION SPECIMENS OF HYDROSTONE PLASTER

TABLE 1. ELASTIC AND FRACTURE DATA FROM HYDROSTONE SIZE-EFFECT COMPRESSION SPECIMENS

Size No. 1 (Small)				Size No. 5 (Large)			
Specimen No.[a]	Modulus of Elasticity, 10^6 psi	Poisson's Ratio (-)	Axial Stress at Fracture, psi	Specimen No.[a]	Modulus of Elasticity, 10^6 psi	Poisson's Ratio (-)	Compression Strength, psi
1-H10C-1	2.57	-	-	1-H50C-1	2.37	0.259	-
-2	-	0.528[b]	-	-2	2.36	0.262	-
-3	2.51	-	-				
2-H10C-4	2.53	-	-	2-H50C-3	2.34	0.246	-
-5	-	0.203	-	-4	2.36	0.257	-
-6	2.59	-	-				
3-H10C-7	2.54	-	-	3-H50C-5	2.33	0.251	-
-8	-	0.237	-	-6	2.31	0.242	-
-9	2.75	-	-				
4-H10C-10	2.49	-	9900[b]	4-H50C-7	2.40	0.248	7990
-11	-	0.295	7760	-8	2.31	0.246	6070
-12	2.50	-	8490				
5-H10C-13	2.30	-	8100	5-H50C-9	2.25	0.208[b]	7720
-14	-	0.228	7160	-10	2.41	0.239	7210
-15	2.35	-	7510				
6-H10C-16	-	0.249	6630	6-H50C-11	2.32	0.245	5390
-17	2.38	-	8140	-12	2.27	0.237	7920
18	2.28	-	7990				
7-H10C-19	2.26	-	-	7-H50C-13	2.29	0.240	-
-20	2.31	-	-	-14	2.27	0.247	-
-21	-	0.298	-				
Mean value	2.45 ± 0.02	0.252 ± 0.034	7720 ± 430	Mean value	2.33 ± 0.02	0.248 ± 0.004	7130 ± 850
Std. deviation	0.05	0.038	600	Std. deviation	0.05	0.008	940 (to nearest 10)

(a) First number of Specimen No. indicates batch.

(b) Data were rejected from computation of mean on basis of Chauvenet's criterion. (See Appendix II.)

Strength". It may suffice here to say that the results of compression tests indicated an effect of size on the nominal compression strength of Hydrostone plaster.

From the elastic data in Table 1, it would appear that, in compression, small specimens of Hydrostone have a higher modulus of elasticity than large specimens of Hydrostone. The data also indicate a variation of Poisson's ratio between the two sizes of about 1.5 per cent, or less than the probable error in the mean value of Poisson's ratio for both sizes. Hence, it would appear that the two sizes exhibited essentially the same Poisson's ratio in compression.

Typical stress-strain curves for No. 1-size and No. 5-size specimens are shown in Figure 3. The variations in modulus and fracture strength with size are immediately apparent from a comparison of these curves. It is of interest that the stress-strain curves of the large and small specimens were not linear all the way to fracture. This was observed in varying degrees for these compression specimens.

These data raise the important question of whether different sizes of ceramic bodies exhibit different moduli. The mechanistic theories of fracture do predict a variation in fracture strength similar to that observed here, but they anticipate no decrease in elastic modulus with size. Nevertheless, these data indicate a 5 per cent variation in Young's modulus with a fivefold increase in size.

In anticipation of a variation of modulus with size, the first three batches of compression specimens were not fractured. Instead, they were returned to the curing oven and allowed to continue curing. These specimens were removed periodically, tested, and returned to curing. When these aging tests were initiated, it was felt that the observed variation of modulus with size might result from a transient curing phenomenon. However, the data in Table 2 tend to refute this explanation, indicating that, even after 127 days of curing, there is no significant change in the elastic properties of either large or small compression specimens. Hence, it appears that the variation in elastic properties with size observed in the compression size-effect tests did not result from a transient curing phenomenon.

Tests were conducted also to determine whether the type of loading had any effect on the elastic properties of Hydrostone in compression. Compression specimens of both sizes were loaded through three cycles of continuous loading and three cycles of incremental loading. The results of these tests were as shown on page 17.

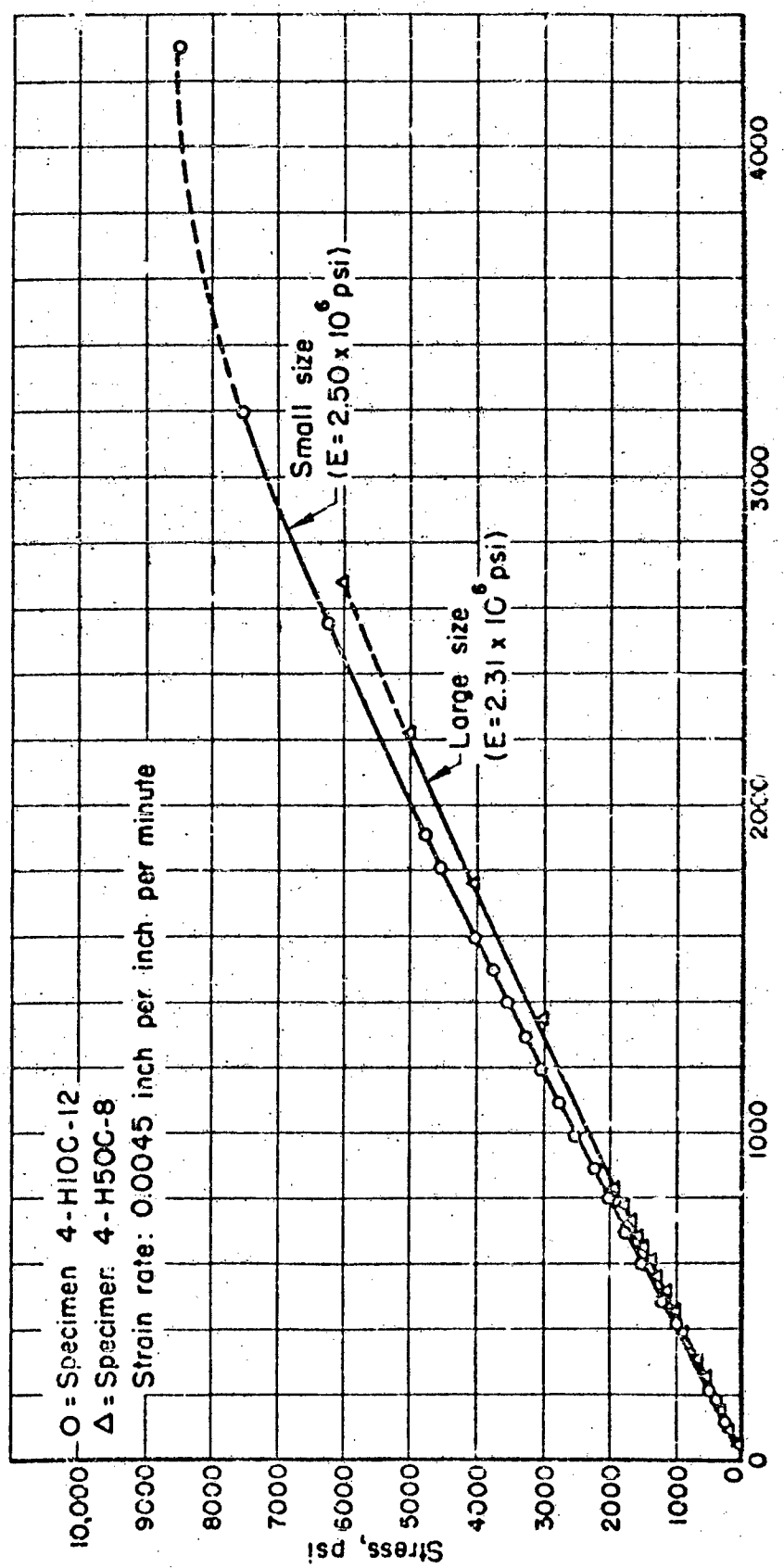

FIGURE 3. COMPRESSION STRESS-STRAIN CURVES FOR HYDROSTONE SIZE-EFFECT SPECIMENS

TABLE 2. EFFECT OF CURING TIME ON HYDROSTONE SIZE-EFFECT COMPRESSION SPECIMENS

Specimen No.	Curing Time, days	Modulus of Elasticity, 10^6 psi	Net Change in Modulus, per cent	Poisson's Ratio (-)	Net Change in Poisson's Ratio, per cent
1-H50C-1	14	2.37	--	0.259	--
(Large)	28	2.38	0.5	0.263	1.5
	41	2.35	0.8	0.257	0.8
	127	2.32	2.1	0.255	1.6
1-H50C-2	14	2.36	--	0.263	--
(Large)	28	2.38	0.8	0.271	3.0
	41	2.36	0.0	0.285	8.4
	127	2.36	0.0	0.277	5.3
1-H10C-1	14	2.57	--	--	--
(Small)	41	2.53	1.6	--	--
	127	2.52	1.9	--	--
1-H10C-3	14	2.51	--	--	--
(Small)	41	2.48	1.2	--	--

Specimen No.	Type of Loading	Modulus of Elasticity, 10^6 psi (Average of Three Tests)
3-H50C-5	Continuous	2.23
	Incremental	2.22
3-H50C-9	Continuous	2.57
	Incremental	2.61

These data indicate no significant difference in elastic properties with the two types of loading; however, incremental loading produced somewhat more erratic data than continuous loading.

In addition to the curing tests described above, the plaster from a large compression specimen was subjected to chemical analysis. The results of this analysis were compared with the results of a similar analysis on a small compression specimen. The moduli of these specimens were as follows:

Specimen No.	Modulus of Elasticity, 10^6 psi (Average of Two Tests)
8-H10C-22 (Small)	2.40
8-H50C-15 (Large)	2.25

The chemical analysis of the plaster from these specimens gave:

Specimen No.	Composition, per cent						
	$CaSO_4$	SiO_2	Al_2O_3	CaO	MgO	H_2O	MnO, SrO, Fe, Cu
8-H10C-22 (Small)	50.7	0.5	0.2	28.5	0.5	19.5	0.03-0.25
8-H50C-15 (Large)	47.9	0.5	0.2	31.1	0.5	19.7	0.03-0.25

The results of these analyses indicate that there was little difference between the plasters of the large and the small specimens. The only difference occurred in the amount of CaO present in each. Whether this small difference (2.6 per cent) in CaO can account for the observed variation in modulus of elasticity is unknown at this time.

There appear to be two possible explanations for the observed variation of compression modulus with size in Hydrostone plaster. One explanation is that the variation results from a difference in the materials themselves. It is possible, owing to variations in the thermal and curing histories of the

two sizes, that the plaster in the small specimen was not the same as the plaster in the large specimen, and that this difference did not disappear with age. The other possible explanation is that this variation in modulus with size was a true size effect. It is interesting that Reinkober[17] found that both the modulus of elasticity and the modulus of rigidity of silica fibers depended on the fiber thickness.

It is important to note that here the variation in moduli between batches of the same size was of the order of 5 per cent in some cases, and that the variation of the mean values (4.7 per cent) of the two sizes was not much greater than the probable error in the means. When these observations were combined with the analysis of the elastic data from other stress states, it was felt that this variation in modulus with size was somewhat anomalous.

As for the existence of a size effect in plaster in compression, the tests so far conducted on plaster indicate that the strengths of compression specimens are affected by their size.

Tension Tests

Elastic and fracture data were obtained from the tension, size-effect tests. Elastic data were used to establish control of the tests and in the correlation of fracture data. Fracture data were recorded in an effort, first, to determine whether an effect of size on strength existed, and, second, to study the quantitative effects of size and stress state on fracture data.

Specimens. Considerable difficulty has been encountered in tension tests of ceramic materials. One of the major sources of difficulty has been the maintenance of axiality of loading during the test. With the specimens used previously in this investigation (see AF Technical Report No. 6512, Figure 1), the specimens tended to change alignment during the test, introducing extraneous bending stresses. An alternate tension specimen employing "cast-in" pins or bushings was developed during this period in an effort to eliminate this difficulty. With pins or bushings accurately located on the center line and with a Universal-type loading, the alignment should not change during the test.

The two sizes of this alternate tensile specimen used in the size-effect study are shown in Figure 4. Some success was obtained with these specimens in maintaining alignment. However, some difficulty arose in maintaining accurate location of the bushings in the casting.

It should be noted that these two size-effect tension specimens were not geometrically similar in the region of the pin. Initial tests with specimens exactly 4 times the size of the No. 1 specimen produced an undesirable number of fractures across the head section. As a result, this portion of

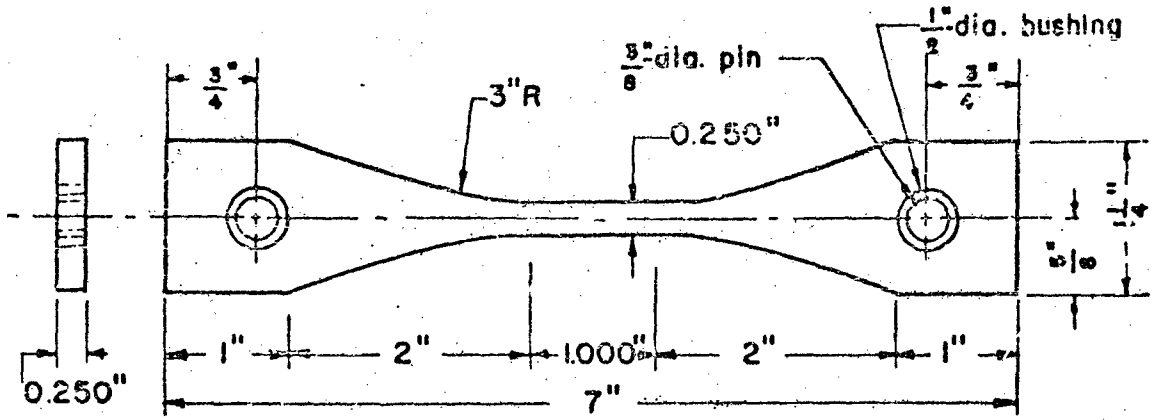

No. 1 size

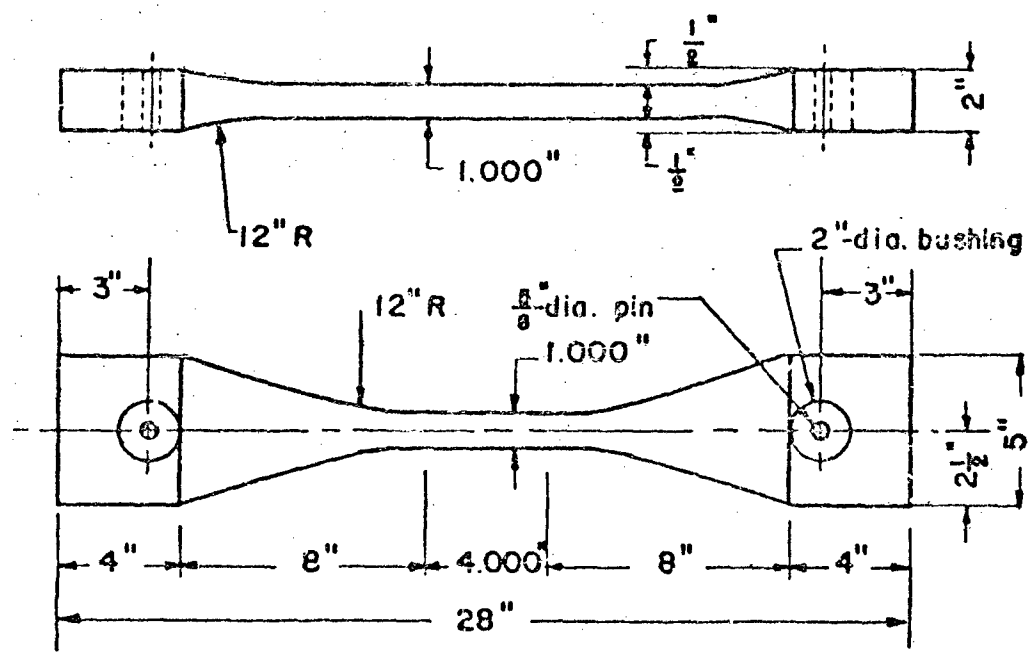

No. 4 size

FIGURE 4. ALTERNATE SIZE-EFFECT TENSION SPECIMENS

A-4682

the No. 4 specimen was widened to reduce the gross stress at the pin. At the same time, geometric similarity of the two specimens in the region of the gage section was maintained to retain similarity of stress distribution. Tests conducted on the redesigned No. 4 specimen produced acceptable fracture data. Figure 5 is a photograph of these two size-effect tension specimens of Hydrostone plaster.

The methods used in testing the size-effect tension specimens are described in detail in a later section of this report.

The procedure used in the calculation of the data from the size-effect tension tests is given in detail in Appendix I.

Results. The elastic and fracture data obtained from the tests on the No. 1-size tension specimen are given in Table 3. The elastic and fracture data obtained from the No. 4-size tension specimen are given in Table 4. The values of modulus of elasticity reported in Tables 3 and 4 are, with a few exceptions, the averages of four or more elastic determinations. The value of strength reported is the average axial stress in the specimen at fracture; that is, the load at fracture divided by the cross-sectional area. It is particularly important to note that a certain eccentricity was observed in certain of these tests. This eccentricity appeared to vary from specimen to specimen and, as a result, the strength reported was not the actual maximum stress in the specimen. Consequently, the mean strengths of these specimens were affected by the eccentricity. Analysis of the effect of eccentricity on the strength data obtained from the tensile test indicated that the strength of a specimen (the maximum stress in the specimen at fracture) should increase with increasing eccentricity. (For a more detailed discussion of this subject, see the section entitled "Effect of Superposed Bending Stresses on Tension-Test Data".) As a result, it was felt that the mean strength values were somewhat higher than they would have been had no eccentricity been present.

The data in Tables 3 and 4 indicate that the modulus of elasticity on Hydrostone plaster in tension, within the limits of accuracy of these tests, does not vary with size. It is interesting to note that the existing variation of modulus was opposite to that observed in the size-effect compression tests; that is, here the larger specimen appeared to have the higher modulus. This served to substantiate the hypothesis that the variation observed in the results of the size-effect compression tests was due to experimental causes.

Typical stress-strain curves for the No. 1 and No. 4 tension specimens are given in Figure 6. It can be seen from Figure 6 that little nonlinearity is present in these stress-strain curves. The effect of size on the fracture strength of plaster in tension is also evident in Figure 6.

It is important to point out that the mounting of SR-4 strain gages on the gage section surfaces of the No. 1 tension specimens appears to have strengthened these specimens. This may have caused the mean strength in

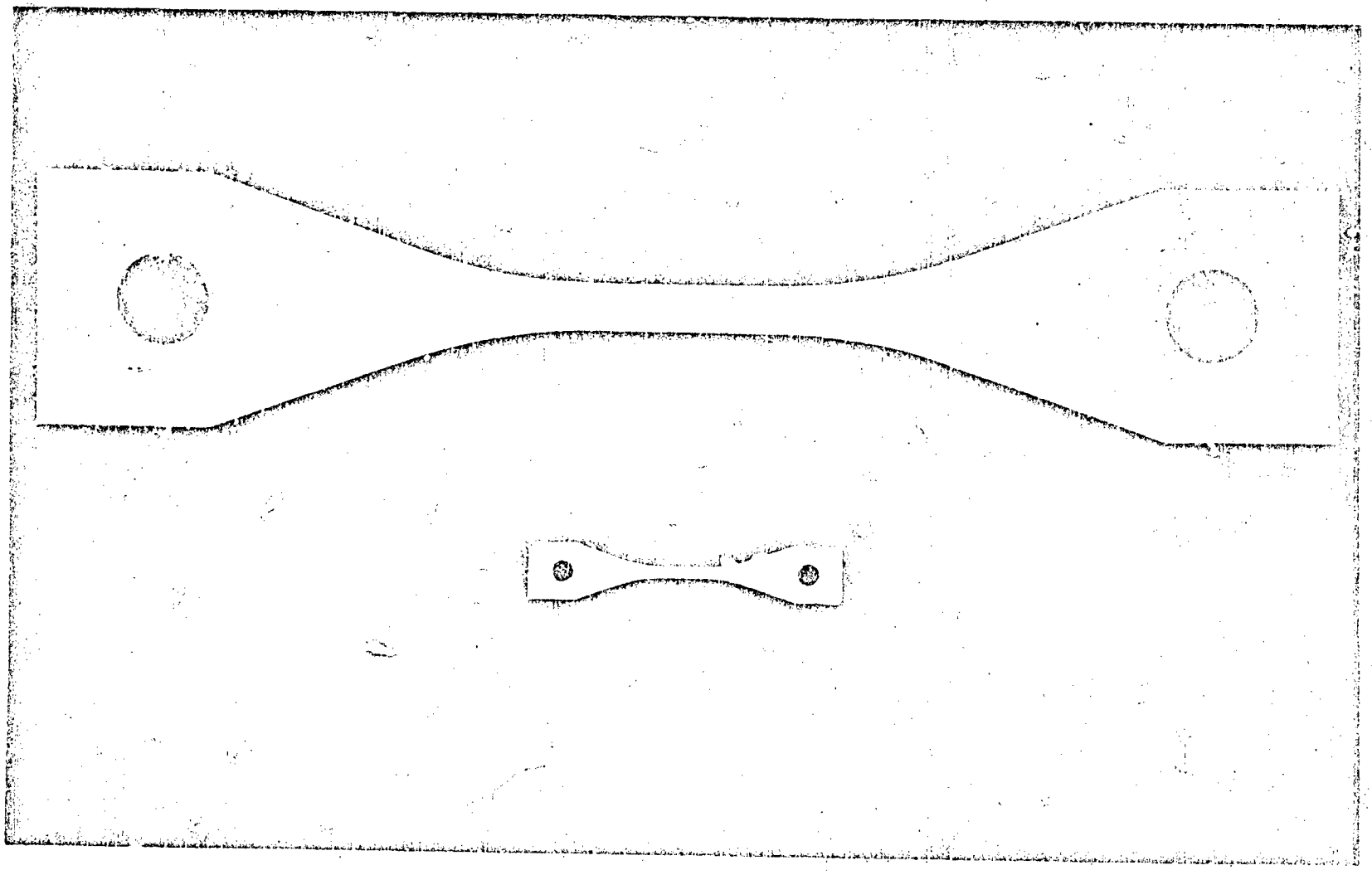

94288

FIGURE 5. SIZE-EFFECT TENSION SPECIMENS OF PLASTER

TABLE 3. ELASTIC AND FRACTURE DATA FROM NO. 1-SIZE PLASTER TENSION SPECIMENS

Specimen No.	Modulus of Elasticity, 10^6 psi	Strength, psi	Specimen No.	Modulus of Elasticity, 10^6 psi	Poisson's Ratio	Strength, psi
H10T-2	2.33	1190	H10T-49			1070
H10T-3	2.27	1145	H10T-50			1240
H10T-5	2.46	--	H10T-54			990
H10T-6	2.48	1335	H10T-55			1070
H10T-8	2.34	1300	H10T-56			1070
H10T-9	2.69	--	H10T-57			705
H10T-10	2.52	1280	H10T-58			960
H10T-11	2.50	1380	H10T-59			1235
H10T-12	2.47	--	H10T-60			1410
H10T-13	2.52	1370	H10T-61			1145
H10T-14	--	1360	H10T-62			1300
H10T-16	2.30	1170	H10T-63			1365
H10T-17	2.30	--	H10T-65			1345
H10T-19	2.36	--	H10T-66			1080
H10T-20	2.20	1310	H10T-68			1235
H10T-21	2.36	1290	H10T-70			1420
H10T-23	2.58	1520	H10T-71			1340
H10T-25	2.27	1130	H10T-72			1375
H10T-26	2.31	1300	H10T-73		0.229	1370
H10T-31	2.30	1240	H10T-74		0.281	1295
H10T-32	2.24	1375	H10T-75		0.306	1105
H10T-33	--	1365	H10T-76			1150
H10T-35	--	1350	H10T-77			975
H10T-40	--	1205	H10T-78		0.245	1390
H10T-44	--	1120,	H10T-79		0.199	1160
H10T-47	2.52	--	H10T-80		0.290	1170
H10T-48	2.39	--	Mean Value	2.40 ± 0.05	0.258 ± 0.037	1245 ± 35
			Standard Deviation	0.13	0.041	135

TABLE '. ELASTIC AND FRACTURE DATA FROM NO. 4-SIZE PLASTER TENSION SPECIMENS

Specimen No.	Modulus of Elasticity, 10^6 psi	Poisson's Ratio	Strength, psi	Specimen No.	Modulus of Elasticity, 10^6 psi	Poisson's Ratio	Strength, psi
H40T-3	2.38	--	--	H40T-27	2.25		--
H40T-4	2.47	0.265	--	H40T-28	2.23		785
H40T-5	2.56	0.225	--	H40T-29	2.10		
H40T-6	2.40	0.224	--	H40T-30			945
H40T-7	2.59	0.255	835	H40T-31			915
H40T-8	2.48	0.218	--	H40T-32			1005
H40T-9	2.50	0.252	--	H40T-33			1090
H40T-10	2.44		--	H40T-34			1060
H40T-11	2.41		--	H40T-36			970
H40T-12	2.43		--	H40T-37			830
H40T-13	2.37		955	H40T-38			945
H40T-14	2.40		--	H40T-39			915
H40T-15	2.42		--	H40T-43			895
H40T-16	2.36		760	H40T-44			770
H40T-17	2.35		--	H40T-46			830
H40T-18	2.39		--	H40T-47			1110
H40T-20	2.24		550	H40T-53			1035
H40T-21	2.40		695	H40T-55			750
H40T-23	2.37		--	H40T-56			1035
H40T-24			645				
H40T-25			920	Mean Value	2.39 ± 0.09	0.240 ± 0.018	875 ± 55
H40T-26			690	Standard Deviation	0.11	0.020	150

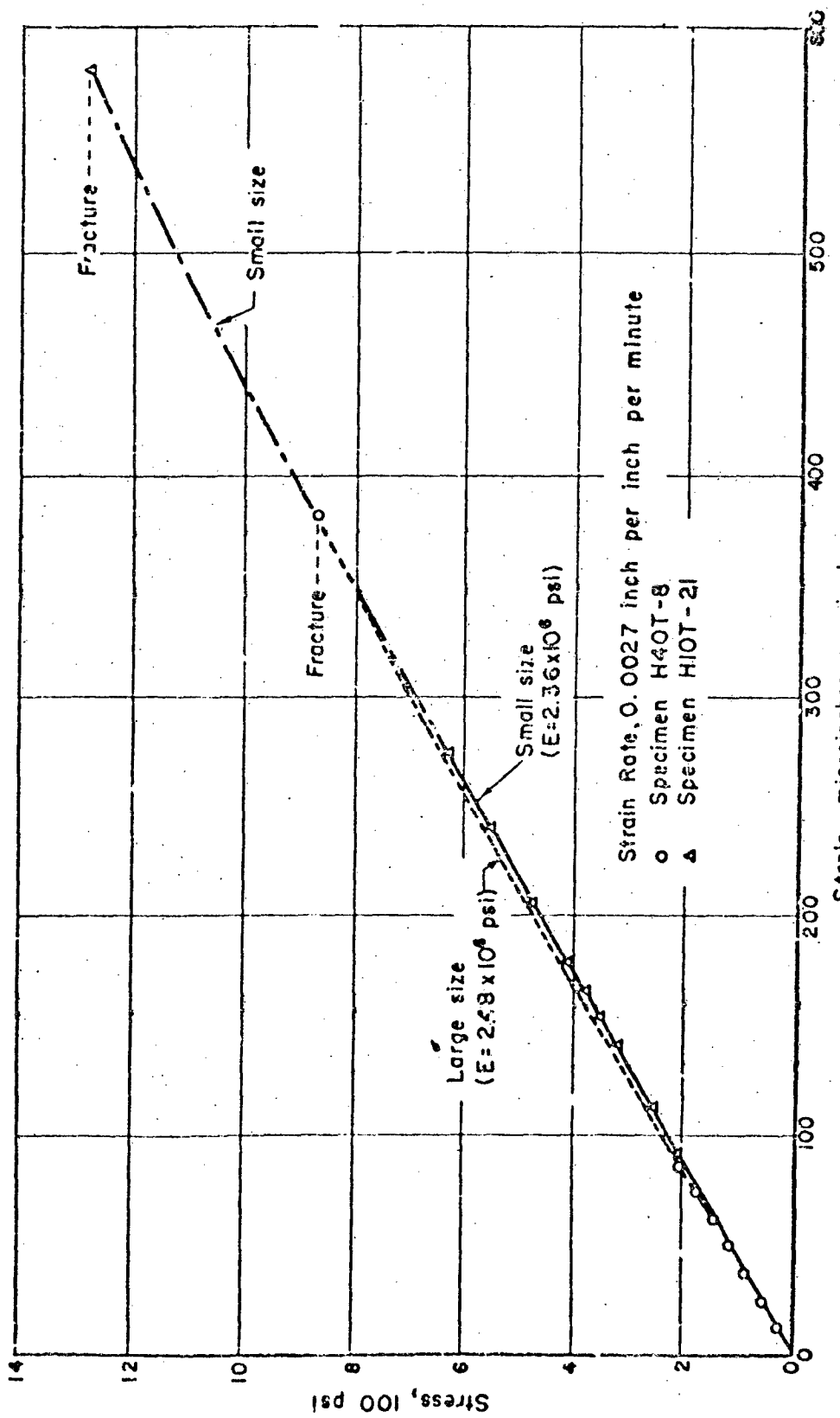

FIGURE 6. TENSION STRESS-STRAIN CURVES FOR HYDROSTONE SIZE-EFFECT SPECIMENS

A-4691

Table 3 to be fictitiously high. A comparison of the fracture strengths from gage-free specimens with strengths from specimens with gages led to the following:

Condition	Number of Specimens	Tensile Strength, psi
With gages	21	1280
Without gages	25	1195

This comparison suggested comparing the mean strength reported in Table 3, 1245 psi, with the mean strength in Table 4, 875 psi. The latter value was obtained from specimens almost all of which were free of gages, while the former value was obtained from specimens of both types. As a result, the following mean strengths were reported for the No. 1- and No. 4- size specimens without gages:

Specimen	Mean Strength, psi	Standard Deviation	Number of Specimens
No. 1	1195 ± 60	175	25
No. 4	915 ± 55	135	19

It should be noted in the case of those No. 1 tension specimens with gages that fracture was observed to take place both through and outside the gage.

Additional tests were made to determine whether the type of loading had any effect upon elastic data obtained from the tension tests. Several No. 1-size specimens were tested under both incremental and continuous loading and the data compared. Each tensile specimen was subjected to three incremental loadings and to three continuous loadings. The results of these tests are given below:

Specimen No.	Type of Loading	Modulus of Elasticity, 10^6 psi
H10T - 31	Continuous	2.30
	Incremental	2.35
H10T - 32	Continuous	2.25
	Incremental	2.23

These data indicate that the type of loading had little effect upon elastic properties obtained from the small tension specimen. It was noted, however, that data taken from incrementally loaded specimens tended to be more erratic than data from continuously loaded specimens.

It should be pointed out that specimens H40T - 7, H40T - 13, and H40T - 16 (see Table 4) were specimens of the old design (exactly 4 times the size of the No. 1 specimen) and, hence, not of the same design as the

remaining specimens in Table 4. The mean strength reported in Table 4 includes these specimens. If the strengths of these specimens are excluded, a mean strength of 880 ± 60 psi and a standard deviation of 155 psi are obtained. These fracture data and the data in Tables 3 and 4 do indicate, however, that the fracture strength of Hydrostone plaster in tension decreases about 30 per cent with a fourfold increase in size. The data in Table 3 and Table 4 would seem to indicate that the standard deviation of the strength might increase with size, however, no such conclusion should be drawn yet, since the individual deviations were determined from unequal numbers of specimens. It is noteworthy, though, that the observed effect of size on strength agreed qualitatively with the effect predicted by the mechanistic theories.

In all of these tests, the fracture of these specimens appeared typically brittle, that is, normal to the maximum tensile stress. It is important to add that, in many instances, fracture appeared to initiate at the surface of the specimen. The actual relative influence of the surface or possible surface "flaws", although certainly important, was not considered at this stage of the investigation.

Bend Tests

As a part of the program to determine the effect of size upon fracture phenomena, bend tests were conducted on plaster bend specimens of two different sizes. The fracture data from these tests were recorded in an effort, first, to determine whether an effect of size existed on strength, and, second, to study the quantitative effects of size and stress state. Elastic and fracture data were obtained from these tests. The elastic data were used to establish control of the tests and for correlation of the fracture data.

Specimens. The bend test is a common test used by ceramic engineers to determine the mechanical properties of ceramic bodies. The bend test was chosen to be used in this investigation for the evaluation of ceramic bodies; however, the nature of this investigation required that the data obtained from the bend test be as quantitatively precise as possible.

In previous periods of this study, bend tests were conducted on specimens of the design shown in Figure 9 of AF Technical Report No. 6512. Specimens of this design were loaded in the manner shown in Figure 8 of that report, i.e., as a solid beam in bending. In this type of loading, the bend specimen is not loaded at the neutral axis. As a result, undesirable friction forces are introduced. Since, by their nature, these frictional forces are unknown, they introduce errors into the resulting bend data. (For a discussion of the significance of friction in bend tests, see WADC Technical Report 52-67.)

In order to alleviate friction forces, an alternate bend specimen was designed for the size-effect program which permitted loading at the neutral axis. This alternate design provided for the use of bushings in the specimen. These bushings were located accurately on the neutral axis of the specimen, and were cast into the plaster specimen. The load was transmitted through hardened steel pins inserted through the bushings. Thus, a pure bending moment could be transmitted to the gage section of the specimen without introducing unknown friction forces. The two sizes of this alternate bend specimen used for the size-effect study on plaster are shown in Figure 7.

Figure 8 shows alternate bend specimens of the two sizes used in this program. It should be noted that 1/2-inch-diameter brass bushings were used in the No. 5-size bend specimen. No bushings were used in the No. 1-size specimen; instead, the pins were cast directly into the specimen.

These specimens of Hydrostone were cured in the same manner as the size-effect compression specimens. Each specimen was marked as it was removed from the mold, in order to insure the same relative orientation in each test.

The methods used in testing these bend specimens are given in detail later in this report.

Results. The procedure followed in the calculation of data from these bend specimens is outlined in detail in Appendix I. Data obtained from the tests on small, No. 1-size bend specimens are given in Table 5. Elastic data obtained from large, No. 5-size bend specimens are given in Table 6. Fracture data from the No. 5-size specimens are given in Table 7.

It should be noted that the moduli reported in Table 5 for the small bend specimens were not equal. If it is assumed that the modulus of elasticity is the same in tension as in compression, the values in Table 5 represent a measure of the state of stress in each bend specimen. Theoretically, if the recorded tension and compression moduli were equal, a state of pure bending would have existed in the specimen. The fact that the strains on the top and bottom surfaces were not equal indicates that this assumption is faulty, or that extraneous axial stresses shifted the neutral axis. It does not seem logical to assume that the consistently greater strain on the tension surface was due to random stresses. It seems more logical that the two strains, tension and compression, were unequal as a result of different tensile and compressive properties or as a result of a consistent axial tensile stress.

It is interesting to note that the elastic data on the large bend specimen (Table 6) indicated an inequality of moduli opposite to that observed on the small bend specimen. It does not seem logical that such a reversal should result from the basic designs of the specimens, but, rather, from a difference in the loadings of the specimens. Both of these variations could have

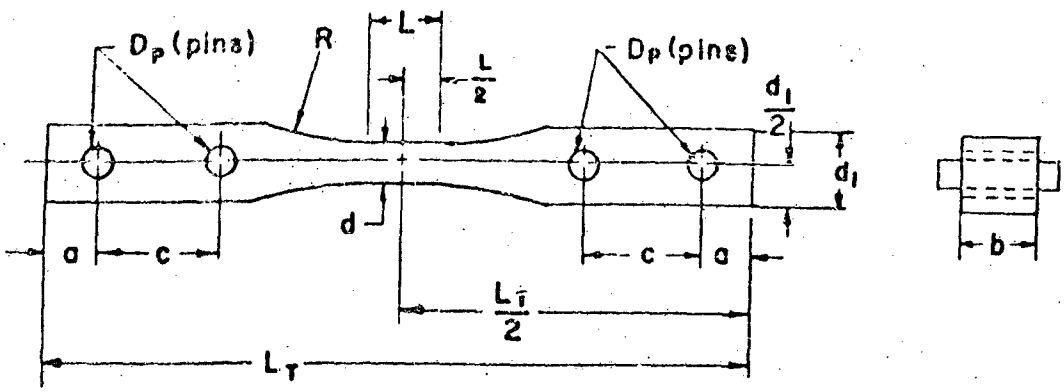

Specimen Size	b	d	L	c	a	R	D_p	L_T	d_1
1	0.313	0.188	0.313	$\frac{1}{2}$	$\frac{7}{32}$	$1\frac{9}{16}$	$\frac{1}{8}$	$2\frac{10}{16}$	0.313
5	1.563	0.938	1.563	$2\frac{1}{2}$	$1\frac{3}{32}$	$7\frac{13}{16}$	$\frac{5}{8}$	$14\frac{11}{16}$	1.563

Dimensions in Inches

FIGURE 7 ALTERNATE SIZE-EFFECT BEND-TEST SPECIMENS OF HYDROSTONE PLASTER

A-4697

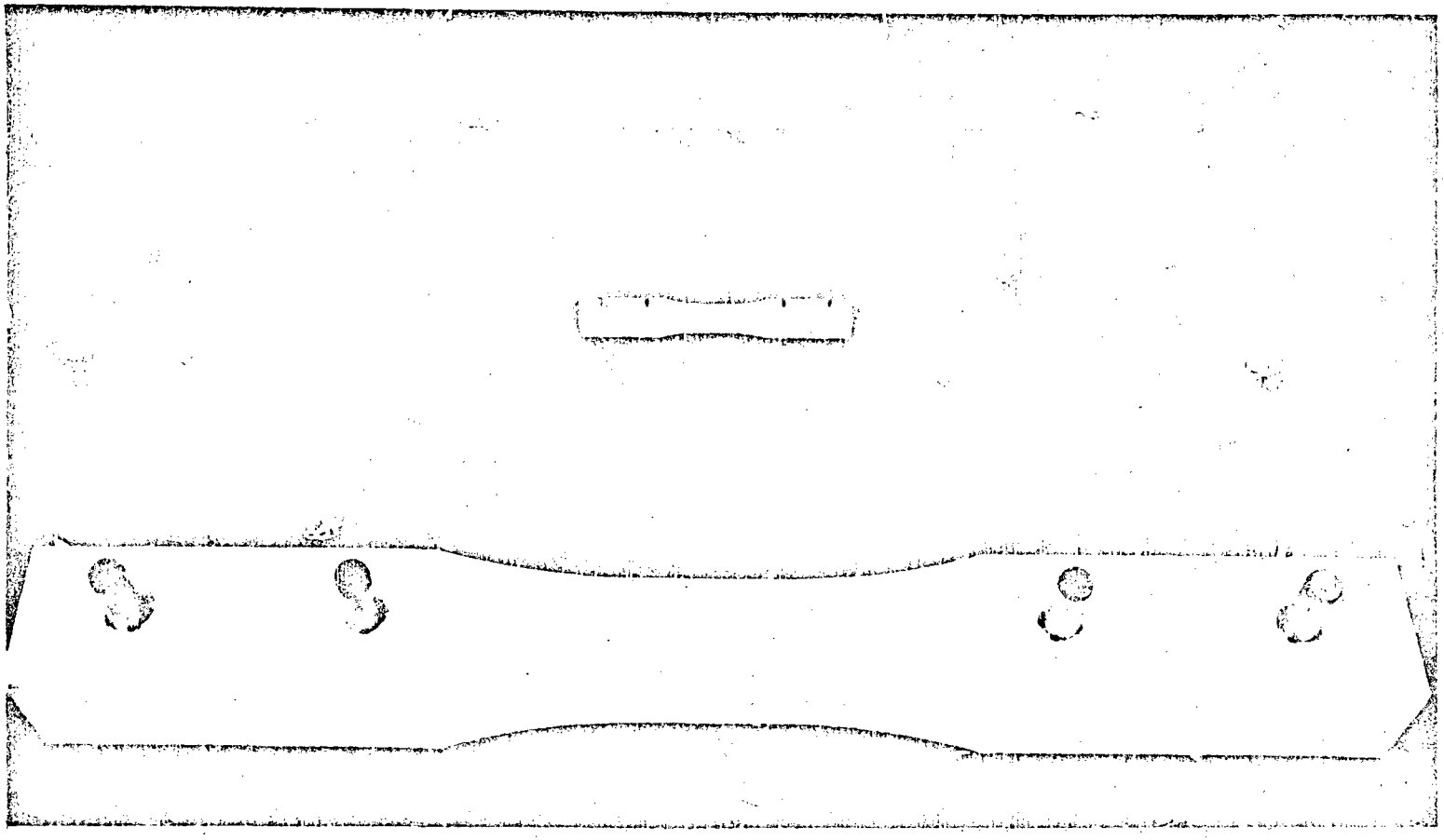

91319

FIGURE 8. ALTERNATE SIZE-EFFECT BEND-TEST SPECIMENS OF HYDROSTONE PLASTER

TABLE 5. ELASTIC AND FRACTURE DATA FROM NO. 1-SIZE PLASTER BEND SPECIMENS

Specimen No.	Modulus of Elasticity, 10^6 psi		Strength, psi	Specimen No.	Modulus of Elasticity, 10^6 psi		Strength, psi
	Tension	Compression			Tension	Compression	
H10B-1			2340	H10B-27	2.42	2.27	1650
H10B-2			2285	H10B-28			1510
H10B-4			1825	H10B-29	2.71	2.48	2275
H10B-5			1930	H10B-31	2.60	2.32	1791
H10B-7			1835	H10B-32	2.45	2.53	
H10B-8			1785	H10B-33	2.37	2.66	1810
H10B-9			1910	H10B-34			1635
H10B-10			2010	H10B-35			1705
H10B-11			1815	H10B-36			2170
H10B-12			1740	H10B-37			1665
H10B-13			2035	H10B-38			1690
H10B-14			1950	H10B-39	2.73	3.28	1780
H10B-15			1870	H10B-40			1715
H10B-16			1845	H10B-41			1905
H10B-17			1860	H10B-42			1765
H10B-18			2185	H10B-43			1665
H10B-19			2015	H10B-44			1935
H10B-20			1765	H10B-45			1960
H10B-21			1780	H10B-46			1950
H10B-23			1560	H10B-47			1730
H10B-24	2.33	2.46	1575	H10B-49			1370
H10B-26	2.49	2.23	1590	H10B-50			1485
				Mean Value	2.51 ± 0.11	2.53 ± 0.14	1830 ± 55
				Standard Deviation	0.15	0.20	210

TABLE 6. ELASTIC DATA FROM NO. 5-SIZE PLASTER BEND SPECIMENS

Specimen Number	Tension		Compression		Average	
	Modulus of Elasticity, 10^6 psi	Poisson's Ratio	Modulus of Elasticity, 10^6 psi	Poisson's Ratio	Modulus of Elasticity, 10^6 psi	Average Poisson's Ratio
H50B-8	2.44	—	2.33	—	2.39	—
H50B-10	2.46	0.256	2.41	0.238	2.44	0.247
H50B-11	2.41	0.251	2.42	0.266	2.42	0.259
H50B-12	2.51	0.200(1)	2.44	0.206(1)	2.48	—
H50B-13	2.50	0.239	2.48	0.233	2.49	0.236
H50B-14	2.46	0.225	2.45	0.233	2.46	0.229
H50B-15	2.45	0.227	2.28	0.233	2.37	0.230
H50B-22	2.34	—	2.17	—	2.26	—
H50B-23	2.31	—	2.17	—	2.24	—
H50B-25	2.20	—	2.07	—	2.14	—
H50B-27	2.40	—	2.25	—	2.33	—
H50B-28	2.31	—	2.23	—	2.27	—
H50B-32	2.24	0.220	2.20	0.262	2.22	0.241
Mean Value	2.39 ± 0.05	0.236 ± 0.013	2.30 ± 0.07	0.244 ± 0.014	2.35 ± 0.06	0.240 ± 0.010
Standard Deviation	0.10	0.015	0.13	0.016	0.11	0.011

(1) Rejected from computation of mean.

TABLE 7. FRACTURE DATA FROM NO. 5-SIZE PLASTER BEND SPECIMENS

Specimen No.	Strength, psi	Specimen No.	Strength, psi
H50B-8	1345	H50B-32	950
H50B-9	1325	H50B-33	1265
H50B-10	1535	H50B-34	1245
H50B-11	1170	H50B-35	1055
H50B-12	1355	H50B-36	1230
H50B-13	1270	H50B-37	1265
H50B-14	1420	H50B-38	1345
H50B-15	1555	H50B-39	1225
H50B-16	1490	H50B-40	1015
H50B-18	1555	H50B-41	1030
H50B-19	1675	H50B-42	1110
H50B-20	920	H50B-43	1265
H50B-21	1300	H50B-44	1380
H50B-22	1125	H50B-45	1010
H50B-23	1265	H50B-46	1430
H50B-24	1225	H50B-47	1120
H50B-25	1060	H50B-48	1570
H50B-26	1040	H50B-49	1510
H50B-27	790	H50B-50	1700
H50B-28	835		
H50B-29	1175	Mean Value	1250 ± 55
H50B-30	1240		
H50B-31	1105	Standard Deviation	215

resulted from variations in the distance between the innermost bushings, too short a distance causing an axial tension and too long a distance causing an axial compression.

In an effort to determine whether or not the relative orientation of the specimen in the test (and, hence, its orientation in the mold) influenced the moduli data, experiments were conducted on both No. 1- and No. 5-size specimens loaded under "normal" and "inverted" orientations. A "normally" oriented specimen was tested with its bottom side in the mold in tension. An "inverted" orientation placed the bottom side in compression. The data from these tests are given below:

Specimen No.	Orientation	Modulus of Elasticity, 10^6 psi	
		Tension	Compression
		(Average of Two Determinations)	
H10B - 24	Normal	2.33	2.46
	Inverted	2.47	2.43
H10B - 30	Normal	2.32	2.60
	Inverted	2.40	2.57
		(Average of Three Determinations)	
H50B - 13	Normal	2.50	2.48
	Inverted	2.43	2.46
H50B - 22	Normal	2.34	2.17
	Inverted	2.16	2.32
H50B - 23	Normal	2.31	2.17
	Inverted	2.09	2.30

In general, these data indicate that the observed inequality between tension and compression moduli was reversed by inverting the specimen in the loading jig. These data tend to refute the explanation that the differences in moduli were due to extraneous axial stresses, since these stresses should not have been reversed by inverting the specimen.

Additional tests were conducted on No. 5 bend specimens to determine whether the rate of loading had any effect on observed elastic data. No. 5 bend specimens were subjected to three continuous loadings and to three incremental loadings, in which the load was applied in steps or increments. The data from these tests are given below:

Specimen No.	Type of Loading	Modulus of Elasticity, 10^6 psi	
		Tension	Compression
H50B - 8	Incremental	2.34	2.24
	Continuous	2.29	2.22
H50B - 13	Incremental	2.50	2.48
	Continuous	2.47	2.46

These data indicate that there was no significant difference between elastic data obtained from the differently loaded specimens; however, data from the incrementally loaded specimens tended to be more erratic than data from specimens loaded continuously.

No possible explanation could be found for the reversal of moduli data reported above other than that the elastic properties of the specimen vary from top to bottom in the mold. That such a large variation between tension and compression moduli could be attributed to orientation was not obvious.

In summary, it does not seem necessary for the elastic properties of a body to be the same in tension and compression, nor does it seem plausible that material variables could cause such a large variation over such a small depth. At the same time, it should be noted that the variation between moduli was for both specimens within the probable error in the data. As a result, it was felt that these differences in moduli reflected experimental errors of unknown origin, and that, for all practical purposes, the tension and compression moduli were equivalent.

The fracture data in Tables 5 and 7, on the two sizes of bend specimen indicate that small bend specimens of Hydrostone plaster were stronger than large specimens of similar design. For the size variation studied, this variation in strength was of the order of 31 per cent. This variation was similar to the qualitative effect of size on strength predicted by the mechanistic theories. It should be noted, however, that the standard deviation of the strength did not decrease with size as predicted by these theories. In light of these data, it seems plausible to conclude that the size of a Hydrostone plaster body does affect its strength in bending; that is, that an effect of size on strength does exist, at least in bending.

The quantitative significance of these results is discussed in more detail later in this report.

Torsion Tests

As another part of the program to determine the effect of size upon fracture phenomena, torsion tests were conducted on plaster torsion specimens of two different sizes. These tests were conducted to determine whether an effect of size on strength existed and to study the effects of size and stress state. No elastic data were obtained from the small torsion specimens due to their small size. Elastic data were obtained, however, on the No. 5-size torsion specimens. Fracture data were obtained for both sizes.

Specimens. The torsion specimens used in this size-effect study are shown in Figure 9. The dimensions of these two sizes, the large and the small, are given in Figure 10. As in the case of the bend and compression

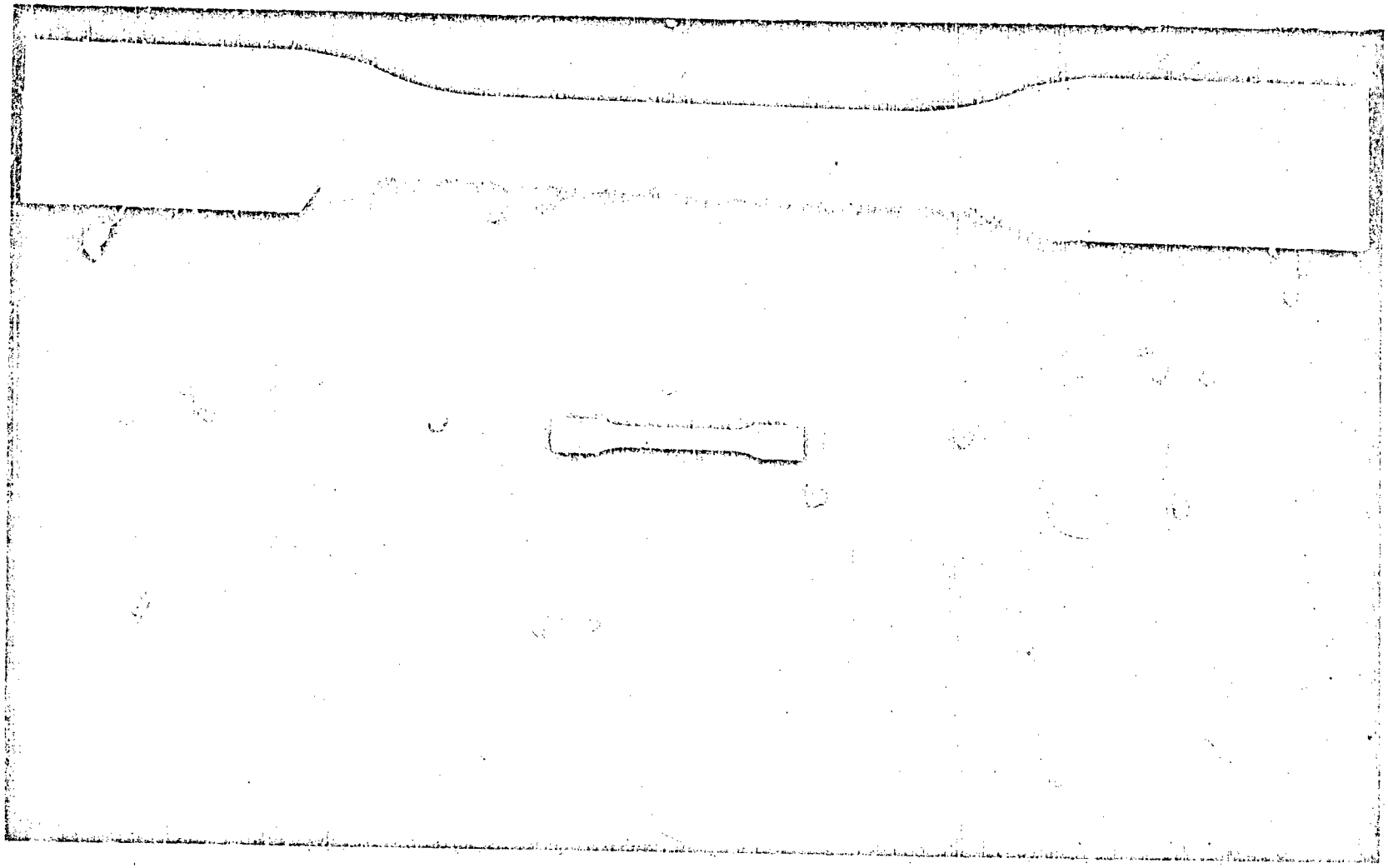

97721

FIGURE 9. SIZE-EFFECT TORSION SPECIMENS OF HYDROSTONE PLASTER

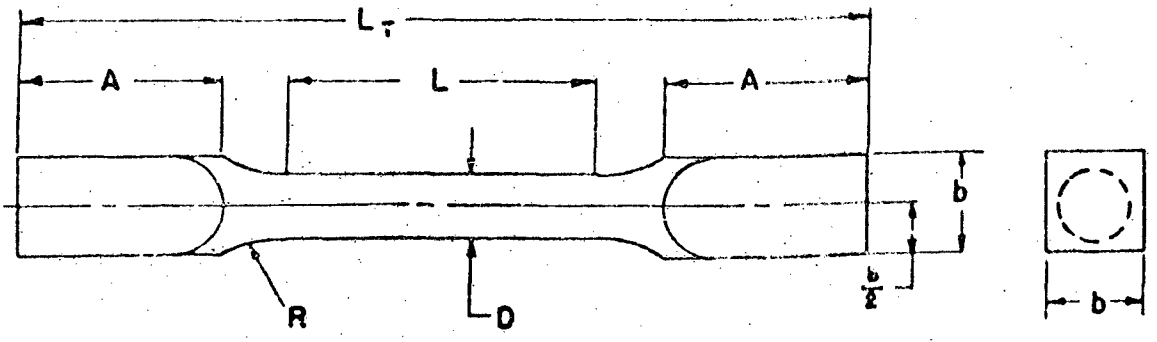

$\frac{L}{D} = 4.50$

Specimen Size	D	L	A	R	L_T	b
1	0.250	1.250	$\frac{3}{4}$	$\frac{1}{2}$	$3\frac{1}{8}$	$\frac{3}{8}$
5	1.250	5.625	$3\frac{3}{4}$	$2\frac{1}{2}$	$15\frac{5}{8}$	$1\frac{7}{8}$

Dimensions in inches

FIGURE 10. SIZE-EFFECT TORSION SPECIMENS

A-4898

specimens, the No. 5-size torsion specimen was 5 times the size of the No. 1-size torsion specimen, a volume ratio of 125.

These specimens, like the other size-effect specimens, were cast in Lucite molds. The procedures for casting and curing these specimens were the same as those used for the size-effect compression specimens. All of the torsion tests were conducted on the 14th day after casting.

The procedures used in conducting the size-effect torsion tests are given in a later section of this report.

Results. In the calculation of the torsion strengths, the standard elastic formula was used, that is:

$$\sigma_T = \frac{16M_t}{\pi D^3} \qquad (1)$$

where

σ_T = torsion strength, psi,

M_t = applied moment at fracture, inch-pound,

D = diameter of gage section, inches.

The elastic data obtained from the No. 5-size torsion specimens of Hydrostone plaster are given below:

Specimen No.	Modulus of Rigidity, 10^6 psi (Average of 3 Determinations)
H50S - 11	0.810
H50S - 12	0.799
H50S - 13	0.835
H50S - 14	0.863
H50S - 15	0.845
Mean	0.830 ± 0.026

If these data are used to determine the modulus of elasticity, E, from the relation

$$E = 2(1+\nu)G, \qquad (2)$$

where G is the modulus of rigidity and ν is Poisson's ratio, and a typical value of $\nu = 0.250$ is used, E is found to have a value of 2.08×10^6 psi. This value is somewhat low when compared with values of E determined from other size-effect tests. This discrepancy was considered to be due to a low experimental value for the modulus of rigidity, G. Although the value of 2.08×10^6 psi for E is reasonable and of the correct order of magnitude, more data on the modulus of rigidity would be required before the relation between the two moduli could be clarified completely.

The fracture data obtained from the No. 1-size torsion specimens are given in Table 8 and the fracture data for the No. 5-size torsion specimens are given in Table 9.

These data indicate that both the strength and the standard deviation decrease with an increase in size. These data show a decrease in strength of approximately 30 per cent with a fivefold increase in size. This effect of size on strength and standard deviation agreed qualitatively with that predicted by the mechanistic theories of strength. The quantitative significance of these data is discussed later in this report.

In all cases, these specimens, No. 1 size and No. 5 size alike, fractured in a brittle manner; that is, normal to the maximum tensile stress in the body. These specimens fractured on a helical surface oriented at 45 degrees to the axis of the specimen (this type of fracture surface is typical of brittle materials). In almost every case, fracture appeared to initiate at or very near the outside surface. This served as another indication that conditions at the surface of bodies of this material may influence fracture.

Summary of Size-Effect Data on Hydrostone Plaster

Table 10 contains a summary of all the elastic data obtained from plaster specimens as a part of the program to determine the effect of size on the fracture of brittle materials. These data indicate that there is no significant effect of size on modulus in tension. The bend and compression data appear to indicate such an effect; however, the significance of the variation of modulus with size cannot be resolved at this stage of the investigation.

Table 11 contains a summary of all the fracture-strength data obtained from the plaster size-effect specimens. These data indicated that an effect of size on the strength of Hydrostone plaster does exist. In turn, this effect agrees qualitatively with that predicted by the mechanistic theories of strength; that is, the strength and the standard deviation of the strength decreased with an increase in size. This decrease in strength was of the order of 30 per cent for a fivefold increase in size.

TABLE 8. FRACTURE DATA FROM NO. 1-SIZE PLASTER TORSION SPECIMENS

Specimen No.	Strength, psi
H10S-2	1605
H10S-3	1540
H10S-5	1465
H10S-8	2460(1)
H10S-9	1600
H10S-10	1385
H10S-12	1490
H10S-14	1375
H10S-18	1755
H10S-19	1740
H10S-20	1340
H10S-21	1580
H10S-22	1725
H10S-23	1715
H10S-24	985
H10S-25	1590
H10S-27	1440
H10S-33	1640
H10S-35	1595
H10S-37	1480
H10S-38	1440
H10S-39	1340
H10S-40	1635
H10S-41	1895
H10S-42	2035
H10S-43	1805
H10S-44	1530
H10S-45	1560
H10S-46	1160
H10S-47	1500
H10S-48	1620
H10S-50	1260
Mean Value	1545 ± 65
Standard Deviation	210

(1) Rejected from computation of mean.

TABLE 9. FRACTURE DATA FROM NO. 5-SIZE PLASTER TORSION SPECIMENS

Specimen Number	Strength, psi	Specimen Number	Strength, psi
H50S-1	1195	H50S-36	1375
H50S-3	1010	H50S-42	1260
H50S-4	1005	H50S-43	1070
H50S-5	880	H50S-44	1090
H50S-7	970	H50S-46	955
H50S-9	1190	H50S-47	935
H50S-11	740	H50S-48	1050
H50S-12	970	H50S-51	1285
H50S-13	915	H50S-52	1310
H50S-14	940	H50S-53	1215
H50S-15	1050	H50S-54	1280
H50S-16	680	H50S-55	1160
H50S-17	840	H50S-58	1380
H50S-22	840	H50S-59	1205
H50S-25	1240	H50S-60	1365
H50S-27	1250	H50S-61	1220
H50S-29	1175	H50S-62	1110
H50S-32	1310	H50S-63	1115
H50S-35	1600		
		Mean	1115 ± 55
		Standard Deviation	200

TABLE 10 CUMULATIVE ELASTIC DATA FROM PLASTER SIZE-EFFECT SPECIMENS

Specimen	Property	Mean Value	Standard Deviation(1)	Probable Error (±)(1)	Number of Specimens
Small tension (No. 1 size)	Modulus of elasticity, 10^6 psi	2.40	0.13	0.05	22
	Poisson's ratio	0.258	0.041	0.037	6
Large tension (No. 4 size)	Modulus of elasticity, 10^6 psi	2.39	0.11	0.09	22
	Poisson's ratio	0.240	0.020	0.018	6
Small torison (No. 1 size)	Modulus of rigidity, 10^5 psi	---	---	---	--
Large torsion (No. 5 size)	Modulus of rigidity, 10^6 psi	0.830	0.026	0.028	5
Small bend (No. 1 size)	Tension modulus of elasticity, 10^6 psi	2.51	0.15	0.11	8
	Compression modulus of elasticity, 10^6 psi	2.53	0.20	0.14	8
Large Bend (No. 5 size)	Tension modulus of elasticity, 10^6 psi	2.39	0.10	0.05	13
	Compression modulus of elasticity, 10^6 psi	2.30	0.13	0.07	13
	Poisson's ratio	0.240	0.011	0.010	6
Small compression (No. 1 size)	Modulus of elasticity, 10^6 psi	2.45	0.05	0.02	14
	Poisson's ratio	0.252	0.038	0.034	7
Large Compression (No. 5 size)	Modulus of elasticity, 10^6 psi	2.33	0.05	0.02	14
	Poisson's ratio	0.248	0.008	0.004	14

(1) See Appendix II.

TABLE 11. CUMULATIVE FRACTURE DATA FROM PLASTER SIZE-EFFECT SPECIMENS

Specimen	Condition	Strength, psi	Standard Deviation, (1) psi	Probable Error, (1) psi	Number of Specimens
Small tension (No. 1 size)	Gage-free	1195	175	60	25
	Combined(2)	1245	135	35	46
Large tension (No. 4 size)	Gage-free	915	135	55	19
	Combined	875	150	55	25
Small compression (No. 1 size)	With gages	7720	600	430	9
Large compression (No. 5 size)	With gages	7130	940	850	6
Small torsion (No. 1 size)	Gage-free	1545	210	65	32
Large torsion (No. 5 size)	Gage-free	1115	200	55	37
Small bend (No. 1 size)	Gage-free	1845	210	60	36
	Combined	1830	210	55	43
Large bend (No. 5 size)	Gage-free	1270	205	65	29
	Combined	1250	215	55	42

(1) See Appendix II.

(2) Includes specimens with and without strain gages.

Correlation of Size-Effect Data on Plaster With Weibull's Statistical Theory of Strength

One of the intermediate objectives of this investigation has been to determine whether any of the existing theories of strength apply to the fracture of ceramic materials. It was pointed out previously in this report that Weibull's statistical theory of strength[18, 19] predicts an effect of size on strength. Since the size-effect tests on plaster indicated a size effect, an attempt was made during this period to determine the applicability of Weibull's theory.

Weibull developed expressions relating the size of a body and its statistical strength in the stress states of tension, bending, and torsion. These expressions were used to determine the constants for Weibull's theory and to compare the observed strengths with those predicted by his theory. In addition, Weibull developed expressions purporting to relate the strengths in the various stress states. The significance of the effect of stress state on fracture strength is discussed in a later section of this report. The specific equations used to obtain the predicted strengths appear in Appendix III of this report, along with a detailed discussion of Weibull's theory.

Table 12 gives the size-effect data and the value of the material constant, m, determined from each stress state. In addition to these data, the bend data reported in Table 4 of WADC Technical Report 52-67 were analyzed by the method described in Appendix III. An average value of $M = 12$ was determined from these bend data as compared to a value of $m = 12.9$ in Table 12. The data in Table 12 indicate an approximate average value of $m = 14$. The scatter in the values of m is quite large and may be significant of the consistency of the size-effect data.

It must be pointed out that analyses of initial portions of these data indicated a value of m of approximately 12. Due to the complexity of these determinations, it was found expedient to use a value of $m = 12$ in the correlations and calculations from Weibull's theory which appear in this report.

Mathematical methods have been used throughout this report in the application of Weibull's theory to the fracture data on Hydrostone. Weibull's statistical constants have been determined from mathematical treatments of the data; however, Weibull has developed graphical methods for the determination of these constants. In regard to this problem, he points out[20]:

"For determining the most probable values of the distribution constants for a given test series either geometrical or arithmetical methods may be used. An advantage of the former is that they immediately indicate statistical anomalies in the series. Therefore, it seems to be advisable that the observations should first be treated by graphic methods, while the arithmetical methods should not be used unless the results of the graphical treatment call for their application."

TABLE 12. MATERIAL CONSTANTS FOR HYDROSTONE PLASTER

Stress State	Specimen Size	Average Volume, $in.^3$	Mean Strength, psi	Standard Deviation of Mean Strength, psi	Material Constant, (1) m
Tension	1	0.0633	1195	175	15.6
	4	4.10	915	135	
Torsion	1	0.0633	1545	210	14.4
	5	6.92	1115	200	
Bending	1	0.0190	1845	210	12.9
	5	2.33	1270	205	

(1) See Appendix III.

In the analysis of the size-effect data of this investigation, an attempt was made to apply the graphical methods to which Weibull refers; however, difficulty was experienced in these initial attempts. Additional, more refined methods are available at this time for the determination of these distribution constants, but these new methods have not been attempted.

It is also very important to point out that the distribution function used in this study of Hydrostone plaster was a greatly simplified one, and that more refined distribution functions are available[18, 21].

Table 13 gives a comparison of the observed strengths and the strengths predicted from Weibull's theory for the large-size specimen. The predicted values were calculated to show the order of variation resulting from the use of different values of m.

In addition to the analyses of strength data, the standard-deviation data obtained from these size-effect tests were analyzed and compared with deviations predicted from Weibull's theory. Expressions were developed relating specimen size and standard deviation in particular stress states. The specific equations used in obtaining the predicted deviations appear in Appendix III. The analysis of the standard-deviation data from the Hydrostone size-effect specimens is given in Table 14. It can be seen from Table 14 that the experimental deviation for the specimens treated was not in good agreement with the deviations predicted from Weibull's theory. The values

TABLE 13. COMPARISON OF EXPERIMENTAL STRENGTHS OF LARGE PLASTER SIZE-EFFECT SPECIMENS WITH STRENGTHS PREDICTED FROM WEIBULL'S THEORY

Specimen	Experimental Strength, psi	Predicted Strength, psi[1]	
		m = 12	m = 14
Large torsion	1115	1045	1105
Large tension	915	845	885
Large bend	1270	1235	1310

(1) See Appendix III, Equations (47), (48), and (49).

TABLE 14. COMPARISON OF EXPERIMENTAL STANDARD DEVIATIONS OF STRENGTH OF LARGE PLASTER SIZE-EFFECT SPECIMENS WITH DEVIATIONS PREDICTED FROM WEIBULL'S THEORY

Specimen	Experimental Standard Deviation, psi	Predicted Standard Deviation, psi[1]	
		m = 12	m = 14
Large torsion	200	140	150
Large tension	135	125	130
Large bend	205	140	150

(1) See Appendix III, Equations (66), (71), and (77).

of the observed standard deviations can be expected to change as the number of specimens tested is increased. As the number of tests in each group becomes quite large, the observed standard deviation, as a property, becomes more reliable. It is important to note here that the standard deviation of the strength of a series of specimens is as much a property of the series as the mean strength. It has been pointed out in another section of this report that the second moment of the distribution about the mean is equivalent to the square of the standard deviation. Also, it is important to note that the third and fourth moments of the distribution are also properties of a set of specimens, and that, if a complete statistical analysis is to be made of the fracture of a material, each of the pertinent statistical properties must be studied.

Weibull also developed expressions for predicting the effects of various stress states upon the standard deviation of the strength. The correlations of the size-effect data on Hydrostone with these predictions appear in a later section of this report.

The results of these analyses of size-effect data indicate that it may be possible to predict the effect of size on the strength of Hydrostone plaster by using Weibull's theory.

Size-Effect Experiments on Porcelain

It will be recalled that the size-effect tests on Hydrostone-plaster compression specimens raised an important question: Do ceramic bodies of different sizes exhibit different moduli of elasticity? The data from these compression tests on plaster (see Table 1) indicated that, in compression, small specimens of Hydrostone have a higher modulus of elasticity than large specimens. The mechanistic theories of fracture do predict a variation in fracture strength similar to that observed here, but they anticipate no decrease in elastic modulus with size. It is possible that this variation resulted from differences in thermal histories, or, on the other hand, from a true size dependence of modulus.

In an effort to determine whether this variation of modulus was characteristic of ceramics other than plaster, a series of tests was conducted on compression specimens of porcelain, of the same design and dimensions as the size-effect compression specimens of plaster (see Figure 1). These porcelain specimens were fabricated by the Champion Spark Plug Company of Detroit. The preparation and the testing of these specimens were the same as the preparation and testing of the No. 1- and No. 5-size plaster compression specimens. The moduli and Poisson's-ratio data were calculated in the same manner, that is, using the techniques outlined in Appendix I.

Table 15 gives the results of these tests. Only elastic data are given on No. 1-size and No. 5-size specimens. These specimens were not fractured.

The data in Table 15 reveal only a very small variation in elastic modulus between the two sizes of specimens. Although this difference in moduli was in the same direction as the variation observed in Hydrostone plaster, the difference for porcelain was of such a small magnitude that no definite statement is justified as to whether the variation of the compression modulus of Hydrostone was due to a true size effect or due to a material variable. It is interesting to note, however, that the data for the Hydrostone size-effect bend specimens (see Tables 5 and 6) exhibit the same effect of size on modulus. At the same time, the Hydrostone size-effect tension specimens exhibited practically no variation in modulus with size. Together, these observations would seem to indicate that a real variation of elastic modulus with the size of ceramic bodies does not exist, or is of such a magnitude that it cannot be discerned with present techniques.

TABLE 15. ELASTIC DATA FROM CHAMPION PORCELAIN SIZE-EFFECT COMPRESSION SPECIMENS

Size No. 1 (Small)			Size No. 5 (Large)		
Specimen No.	Modulus of Elasticity, 10^6 psi	Poisson's Ratio	Specimen No.	Modulus of Elasticity, 10^6 psi	Poisson's Ratio
C10C-1	40.7	--	C50C-1	40.4	0.237
C10C-2	40.7	--	C50C-2	40.7	0.236
C10C-3	41.5	--	C50C-3	40.6	0.232
C10C-4	42.9*	0.244	C50C-4	40.0	0.239
C10C-5	40.7	0.215	C50C-5	40.6	0.230
C10C-6	40.6	--	C50C-6	40.3	0.234
C10C-7	40.0	--	C50C-7	40.0	0.238
C10C-8	40.5	--	C50C-8	40.5	0.240
C10C-9	41.4	--	C50C-9	40.5	0.251*
Mean Value	40.8 ± 0.3	0.230	Mean Value	40.4 ± 0.2	0.236 ± 0.002
Std. Deviation	0.5	--	Std. Deviation	0.3	0.003

*Rejected from computation of mean.

THE EFFECT OF STRESS STATE ON MECHANICAL PROPERTIES

It has long been observed that the state of stress in a body has an influence on its fracture. For example, the compression strength (defined by the ordinary compression test) of a brittle material is much higher than its tensile strength, sometimes being of the order of eight times the tensile strength. In the present investigation, the compression strength of Hydrostone plaster was found to be about six times greater than the tensile strength. In the case of cast iron, which is not truly a brittle material, even the stress-strain curves in tension and compression differ. Another striking example is the effect of high hydrostatic compression stresses on the behavior of brittle materials, illustrated by the fact that under the tremendous pressures in the earth's crust, igneous and sedimentary rocks which are quite brittle in ordinary compression have been caused to flow like a viscous fluid.

How well, then, do the phenomenological and mechanistic theories of strength predict the behavior of brittle materials under varying states of stress?

It was pointed out earlier that the phenomenological theories of strength belong to the classical group of theories that predict a unique fracture strength for a material. The phenomenological theory most commonly applied to brittle materials, the maximum-tensile-stress theory, postulates that fracture will occur when the maximum tensile stress in a body reaches a certain value. This theory has been found to agree qualitatively with fracture data on brittle materials at normal temperatures and pressures. However, this theory predicts that the fracture of a brittle material is independent of the other two principal stresses. This would mean that the strength of brittle materials should be the same in triaxial tension as in uniaxial tension, which is contrary to observation. At the same time, this theory in no way predicts the behavior observed at high hydrostatic pressures. On the other hand, many of the phenomenological theories, such as the octahedral-shear-stress theory, the effective-stress theory, the distortion-energy theory, the maximum-shear-stress theory, and the maximum-strain-energy theory, are not valid for truly brittle materials, since they propose criteria which are more valid for flow than for fracture. This becomes obvious when it is noted that each of these theories predicts that a material will not fail in triaxial tension. To these limitations of the phenomenological theories must be added the limitation that these theories predict that the strength of a body is that of its elements, regardless of its size.

The mechanistic theories are typified best by Griffith's theory (22) and by the statistical theories of strength. According to Griffith's theory, the strength of a body is equal to the microscopic stress in a very small volume at the instant that a critical crack in this volume begins to propagate. The effects of other cracks and of the distribution of these cracks in a body are neglected by Griffith.

It has been pointed out that the phenomenological theories consider that fracture will occur when any one element in a body reaches a critical state of stress, and Griffith makes this same assumption. In these theories, the important point is that fracture is considered to occur when this critical element fails, and that the contribution of other elements is considered to be negligible. In the case of the statistical theories of strength, however, consideration is given to every element in a body and its contribution or possible contribution to fracture is taken into account.

Let us compare the maximum-tensile-stress theory, for example, with Weibull's statistical theory of strength. The maximum-tensile-stress theory states that fracture will occur when the tensile stress on some plane of an element reaches a critical value. Weibull's theory, however, proposes that there is a certain probability of fracture associated with every unit volume in a body, and that this probability is a function of the state of stress in the element. What is even more important is that the probability of fracture of a unit volume is not only the probability of fracture associated with one plane of the element, but the probability of fracture associated with all planes in the element. Hence, the probability of fracture at a point in a body becomes a function of the individual probabilities of fracture on every plane through that point on which the normal stress is tensile. This reasoning can be extended to give a probability of fracture for the entire body, taking into consideration the state of stress at every point in the body. If the relation between the tensile stress in an element and the probability of fracture of that element is assumed, then the strength of the element, as the most probable stress at fracture, can be predicted. It is important to point out however, that Weibull's theory assumes that fracture will take place under the action of tensile stresses, that is, in a normal brittle manner. Furthermore, Weibull's theory postulates that the fracture of a body occurs simultaneously with the fracture of any of its elements.

Nevertheless, Weibull's theory predicts a distinct effect of stress state on fracture phenomena. It is true that Griffith's theory and the phenomenological theories also predict an effect of stress state on fracture; however, it appears at this point that more can be gained from a study of Weibull's theory.

In light of the above, special consideration was given during this period to the correlation of fracture data with Weibull's statistical theory of strength. Fracture data obtained from size-effect tests on plaster in the simple stress states of tension, torsion, and bending were correlated with Weibull's theory. In addition, the results of tests to determine the effects of biaxial states of stress on the fracture of plaster have been reported.

Correlation of Tension, Torsion, and Bend Data on Plaster With Weibull's Theory

One of the objectives of this investigation is to determine whether any of the existing theories of strength apply to ceramic materials. Since the tests on plaster indicated a size effect, and since Weibull's theory predicts such an effect, an attempt was made to determine the applicability of Weibull's theory to stress-state data. Weibull developed expressions purporting to relate strengths in tension, bending, and torsion. In addition, he has developed expressions relating specimen size and strength in a particular stress state. Hence, these expressions could be used to predict the strength of Hydrostone plaster in each of these stress states and to compare the theoretical strengths with the observed strengths.

The general principles of Weibull's theory were outlined in detail in WADC Technical Report No. 52-67. These principles were used to develop expressions for predicting the effects of size and stress state on the strength of Hydrostone plaster. Additional expressions were developed for predicting the standard deviations of the strengths of plaster. The specific expressions used for these correlations are outlined in Appendix III of this report.

The general procedure was to determine the material constant, m, for Hydrostone plaster from the size-effect data from one stress state and then to use this value of m in the appropriate equations to predict the strength of Hydrostone in the other stress states. Table 16 gives the size-effect data and the value of the material constant, m, determined from each stress state. The volumes reported in Table 16 are averages for the specimens tested.

Weibull also developed expressions relating the standard deviations of the strengths in the various stress states. As a part of the program to correlate fracture data, these expressions were used to analyze the plaster size-effect data. The results of the comparison of the standard deviations with those predicted from Weibull's theory are given in Table 17.

The results in Table 16 show a fair agreement between the experimental and the predicted strengths. The analysis indicates, however, that more size-effect data (particularly on gage-free specimens) may be required if definite conclusions are to be drawn as to the applicability of Weibull's theory to the fracture of Hydrostone plaster. An extension of the program to some other ceramic material (contemplated for the following contract period) would furnish valuable insight as to the applicability of Weibull's theory to the fracture of brittle ceramics.

The results in Table 17 of the comparison of experimental deviations with deviations predicted by Weibull's theory reveal a poor correlation. This effect may have resulted, however, from the relatively small number of specimens tested. Standard deviation, as a property, appears to be much

TABLE 16. COMPARISON OF EXPERIMENTAL STRENGTHS OF PLASTER SIZE-EFFECT SPECIMENS WITH STRENGTHS PREDICTED FROM WEIBULL'S THEORY

Based on Large Torsion Strength and m = 12

Specimen	Predicted Strength,[1] psi	Experimental Strength, psi	Deviation, %
Small tension	1125	1195	5.9
Large tension	960	915	4.9
Small torsion	1650	1545	6.8
Large torsion	--	1115	--
Small bend	1975	1845	7.0
Large bend	1320	1270	3.9

(1) See Appendix III, Equations (50), (51), and (52).

TABLE 17. COMPARISON OF EXPERIMENTAL STANDARD DEVIATIONS OF THE STRENGTH OF PLASTER SIZE-EFFECT SPECIMENS WITH STANDARD DEVIATIONS PREDICTED FROM WEIBULL'S THEORY

Based on Deviation of Large Torsion Specimen and m = 12

Specimen[2]	Experimental Standard Deviation, psi	Predicted Standard Deviation, psi[1]	Deviation, %
Small tension (25)	175	200	14
Large tension (19)	135	170	26
Small torsion (32)	210	295	41
Large torsion (37)	200	--	--
Small bend (36)	210	355	69
Large bend (29)	205	235	15

(1) See Appendix III, Equations (77), (78), and (79).

(2) Number in parentheses indicates number of specimens tested.

more sensitive to the size of the sample than is the mean. Therefore, a far larger number of tests may be required to obtain suitable deviation data than to obtain reliable strength data.

These correlations of strength and standard-deviation data do indicate that Weibull's statistical theory of strength may offer a reliable means of predicting the statistical strength of a ceramic body. Neither Weibull's theory nor any other theory, however, offers any way of predicting the strength of a single ceramic body. Still, it may be possible, using Weibull's theory, to predict a threshold strength for a ceramic body below which this body will not fail (negligible probability of fracture). However, this threshold strength may prove to be too small to be of practical use to the ceramic engineer.

The Effect of Biaxial Stresses on Mechanical Properties

In the past, this research has been limited to a study of the simple stress states of uniaxial tension and compression and to the states of bending and torsion. It is obvious, however, that limiting the investigation to the study of tension, compression, bending, and torsion states would be unrealistic, as the stress states commonly encountered in practical problems are combinations of these simpler states. If a practical solution is to be found to the problem of the effect of stress state on the fracture of brittle materials, the effects of biaxial stresses should be studied.

A biaxial stress state implies the consideration of a two-dimensional stress system. Figure 11 illustrates a general two-dimensional stress system acting on a small element of material. σ_x and σ_y are normal stresses, which may be either tensile or compressive stresses. τ_{xy} is a shear stress. Figure 11 represents the general stress state in a body subjected to biaxial stresses corresponding to a random orientation of the element in the body. In every case of biaxial loading, however, there is one particular orientation of the element for which the shear stress is zero. This condition occurs when the x and y axes coincide with the principal axes. The principal axes correspond to the directions of the maximum and minimum normal stresses on an element. This orientation is shown in Figure 12. σ_1 and σ_2, the principal stresses, may be either negative or positive, but σ_1 is always algebraically greater than or equal to σ_2.

From the above discussion, it can be seen that any biaxial stress state can be defined completely in terms of the two principal stresses. Furthermore, the type or character of the biaxial state can be expressed in terms of the ratio σ_2/σ_1 of the principal stresses. For example, a tension test would be represented by a ratio $\sigma_2/\sigma_1 = 0$ and a torsion test by a ratio $\sigma_2/\sigma_1 = -1$.

Tests of the biaxial state in which the ratio of the principal stresses is constant throughout the test are designated as constant-stress-ratio tests.

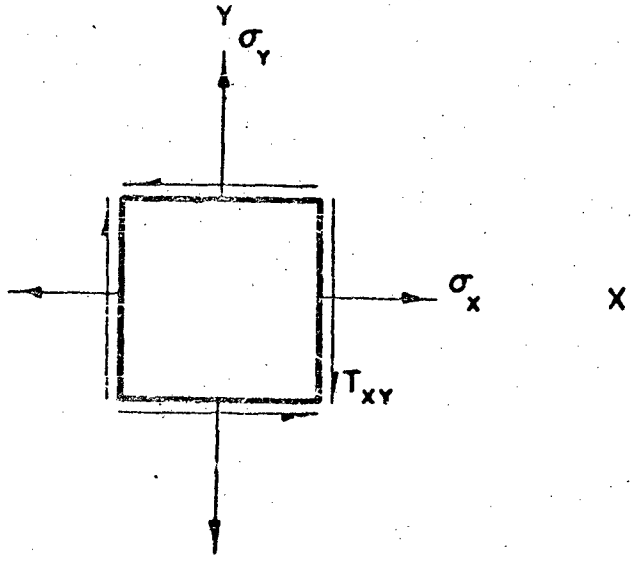

FIGURE 11. GENERAL BIAXIAL STRESS STATE

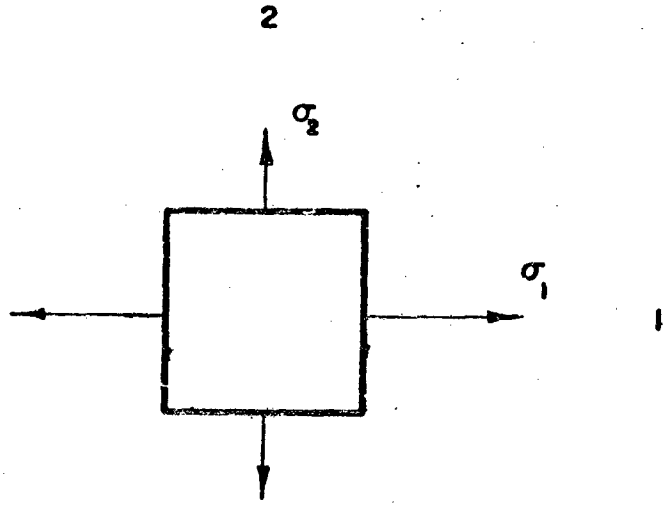

FIGURE 12 ELEMENT SHOWING PRINCIPAL STRESSES CORRESPONDING TO GENERAL BIAXIAL STRESS STATE

A-3666

Essentially, this means that the stress ratio in a body does not change as the body is loaded to fracture. In the past, the method used most commonly to investigate the effect of biaxial stresses has been the constant-stress-ratio test.

In this investigation, the objective is to determine the effects of various biaxial stress states (each represented by a particular stress ratio) on the fracture strength of a brittle material. If it were assumed that biaxial stresses do affect the fracture strength of a material, then it would follow that there is a unique fracture strength for each stress ratio. This concept of a variation of fracture strength with stress ratio is exemplified by the hypothetical curve shown in Figure 13.

In Figure 13, the axes are designated as σ_2/σ_f and σ_1/σ_f, where σ_f has been chosen as the fracture strength in simple tension (for this hypothetical material). Points C and D represent the fracture strength in simple tension. At Point C, for example, σ_2 is zero and $\sigma_1 = \sigma_f$, $\sigma_1/\sigma_f = 1.0$; at Point D, a similar condition exists. A constant-stress-ratio test can be represented by a straight line extending outward from the origin, O. A biaxial test for which $\sigma_2/\sigma_1 = 1/3$ is represented by the line OB. Every point on this line represents a stress condition at some time during the test. As σ_2 and σ_1 are increased, the point representing the stress state moves outward along OB. When σ_2 and σ_1 reach the magnitude represented by Point B, the specimen fractures. Thus, it can be seen that the curve shown in Figure 13 represents the fracture strength for all possible biaxial states of stress.

As a part of the program for studying the effect of stress state on the fracture of ceramic materials, Weibull's theory was analyzed and expressions developed for predicting the fracture of Hydrostone plaster under combined stresses. The results of this analysis of Weibull's theory are presented in Figure 14 in the form of a curve of the type shown in Figure 13. It can be seen from Figure 14 that Weibull's theory predicts a steady increase in fracture strength (value of σ_1 at fracture) with negatively increasing values of σ_2. Figure 14 also shows that, in the region of biaxial tension (σ_2 and σ_1 both tensile), the fracture strength is lower than the strength in uniaxial tension. It should also be noted from Figure 14 that Weibull's theory is quite similar to the maximum-tensile-stress theory, which predicts fracture when the maximum tensile stress in a body reaches the stress at fracture in tension. However, Figure 14 indicates that caution may be necessary in the use of the maximum-tensile-stress theory when both principal stresses are tensile stresses. It is important to note that the curve in Figure 14 is for a unit volume of uniformly stressed Hydrostone plaster ($m = 12$).

The methods used in the determination of Weibull's theory for biaxial stresses on Hydrostone are described in detail in Appendix III.

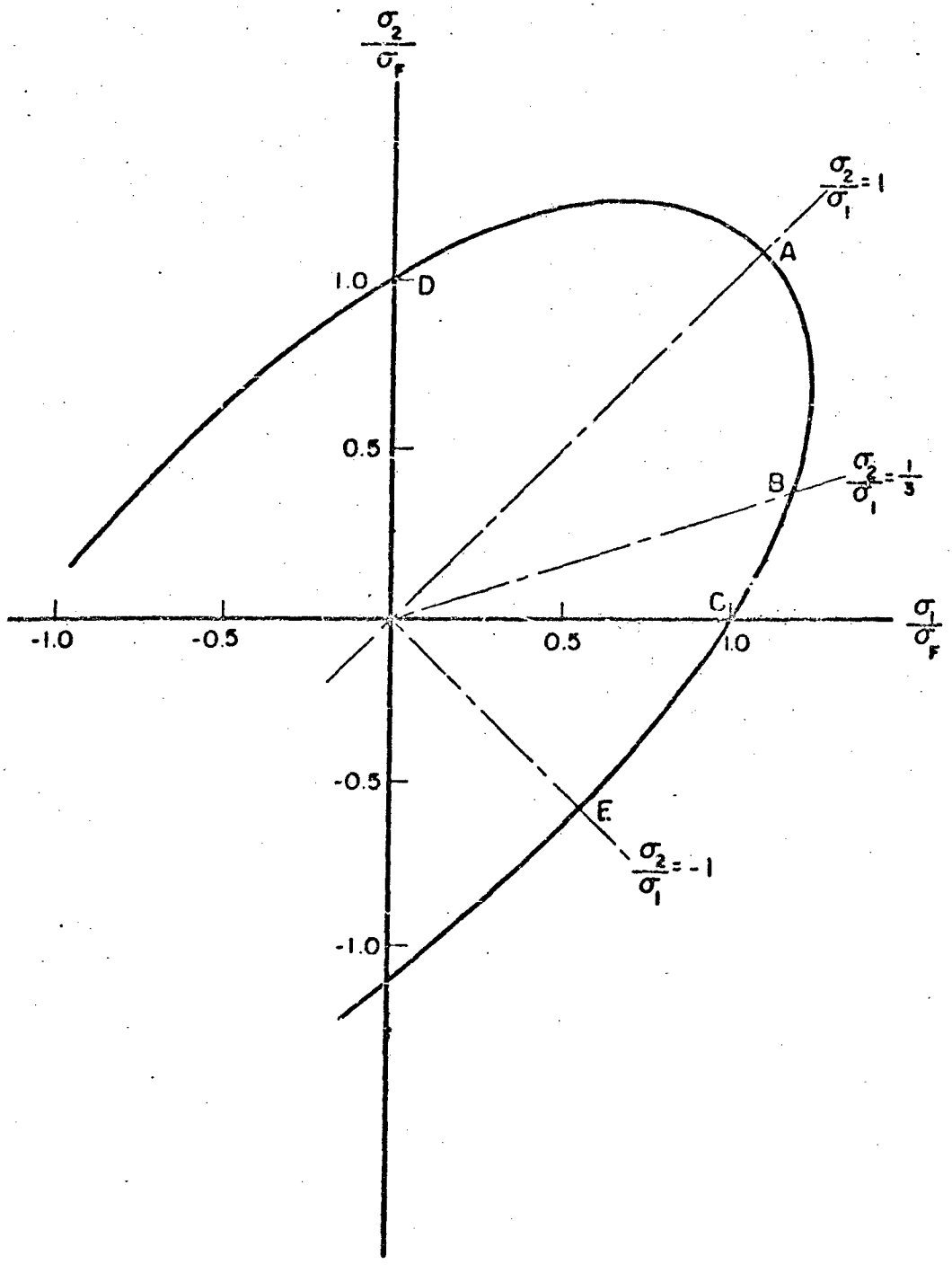

FIGURE 13. HYPOTHETICAL CURVE ILLUSTRATING VARIATION OF FRACTURE STRENGTH WITH PRINCIPAL STRESS RATIO

A-3856

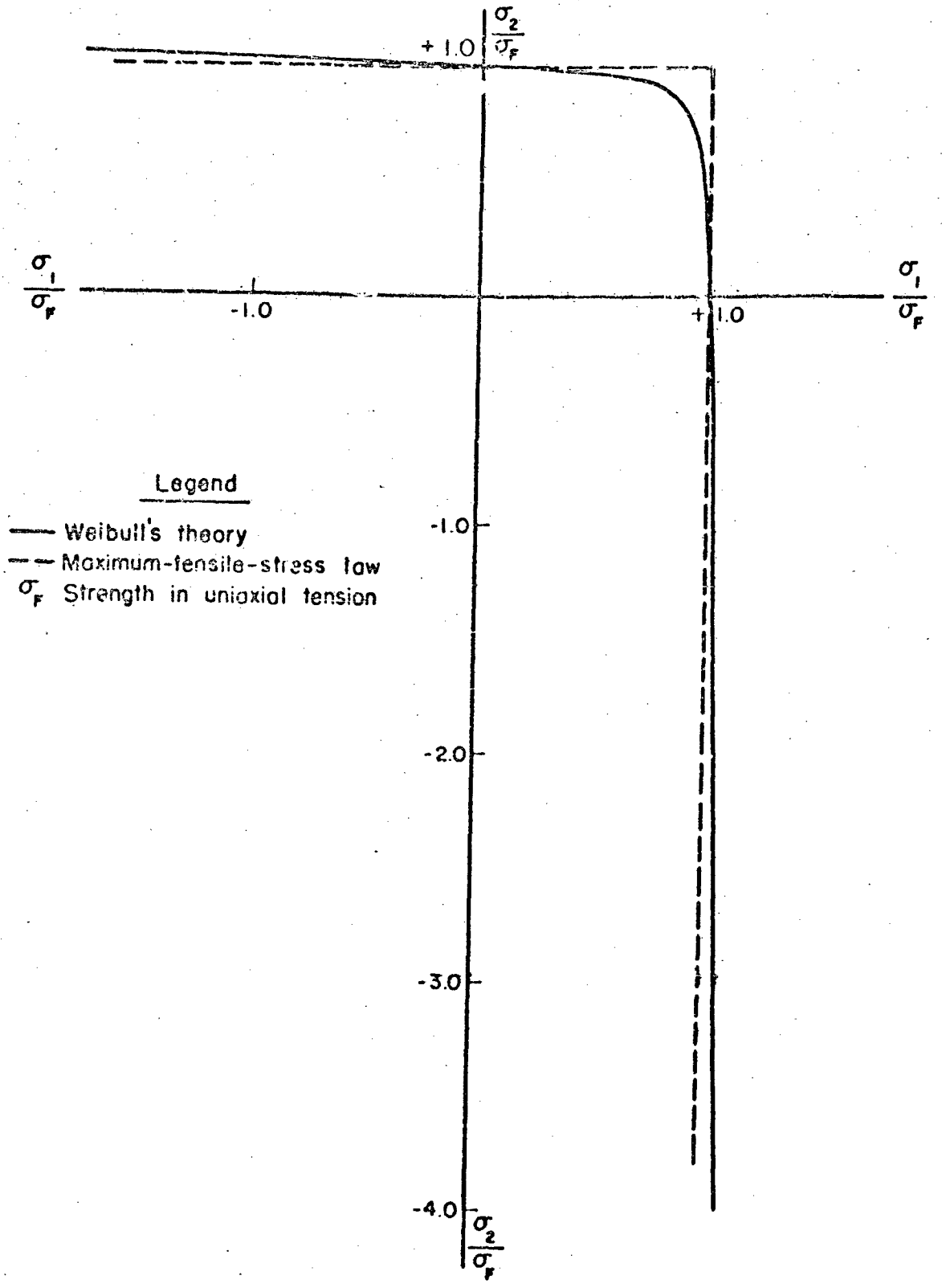

FIGURE 14. WEIBULL'S THEORY OF STRENGTH FOR BIAXIAL STRESSES FOR HYDROSTONE PLASTER (m=12)

A-3857

Combined-Stress Tests on Plaster

A program was set up during this period to study the effect of combined (biaxial) stresses on Hydrostone plaster. To accomplish this, a specimen was designed with which various biaxial stress states might be obtained. This specimen was a hollow cylinder which could be subjected to axial loading and internal pressure. This specimen and the system for loading are described in detail in a later section of this report (see "Development of Test Equipment"). This specimen (see Figure 15) was designed such that fracture data obtained could be analyzed using the theory of thick-walled cylinders. The wall of the specimen was of such thickness (when compared with its internal diameter) that the variation of stresses from the inner surface to the outer surface had to be considered.

In the initial tests conducted during this period, the specimen was subjected to internal pressure loading or to tension loading.

The procedures used in casting and curing these specimens were the same as those used in casting and curing the size-effect specimens of plaster. The plaster used for these specimens was the same as that used in the size-effect specimens.

The methods used in testing these specimens are described in detail in a later portion of this report.

Results

Data from the internal-pressure tests were analyzed using the elastic theory of thick-walled cylinders.[23] This theory indicates that the stresses at the inside surface are higher than those at the outside surface. According to this theory, the transverse stress σ_1, in the specimen is of the form:

$$\sigma_1 = \frac{r_i^2 p}{r_o^2 - r_i^2} \left(1 + \frac{r_o^2}{r^2}\right), \qquad (3)$$

where

r_i = radius of the inside surface,
r_o = radius of the outside surface,
p = internal pressure,
r = radius at which the stress is being determined.

From Equation (3), it can be seen that the transverse stress at the inside surface, σ_{1i}, is (when $r = r_i$):

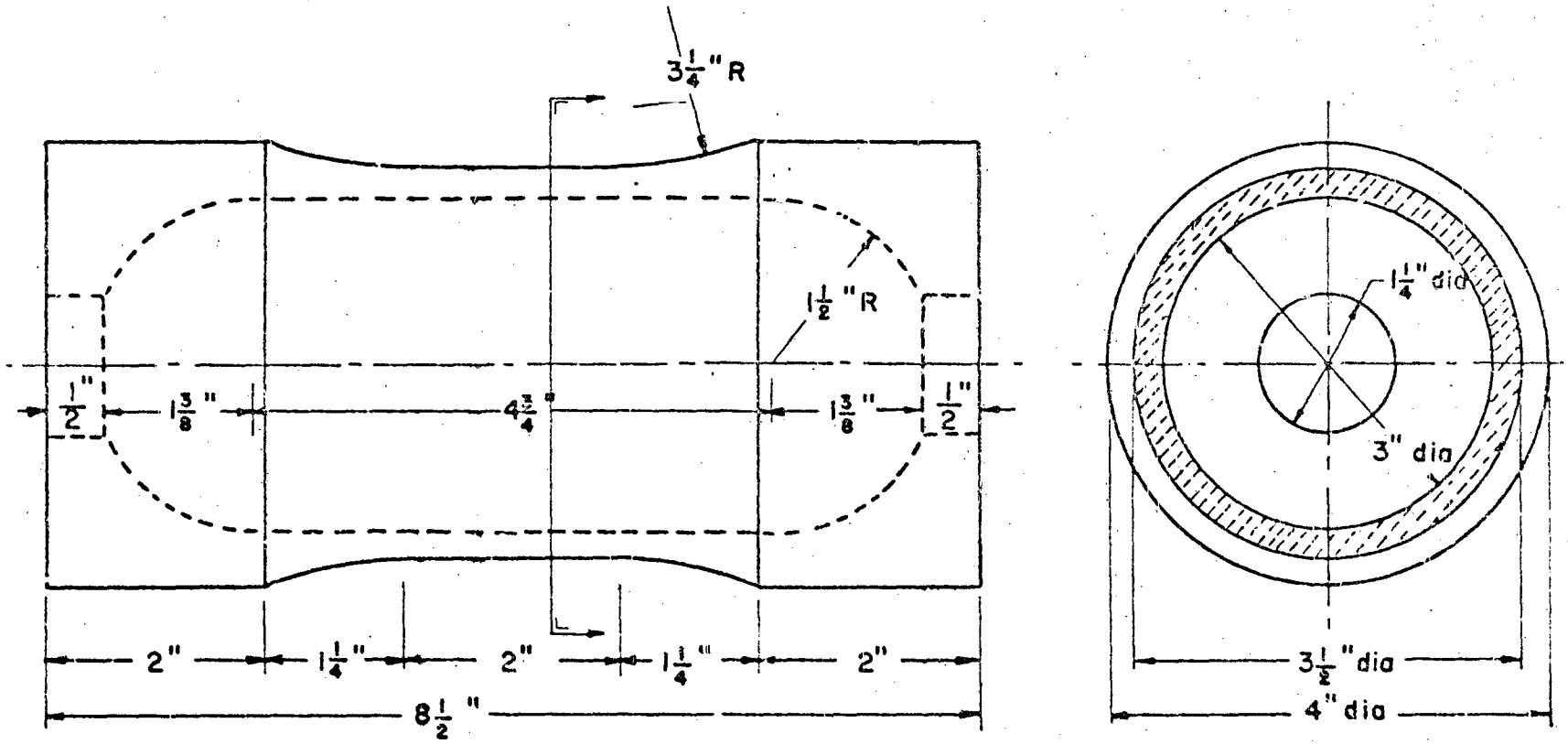

FIGURE 15. BIAXIAL TEST SPECIMEN

A-4693

$$\sigma_{1i} = \frac{r_o^2 + r_i^2}{r_o^2 - r_i^2} p \quad . \tag{4}$$

Then Equation (4) can be rewritten as:

$$\sigma_{1i} = \frac{D_o^2 + D_i^2}{D_o^2 - D_i^2} p \quad , \tag{5}$$

where D_o is the outside diameter and D_i is the inside diameter. Similarly, the transverse stress at the outside surface, σ_{1o} is:

$$\sigma_{1o} = \frac{2D_i^2}{D_o^2 - D_i^2} p \quad . \tag{6}$$

The internal pressure distributed over the ends of the inside of the specimen is assumed to produce a uniform axial stress, σ_2, of the form:

$$\sigma_2 = \frac{D_i^2}{D_o^2 - D_i^2} p \quad . \tag{7}$$

Furthermore, it should be noted that σ_2 and σ_1 are principal stresses. Since the elastic theory of thick-walled cylinders assumes that Hooke's law holds for the test material, the principal strains, ϵ_1 and ϵ_2, can be determined from Equations (8) and (9):

$$\epsilon_1 = \frac{1}{E}[\sigma_1 - \nu\sigma_2], \tag{8}$$

$$\epsilon_2 = \frac{1}{E}[\sigma_2 - \nu\sigma_1], \tag{9}$$

where $\epsilon_1 \geq \epsilon_2$, and

E = modulus of elasticity, psi,

ν = Poisson's ratio.

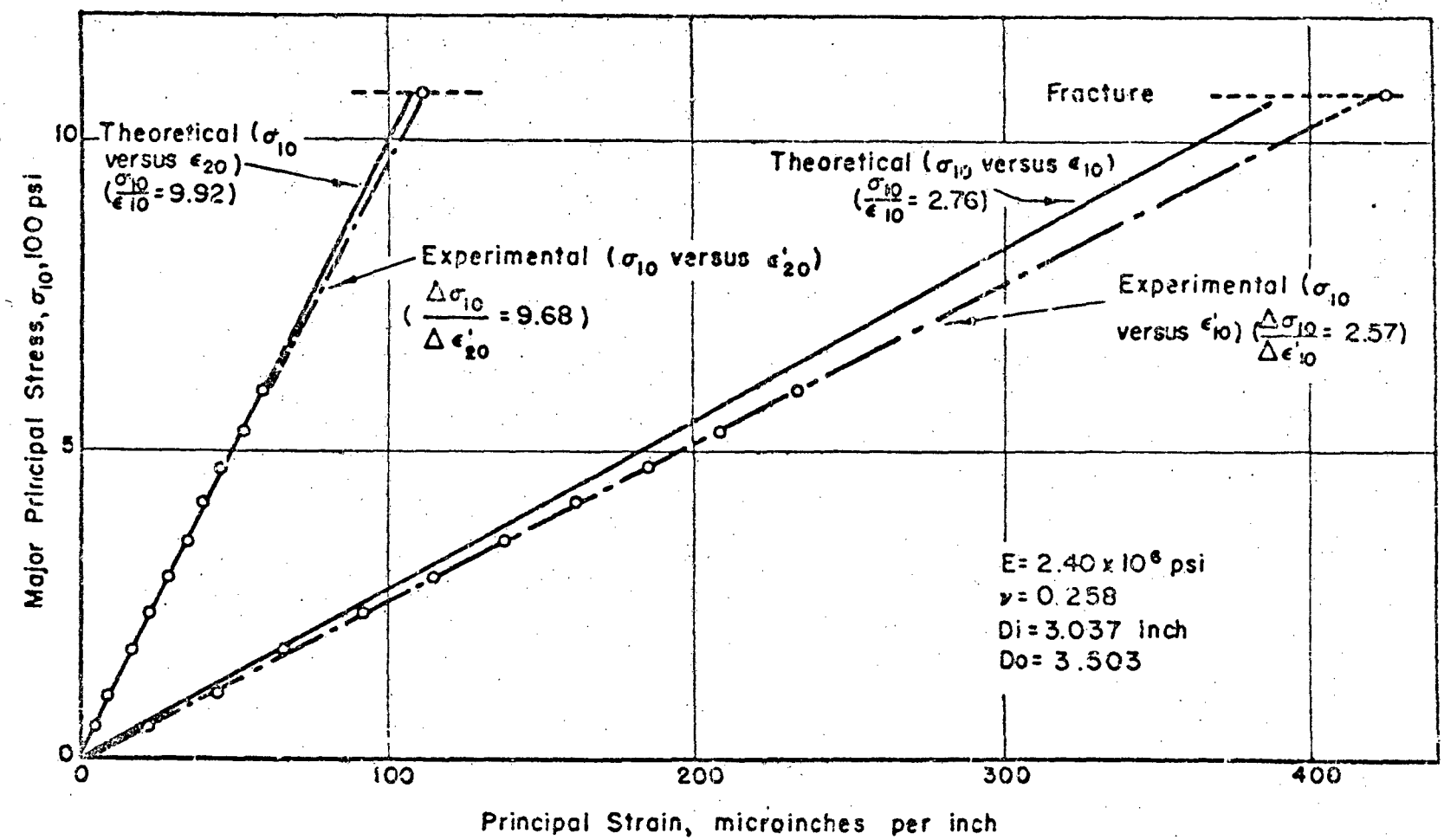

FIGURE 16. COMPARISON OF EXPERIMENTAL DATA FROM BIAXIAL SPECIMEN HOP-6 WITH DATA PREDICTED BY THE THEORY OF THICK-WALLED CYLINDERS

A- 4706

Then the principal strains on the outside surface of the specimen become:

$$\epsilon_{1o} = \frac{1}{E} [\sigma_{1o} - \nu\sigma_2], \tag{10}$$

$$\epsilon_{2o} = \frac{1}{E} [\sigma_2 - \nu\sigma_{1o}]. \tag{11}$$

To determine the applicability of the theory of thick-walled cylinders to these tests on the biaxial specimen, the theoretical strains, ϵ_{1o} and ϵ_{2o}, were compared with the observed values, ϵ'_{1o} and ϵ'_{2o}. The principal strains, ϵ'_{1o} and ϵ'_{2o}, in all instances were corrected for the effects of transverse sensitivity [see Equations (20) and (21) of Appendix I] by comparing the slopes, $\sigma_{1o}/\epsilon_{1o}$, of the theoretical curves of σ_{1o} versus ϵ_{1o} with the slopes, $\Delta\sigma_{1o}/\Delta\epsilon'_{1o}$, of the experimental curves of σ_{1o} versus ϵ'_{1o}. Similarly, the slopes, $\sigma_{1o}/\epsilon_{2o}$, of the theoretical curves of σ_{1o} versus ϵ_{2o} were compared with the slopes, $\Delta\sigma_{1o}/\Delta\epsilon'_{2o}$, of the experimental curves of σ_{1o} versus ϵ'_{2o}. The elastic constants, E and ν, determined for each specimen under tension loading were used to determine ϵ_{1o} and ϵ_{2o} from Equations (10) and (11). These experimental and theoretical curves are shown in Figure 16 for a typical biaxial stress specimen.

The theoretical and observed elastic data obtained from the biaxial stress specimens tested under internal pressure are given in Table 18. These data indicate a variation of approximately 5 per cent between the experimental and theoretical results. The reasonable agreement of these data with the predictions of the elastic theory of thick-walled cylinders was considered an indication that fracture data from this biaxial specimen could be analyzed from the point of view of thick-walled theory. It is significant, in these tests, that the experimental strains were consistently greater than the theoretical strains. The reason for this variation was not determined.

The principal stresses and the theoretical and experimental principal strains at the instant of fracture in these tests are given in Table 19. The principal stresses at fracture were calculated from Equations (5), (6), and (7). The theoretical principal strains, ϵ_{1o} and ϵ_{2o}, were calculated from Equations (10) and (11). The tangential stress, σ_{1i}, at the inside surface was the largest principal stress in the specimen and was taken as a nominal value of the strength of the specimen.

The data in Table 19 indicate fair agreement between theoretical and experimental fracture strains, considering the limited amount of data available.

The elastic and fracture data obtained from those biaxial specimens fractured in axial tension are given in Table 20. The strength obtained from

TABLE 18. ELASTIC DATA FROM BIAXIAL SPECIMENS SUBJECTED TO INTERNAL PRESSURE

Specimen No.	Modulus of Elasticity, 10^6 psi	Poisson s Ratio	$\frac{\sigma_{1o}}{\epsilon_{1o}}$, 10^6 psi	$\frac{\Delta\sigma_{1o}}{\Delta\epsilon'_{1o}}$, 10^6 psi	$\frac{\sigma_{1o}}{\epsilon_{2o}}$, 10^6 psi	$\frac{\Delta\sigma_{1o}}{\Delta\epsilon'_{2o}}$, 10^6 psi
HOP-4	--	--	2.73(1)	2.48	9.23(1)	9.42
HOP-5	2.48	0.243	2.82	2.57	9.65	9.34
HOP-6	2.40	0.258	2.76	2.57	9.92	9.68
HOP-7	2.37	0.266	2.73	2.53	10.13	8.73
HOP-8	2.48	0.206	2.76	2.48	8.44	9.50
HOP-11	2.48	0.234	2.81	2.48	9.32	9.09
HOP-12	2.49	0.238	2.54	2.29(2)	9.50	8.99
HOP-14	2.32	0.240	2.64	2.97	9.67	8.43
HOP-15	2.42	0.227	2.73	2.57	9.20	8.92
HOP-16	2.40	0.263	2.76	2.79	10.13	9.38
Mean Value	2.43 ± 0.04	0.242 ± 0.013	2.73	2.57 ± 0.11	9.52	9.15 ± 0.21
Standard Deviation	0.06	0.019	--	0.17	--	0.32

(1) Based on $E = 2.40 \times 10^6$ psi and $\nu = 0.240$.

(2) Rejected from computation of mean.

TABLE 19. FRACTURE DATA FROM BIAXIAL SPECIMENS SUBJECTED TO INTERNAL PRESSURE

Specimen No.	Principal Stresses, psi			Principal Strains, microinches per inch			
	Outside Surface		Inside Surface,	Experimental		Theoretical	
	Tangential, σ_{1o}	Axial, σ_2	Tangential, σ_{1i}	Tangential, ϵ'_{1o}	Axial, ϵ'_{2o}	Tangential, ϵ_{1o}	Axial, ϵ_{2o}
HOP-4	1050	525	1225	399	116	385	114
HOP-6	1080	540	1255	443	110	391	109
HOP-8	990	495	1155	405	106	359	118
HOP-11	890	445	1035	354	94	317	96
HOP-12	840	420	970	363	94	296	88
HOP-15	790	395	915	314	88	290	89
HOP-16	900	450	1040	324	96	326	89
Mean Value	934 ± 113	467 ± 46	1085 ± 112	372 ± 37	101 ± 8	338	100
Standard Deviation	142	58	141	47	10	--	--

TABLE 20. ELASTIC AND FRACTURE DATA FROM BIAXIAL SPECIMENS SUBJECTED TO AXIAL TENSION

Specimen No.	Modulus of Elasticity, 10^6 psi	Poisson's Ratio	Fracture Stress, σ_2, psi	Fracture Strains, micro-inches per inch	
				Axial, ϵ'_{2o}	Tangential, ϵ'_{1o}
HOP-2	2.37	0.185	500	239	41
HOP-3	2.42	0.255	650	321	87
HOP-10	2.39	0.198	845	398	93
HOP-18	2.43	0.237	565	269	67
HOP-19	2.32	0.243	740	376	81
HOP-22	2.34	0.225	925	439	101
HOP-24	2.49	0.271	1235	519	137
Mean Value	2.39 ± 0.05	0.231 ± 0.025	780 ± 126	366 ± 78	87 ± 24
Standard Deviation	0.06	0.031	159	98	30

these tests in tension, 780 psi, was considerably below the strength obtained from the tests under internal pressure, 1085 psi, which was contrary to expectation. Weibull's theory predicts the opposite; that is, the strength in tension should be higher than the strength under internal pressure. However, it should be remembered that, under internal pressure, the biaxial specimen must be treated as a thick-walled cylinder and, hence, the strength should not be compared directly with the strength in uniaxial tension. When, for comparison, the biaxial specimen was considered to behave as a thin-walled cylinder, then a strength under internal pressure of 1005 psi was obtained. This indicated that, as a thin-walled cylinder, the biaxial specimen was stronger under pressure than in uniaxial tension. It was felt that these initial data were insufficient and too erratic to warrant any firm conclusions concerning the effect of biaxial stresses on the fracture of plaster.

The nature of the fracture in these specimens, subjected to internal pressure, was typically brittle. Fracture appears to have initiated at the inside surface of the specimen and on a plane perpendicular to the transverse stress, σ_{1i}. The region in which fracture initiated usually was typified by a vertical crack in the gage section. Figure 17 shows a biaxial specimen which was fractured under internal pressure. Fracture initiated in the central section of the specimen.

The Effect of Superposed Bending Stresses on Tension-Test Data

If bending stresses are known to be present in a tension test, the question of their effect arises. Present knowledge of brittle materials would lead us to believe that the strength of a specimen is affected by the type of stresses present. For example, the strength data obtained in this investigation on titanium carbide and plaster indicate that the strengths of these materials are not equal in bending, torsion, and tension. It does not seem logical to assume, then, that superposed bending stresses will have no effect on tension data.

In view of the encouraging correlations of size-effect strength data with Weibull's statistical theory of strength, theoretical relations were derived from Weibull's theory during this period for predicting the effect of superposed bending stresses on tensile fracture. The development of these relations is outlined in Appendix III. Essentially, an expression for the ultimate strength of a tension specimen subjected to superposed bending was derived in terms of the eccentricity of the load and an expression for the strength of a similar specimen with uniform tensile loading. It is important to note that these were developed for the bending of a rectangular tension specimen about an axis parallel to one of its edges. It is not always true that bending will take place about this axis only. However, the expressions developed here are meant to provide only a qualitative indication of the effect of superposed bending stresses on the strength of a tension specimen. The specific expression developed is given on page 68:

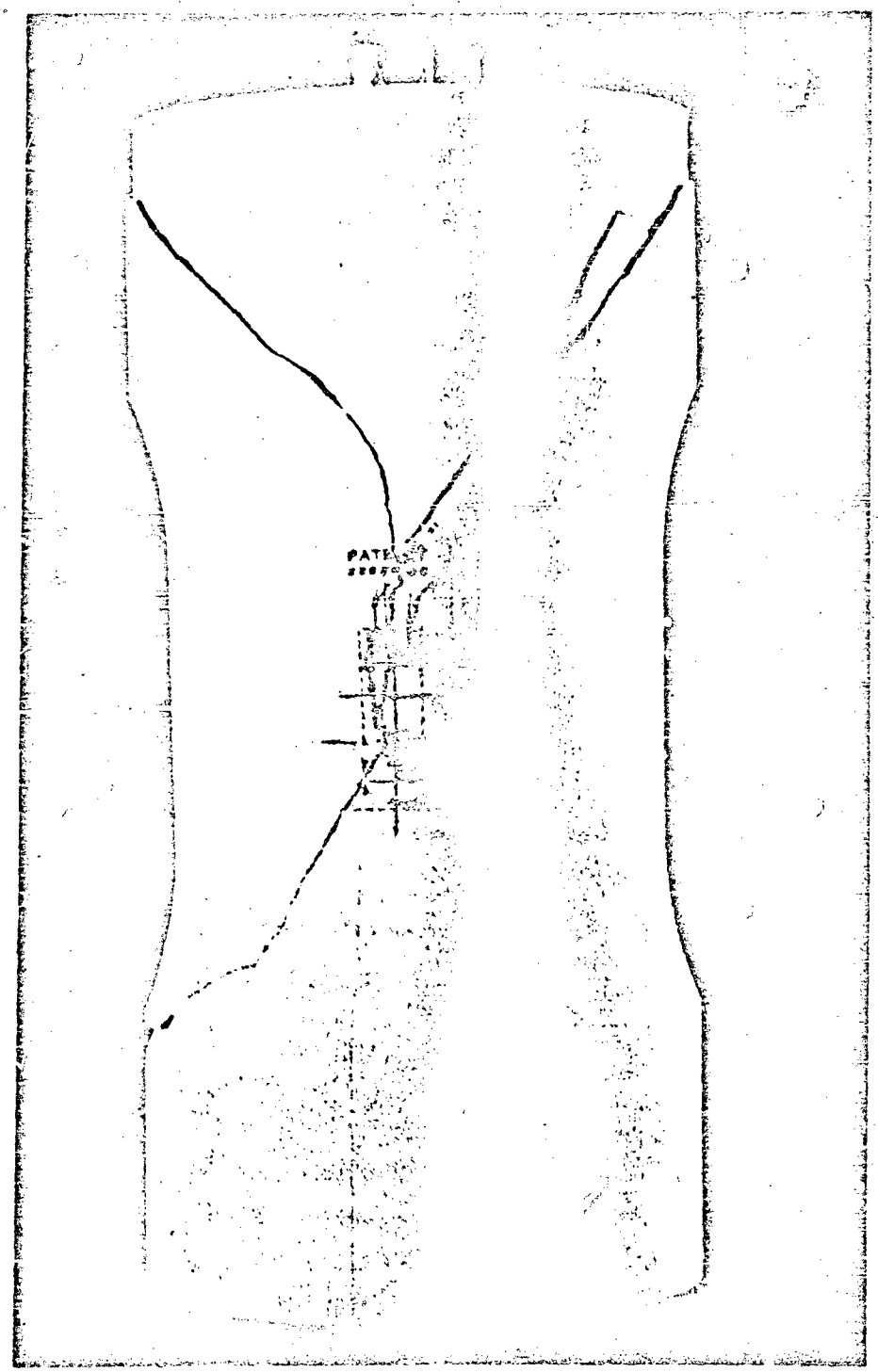

96210

FIGURE 17. PLASTER BIAXIAL SPECIMEN FRACTURED UNDER INTERNAL PRESSURE

$$\frac{\sigma_{bd}}{\sigma_{d'}} = \left(1 + \frac{3e}{h}\right) \left[\frac{V_{d'}}{V_{bd} S_m}\right]^{\frac{1}{m}} , \qquad (12)$$

where

σ_{bd} = strength of a (rectangular) specimen subjected to combined bending and tension, psi,

$\sigma_{d'}$ = strength of a specimen subjected to pure tension (e = o), psi.

e = eccentricity of the load, inches,

h = half the width of the specimen (see Figure 33),

V_{bd} = volume of the gage section of the specimen loaded in combined bending and tension, cubic inches,

$V_{d'}$ = volume of the gage section of the specimen loaded in pure tension, cubic inches,

m = material constant (an integer),

$$S_m = \sum_{r=o}^{r=\frac{m}{2}} \frac{m! \left(\frac{3e}{h}\right)^{2r}}{(m - 2r)!\ (2r + 1)!} . \qquad (13)$$

It can be shown from Equation (12) that the observed strength of a specimen as defined by Weibull should increase with increasing eccentricity of the load.

Effect of Eccentricity on Plaster Tension Data

It has been noted previously in this report that some eccentricity was observed in the tests on the size-effect tension specimens of plaster. It was noted also, from strain measurements taken at the instant of fracture, that the eccentricity tended to vary from specimen to specimen. All fracture data previously reported for the size-effect tension specimens were obtained by dividing the axial load at fracture by the cross-sectional area of the specimen. Hence, these strength data do not take into consideration the presence of any bending stresses. If bending stresses are present in a tension specimen at fracture, the normal stress obtained as the ratio of the maximum load to the cross-sectional area is not the maximum stress in the

specimen at fracture, the bending stress must be added to this normal stress.

An attempt was made during this period to predict the effect of eccentricity in tension loading on the strength of the No. 1-size tension specimen of Hydrostone plaster. For Hydrostone (m = 12, approximately), where $V_{bd} = V_d'$, Equation (12) becomes:

$$\frac{\sigma_{bd}}{\sigma_{d'}} = \frac{\left(1 + \frac{3e}{h}\right)}{S_{12}^{1/12}}, \qquad (14)$$

where

$$S_{12} = \sum_{r=0}^{r=6} \frac{12! \left(\frac{3e}{h}\right)^{2r}}{(12 - 2r)!\ (2r + 1)!}. \qquad (15)$$

Figure 18 presents a theoretical curve derived from Equation (14) depicting the effect of eccentricity on the strength of the No. 1-size-effect tension specimen. Weibull's theory predicts that the strength of an eccentrically loaded tension specimen should increase with increasing eccentricity of the load. The curve in Figure 18 was based on a value of $\sigma_d' = 1245$ psi.

In order to compare the predicted effect of eccentricity with data available on the No. 1 tension specimen, the eccentric strength σ_{bd}, and the eccentricity, e, were determined for a number of these specimens. The stress, σ_{bd}, was calculated as the nominal tensile stress (load ÷ area) plus the bending stress (bending strain x modulus of elasticity). The eccentricity, e, of the load was calculated by means of the relation:

$$e = \frac{EAW\epsilon_b}{6P} \text{ (inches)}, \qquad (16)$$

where

E = modulus of elasticity, 10^6 psi,

A = area of cross section, sq in.,

W = width of cross section, in.,

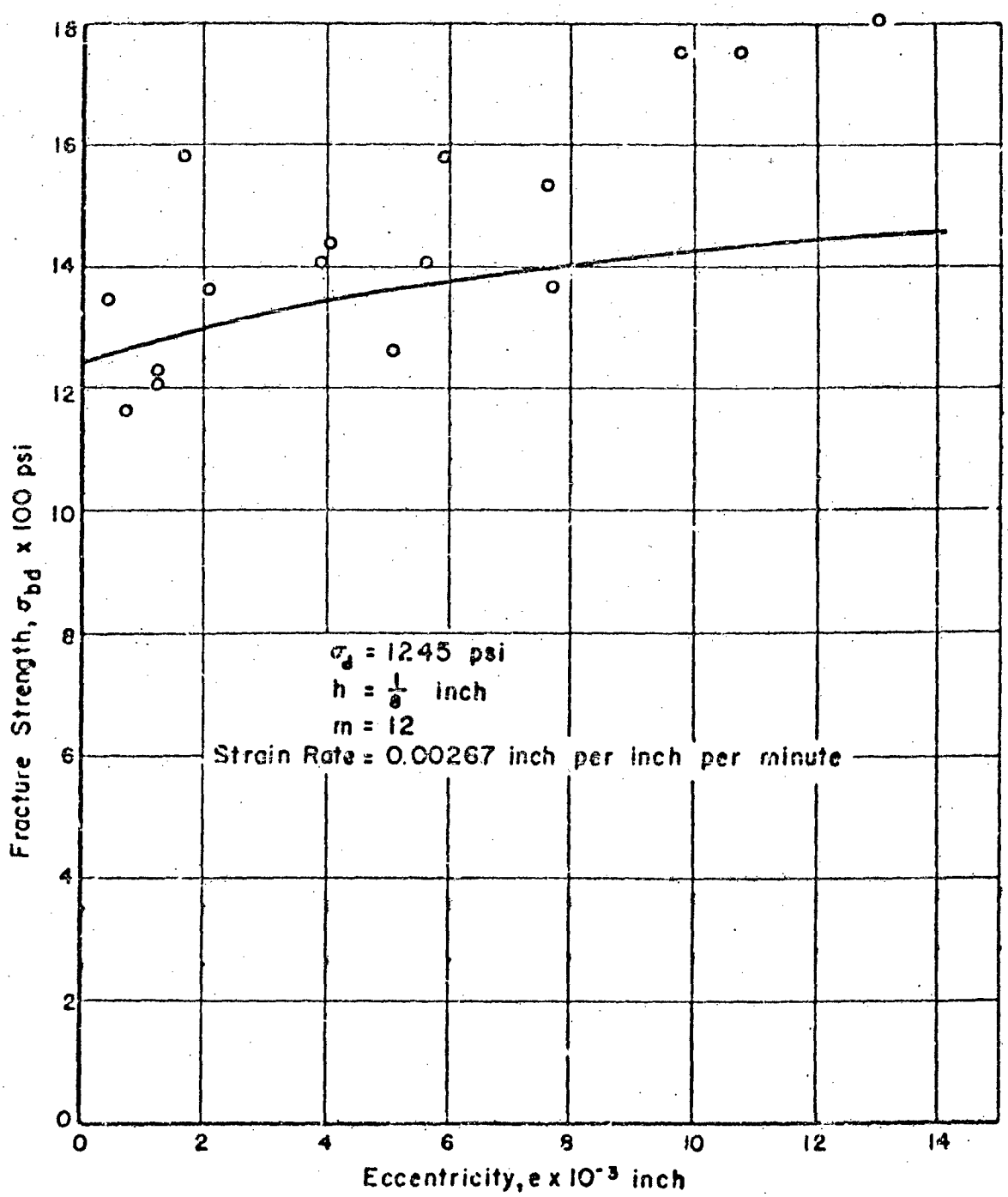

FIGURE 18. EFFECT OF ECCENTRICITY ON FRACTURE STRENGTH OF NO 1 SIZE TENSION SPECIMEN AS PREDICTED FROM WEIBULL'S THEORY

A-4708

ϵ_b = bending strain at fracture, microinches per inch,

P = axial load at fracture, pounds.

The data for these specimens have been plotted in Figure 18. These data reveal only a qualitative verification of the predicted variation of strength with eccentricity. Since the distribution of strengths will change with eccentricity, an entire series of tests at each eccentricity would be necessary in order to verify this effect quantitatively. However, this effect does serve as another indication that the stress state in the body of a brittle material affects its strength.

The Effect of Friction on Compression Strength

The usual compression test is intended to obtain the strength of a material in a uniaxial-compressive-stress state. Of course, the word "uniaxial" implies that there is only one stress acting upon the body and that, in this case, this stress is compressive and has constant magnitude and constant direction throughout the body.

The specimen usually chosen for the purpose of simulating this stress state is a right prism or a right circular cylinder; however, a critical difficulty arises in the loading of these specimens. As the stress must be uniformly compressive throughout, an attempt is made to distribute the load uniformly over the base surfaces by applying the load through flush-fitting plates. Owing to the tendency of the specimen to expand laterally under the longitudinal compressive load, frictional forces set up between the specimen and the end plates destroy the uniformity of the stresses in the region of the end of the specimen. Hence, the fracture strengths obtained from such stressed specimens must be treated with reservation.

Analysis shows that quite a complex stress system exists in the ends of such a specimen and that the resulting stresses tend to strengthen a cone-shaped region, the base of which is the base of the specimen. As a consequence of the frictional forces on the ends of prismatic specimens, a singularity in the stress field develops along the edges of the specimens (see Figure 19). This singularity arises because the shear stress, τ_{zx}, at A along the prismatic element must be zero, while the shear stress, τ_{xz}, at A may have a large finite value; hence, the fundamental criterion that the shear stresses τ_{zx} and τ_{xz} be equal at all points in the body is not satisfied at the corner, A. The result is the conical region of severe destruction shown in Figure 19. The elements of this region make a characteristic angle α with the base of the specimen.

Figure 20 shows a fractured compression specimen of Hydrostone. The conical region at the end of the specimen and the heterogeneous nature of the fracture in this region are revealed strikingly. The angle α has been

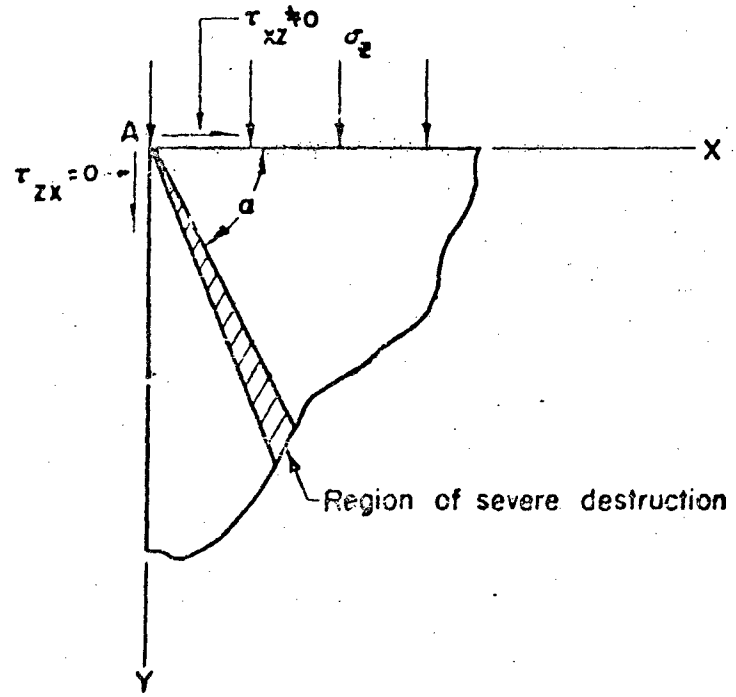

FIGURE 19. SINGULARITY IN STRESS SYSTEM AT EDGE OF PRISMATIC COMPRESSION SPECIMEN

A-2055

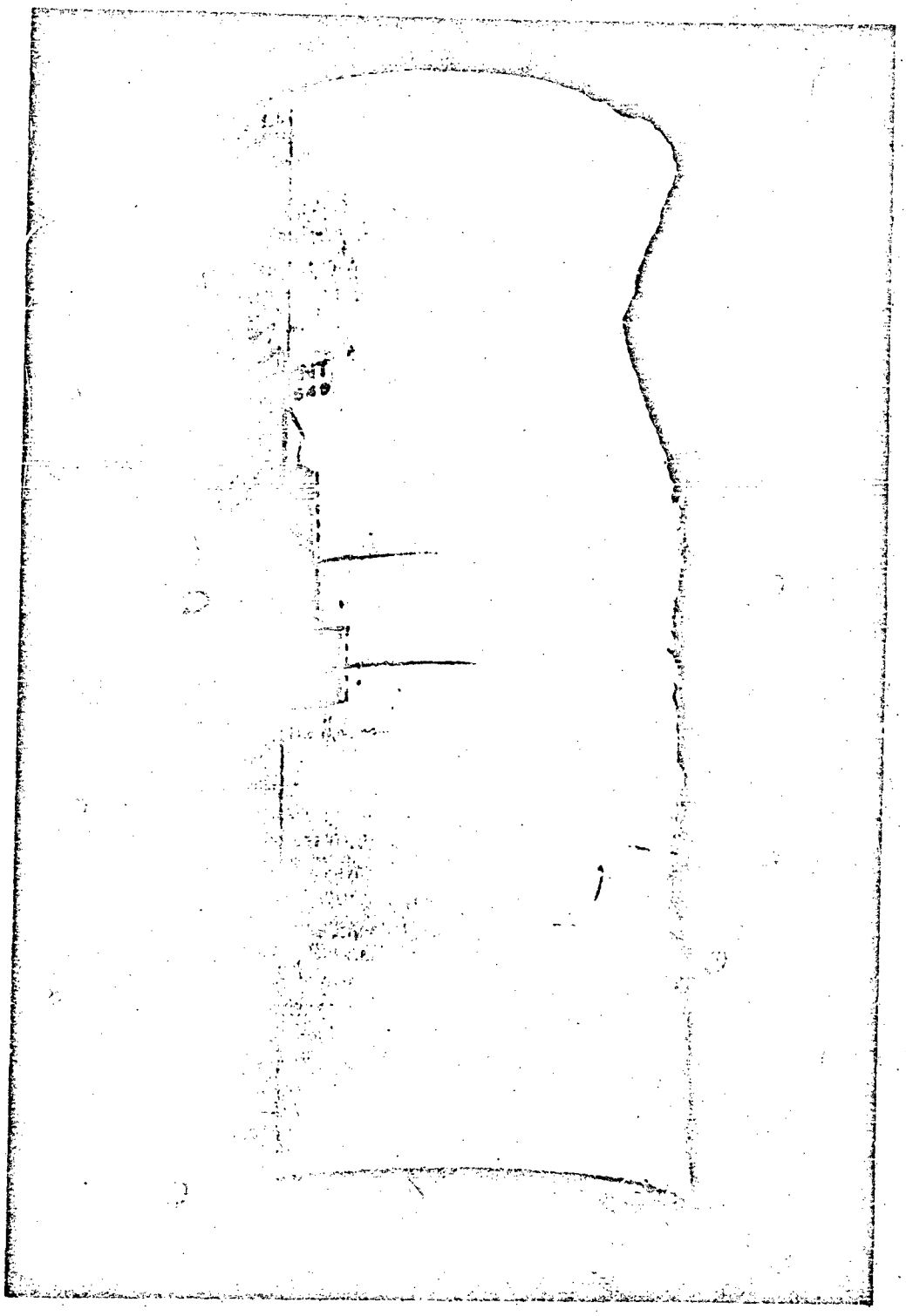

91323

FIGURE 20. COMPRESSION SPECIMEN OF HYDROSTONE PLASTER SHOWING CONICAL REGION OF SEVERE DESTRUCTION

found to depend upon the material, the presence or lack of antifriction materials, and the ratio of the length to the diameter of the specimen[24].

Seibel[25] proposed the use of conically shaped compression plates in an effort to obtain a more uniform stress distribution in the body of a cylindrical specimen. He proposed that the generatrices of the cones be machined with an angle equal to the angle of friction. The problem, of course, is to determine this angle. Some question of the constancy of this angle of friction during the test also arises.

It is of significance that, at the present time, 29 years after Siebel's work, there is still no known test from which the fracture strength of a uniformly stressed, compression specimen can be obtained. With the methods and techniques presently available, it is impossible to determine the true fracture strength of a prismatic specimen, yet no other satisfactory specimen design has been advanced.

Nadai[24] has reported the results of experiments by Lambert and Manjoine on the compression strengths of various hollow cylinders of porcelain, as shown in Figure 21. These specimens of porcelain exhibited different fracture strengths, and the variation in strength from one specimen to another was apparently a function of the shape of the specimen and of the end conditions. Some of the results reported by Nadai appear in Table 21. It can be seen from these results that the shape of a compression specimen greatly influences the compression strength of a particular brittle material. As a consequence of various factors, the experimenter may find that a material does not exhibit a consistent compression strength, and he probably will continue to observe this until a technique is devised which will eliminate the effect of end friction and permit uniform compressive stressing of a body.

Bend Tests on Porcelain

As a part of the effort to determine the effect of stress state on fracture phenomena, a series of bend tests were initiated on specimens of high-alumina porcelain supplied by Champion Spark Plug Company. The objective of these tests was to determine the elastic and fracture properties of this porcelain. The specimens were of the design shown in Figure 9 of AF Technical Report 6512, dated April, 1951. Tests were conducted using the procedures outlined in the above report for the testing of these specimens.

Elastic data were obtained from both top and bottom surfaces, along with the fracture strength.

In these tests, SR-4 strain gages mounted on the top and bottom surfaces of the gage section were used to determine the longitudinal and transverse strains in tension and compression. These strain data were corrected using Equations (20) and (21) of Appendix I. Bending stresses were

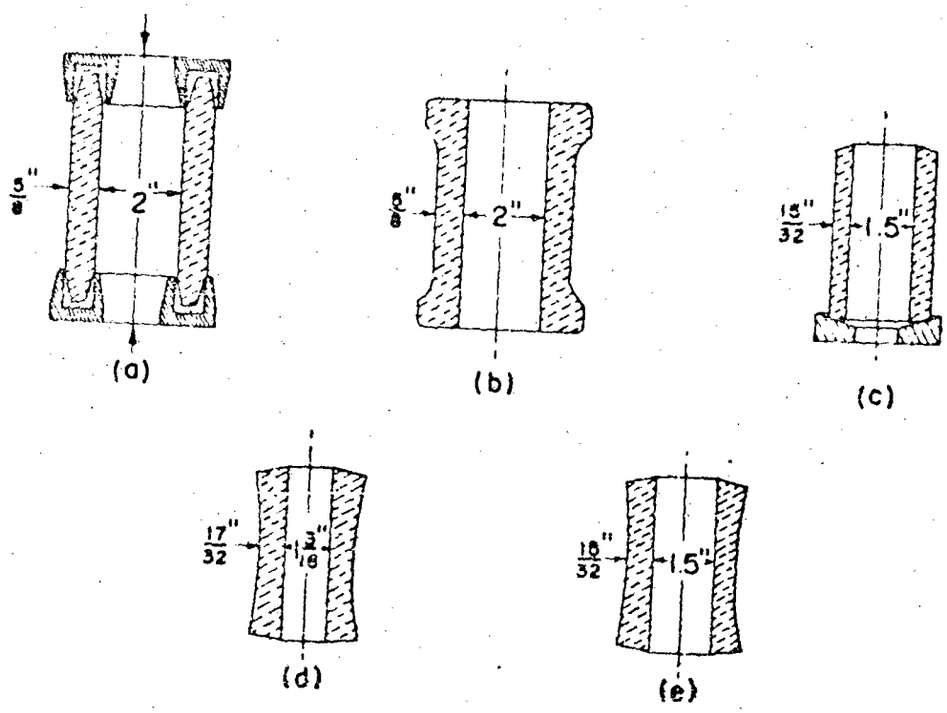

FIGURE 21. PORCELAIN COMPRESSION SPECIMENS

TABLE 21. STRENGTH IN AXIAL COMPRESSION OF HOLLOW PORCELAIN CYLINDERS

Shape	Figure 21	Compression Strength, psi
Cemented ends	a	64,600
Reinforced shoulders	b	50,200
Straight hollow cylinder	c	56,300
Cylinder with curved outside surface	d	121,000(a) 66,000(b)
Cylinder with curved outside surface	e	130,000(a) 117,000(b)
Straight solid cylinder (d= 1½ in., h=3 in.) with plane ground ends	-	73,000

(a) Highest Stress.
(b) Average stress.

calculated from the usual equation for maximum bending stress, σ_b:

$$\sigma_b = \frac{Mc}{I} \quad , \tag{17}$$

where M = applied bending moment,

I = moment of inertia of cross section,

c = half of the depth of cross section.

The value of Poisson's ratio in tension, ν_t, was obtained from the slope, E_t, of the plot of σ_b versus the longitudinal strain in tension, ϵ_{1t}, and from the slope, Q_t, of the plot of σ_b versus the transverse strain in tension, ϵ_{2t}, as

$$\nu_t = \frac{E_t}{Q_t} \quad . \tag{18}$$

The value of Poisson's ratio in compression, ν_c, was obtained from the slope, E_c, of the plot of σ_b versus the longitudinal strain in compression, ϵ_{1c}, and from the slope, Q_c, of the plot of σ_b versus the transverse strain in compression, ϵ_{2c}, as

$$\nu_c = \frac{E_c}{Q_c} \quad . \tag{19}$$

The data obtained from these initial tests on porcelain are given in Table 22. The strengths of these specimens are reported in Table 22 as the bending stress, σ_b, at fracture. These data, like data obtained earlier on similar specimens of Hydrostone plaster (see AF Technical Report 52-67, pp 55-58), indicate a difference between the moduli obtained from the top and the bottom surfaces. This effect is, of course, contrary to expectation. There is some question at the present as to the source of this discrepancy; however, the work conducted during the past year has led to the proposition that frictional forces arising at the load and support points cause this inequality. The values of Poisson's ratio obtained were subject to the same variance as the moduli, and this variation was assumed to arise from the same source.

When the data in Table 22 were combined with data obtained previously, and reported in AF Technical Report 52-67, the average properties were obtained as given on page 30.

TABLE 22. BEND-TEST DATA FROM SPECIMENS OF CHAMPION'S HIGH-ALUMINA PORCELAIN

Specimen No.	Modulus of Elasticity, 10^6 psi		Poisson's Ratio		Bending Stress At Fracture, psi
	Tension (E_t)	Compression (E_c)	Tension (ν_t)	Compression (ν_c)	
COB-26	45.3	40.6	0.262	0.188	-
COB-27	40.2	41.6	0.229	0.226	-
COB-28	41.2	45.5	0.238	0.242	-
COB-29	40.8	41.5	0.217	0.236	-
COB-30	39.8	40.8	0.232	0.229	-
COB-31	40.5	41.1	-	-	35,300
COB-32	41.7	52.5	-	-	37,300
COB-33	39.1	43.1	-	-	33,400
COB-34	46.0	40.7	-	-	31,900
COB-35	40.2	46.8	-	-	36,400
Mean Value	41.5 ± 1.1	43.9 ± 2.5	0.236 ± 0.018	0.224 ± 0.022	34,900 ± 2350
Standard Deviation	1.8	4.1	0.017	0.021	2,200

	Mean	Standard Deviation
Modulus of elasticity (tension), 10^6 psi	41.6 ± 1.1	2.2
Modulus of elasticity (compression), 10^6 psi	42.5 ± 1.5	2.7
Strength, psi	33,600 ± 800	2500

These data will be combined with size-effect and stress-state data to be obtained on porcelain in future phases of this investigation.

THE EFFECT OF STRAIN RATE ON THE MECHANICAL PROPERTIES OF BRITTLE MATERIALS

The rate at which a body is strained appears to have a distinct effect on its fracture strength. The effect of the rate of straining on the mechanical properties of metals, for example, has been the subject of many investigations. Generally, in the case of metals, the effect of increased strain rates is to increase the yield and ultimate strengths. On the other hand, relatively little is known about the effect of the rate of straining on the fracture of brittle materials.

In the case of brittle materials, the terms "rate of straining" and "rate of stressing" frequently are used synonomously, since these materials may behave elastically to fracture. In general, an increase in the rate of straining or stressing a brittle material has been found to increase its fracture strength. For example, Nadai[26] has reported the results of a series of tests on the effect of strain rate on the fracture stress of porcelain tension specimens. The results of these tests are given in Figure 22, where the fracture stresses of the porcelain specimens are plotted against the strain rate (on a logarithmic scale). These results reveal that the stress to cause fracture in this porcelain appeared to increase with increasing rates of straining. In regard to these tests, Nadai states: "From these tests it must be concluded that a brittle material under ordinary conditions when tested in air does not possess a definite tensile strength but that the latter continuously decreases with the time during which a load can act". Watstein [27] conducted compression tests on concrete cylinders at rates of straining ranging from 10^{-5} to 10 inches/inch/second. The compressive strength of the concrete was observed to increase about 80 per cent as the strain rate was increased from 0.003 to 10 inches/inch/second. Watstein also indicated that the entire stress-strain curve for concrete was affected by the rate of stressing.

Other researchers[28 to 34] have noted that the duration of the applied stress appears to affect the fracture of brittle materials. This effect has

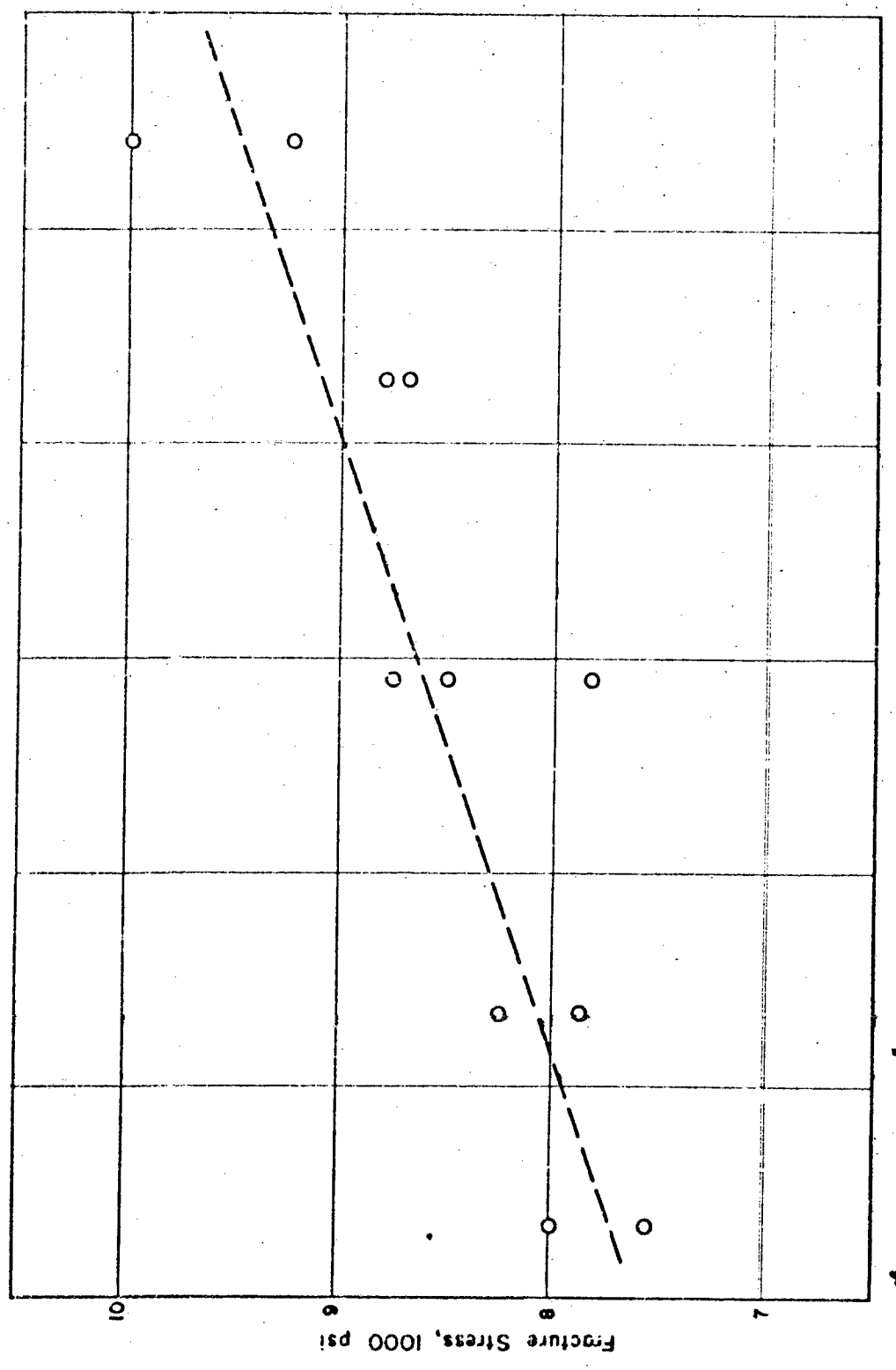

FIGURE 22. EFFECT OF RATE OF STRAINING ON FRACTURE STRESS OF PORCELAIN IN TENSION (AFTER NADAI)

been observed particularly in the cases of glass and porcelain. However, in these tests the applied stress was constant and not varying with time; in short, these materials appeared to fatigue with time. It is important to point out that it may be impossible to separate the latter effect of stress duration (time) from the former effect of rate of stressing or straining. It cannot be said that these two effects are one and the same phenomenon, but it must be pointed out that the two effects appear to be interrelated. In fact, it might be that the duration of stress is the only factor that affects fracture strength, and that the effect illustrated in Figure 22 for porcelain actually represents the effect of duration of stress on strength. That the existing knowledge on the effect of strain rate on the properties of brittle materials is meager is true; nevertheless, it can be stated that the rate at which a brittle material is strained significantly affects its fracture characteristics.

Strain-Rate Tests on Plaster

A program was set up during this period to study the effect of the rate of stressing or straining on the fracture strength of Hydrostone plaster. The initial phases of this program were qualitative in nature in that their only purpose was to determine the existence of such an effect. As a result, it was decided to test the No. 1 tension specimen, the No. 5 bend specimen, and the No. 5 torsion specimen at various strain rates and to note the effect, if any, on their fracture strengths. The results of these initial tests are reported below.

Tension Tests

The No. 1-size alternate tension specimen was selected to study the effect of strain rate on the strength of plaster in tension. The casting and curing procedures for these specimens were the same as those for the size-effect specimens. Strain gages were used on almost all of these specimens.

The same procedure was used in aligning these specimens as was used in the size-effect tests on the No. 1 tension specimen. The strain rates were measured by means of strain gages. After the gages had been prestrained, an initial load was applied to the specimen. Then the Baldwin strain indicators were balanced and the strains recorded. Without changing the setting on one indicator, the setting on the other was increased 100 microinches per inch. The loading rate of the testing machine was adjusted then to give the desired strain rate (lapsed time for 100 microinches per inch). The specimen was then strained to fracture using this loading rate.

The data from these tests were calculated in the same manner as the data from the size-effect tension tests.

Table 23 and Table 24 give the results of the few initial tests conducted on the No. 1 tension specimen. It is important to note that these data were obtained from specimens with gages cemented to their surfaces. It was noted in the size-effect tests that gages appeared to strengthen a specimen, so additional tests must be conducted on gage-free specimens before any valid quantitative results can be obtained. However, a comparison of the results in Tables 23 and 24 with the size-effect data in Table 3 leads to the following:

Strain Rate, in./in./min	Fracture Srress, psi	Number of Specimens
0.00074	1350	12
0.0027	1280*	21
0.0060	1235	12

* From specimens with gages.

The above comparison raises an important question: "Can the effects of strain rate be different for different brittle materials, or are these data misleading?" The work reported by Nadai on porcelain was conducted over a much wider range of strain rates. It may be possible then that the rates used here were sufficiently narrow to permit normal statistical scatter in test data to overshadow the true effect of strain rate. Additional data should be obtained if this question is to be resolved.

Bend Tests

The No. 5-size alternate bend specimen was chosen for the study of the effect of strain rate on the strength of plaster in bending. The procedures used in casting and curing the bend specimens for the strain-rate tests were the same as those used for the size-effect specimens. As in the case of the strain-rate tests in tension, strain gages were used to measure the strain rates. Usually, only one strain gage was cemented to a bend specimen; this gage was placed on the tension surface.

The same procedure was used in aligning, prestraining, and loading these specimens as was used in the size-effect bend tests. The proper loading rate was determined by adjusting the head rate of the machine to obtain the desired strain rate from the strain gage.

Table 27 gives the results of these initial strain-rate tests on Hydrostone plaster bend specimens. A comparison of these data with the data obtained from the size-effect tests on the No. 5 bend specimens leads to the following:

Strain Rate, in./in./min	Bend Strength, psi	Number of Specimens
0.00075	1260	14
0.0027	1250	42

These data indicate that, in bending, the fracture strength of plaster may be practically unaffected by strain rate within the range investigated. It is interesting that these data indicated a very slight decrease in strength with increased strain rate; however, more data at these rates and at other rates are necessary before any definite statements can be made as to the effect of strain rate on the bending strength of plaster.

Torsion Tests

The No. 5 size torsion specimen was chosen for the strain-rate program because it was large enough to permit the use of strain gages for measuring strain rate. The procedures for casting, curing, and testing these specimens were the same as those for the size-effect tests on the No. 5 torsion specimen. In these strain-rate tests, however, it was possible to maintain a constant strain rate from specimen to specimen. Hence, only one specimen was needed to determine the twist rate required to give the desired principal strain rate.

Table 26 gives the results of the initial strain-rate tests on the No. 5 torsion specimen, conducted at a strain rate of approximately 0.0024 inch/inch/minute. If these data are compared with the strengths of those specimens tested at a strain rate of 0.0027 inch/inch/minute, the following data result:

Strain Rate, in./in./min	Torsion Strength, psi	Number of Specimens
0.0024	1135	12
0.0027	1115	37

These data appear to indicate that strain rate had no significant effect on fracture stress for the range of rates investigated. However, this range was relatively quite narrow and, if an effect of strain rate were present, it could be discerned more easily by testing at more widely separated strain rates.

TABLE 23. STRAIN-RATE DATA FROM SMALL, NO. 1-SIZE PLASTER TENSION SPECIMENS

Specimen No.	Strain-Rate, in./in./min	Tension Strength, psi
H10TR-1	0.00075	1095
H10TR-3	0.00072	1350
H10TR-4	0.00072	1375
H10TR-5	0.00073	1360
H10TR-6	0.00071	1270
H10TR-9	0.00075	1655
H10TR-10	0.00075	1490
H10TR-11	0.00075	1370
H10TR-15	0.00075	1380
H10TR-16	0.00075	1380
H10TR-18	0.00075	1270
H10TR-19	0.00075	1195
Mean Value	0.00074	1350 ± 75
Standard Deviation	-	140

TABLE 24. STRAIN-RATE DATA FROM SMALL, NO. 1-SIZE PLASTER TENSION SPECIMENS

Specimen No.	Strain-Rate, in./in./min	Tension Strength, psi
H10TR-23	0.0060	1100
H10TR-27	0.0060	1240
H10TR-36	0.0060	970
H10TR-39	0.0060	1170
H10TR-46	0.0060	1125
H10TR-47	0.0060	1245
H10TR-49	0.0060	1150
H10TR-50	0.0060	1030
H10TR-52	0.0060	1390
H10TR-53	0.0060	1410
H10TR-54	0.0060	1405
H10TR-55	0.0060	1575
Mean Value	0.0060	1235 ± 95
Standard Deviation	-	180

TABLE 25. STRAIN-RATE DATA FROM LARGE, NO. 5-SIZE PLASTER BEND SPECIMENS

Specimen No.	Strain-Rate in./in./min	Bend Strength, psi
H50BR-2	0.00075	1215
H50BR-3	0.00075	1045
H50BR-5	0.00075	1660
H50BR-10	0.00078	1495
H50BR-11	0.00075	1035
H50BR-12	0.00072	1215
H50BR-13	0.00063	1235
H50BR-14	0.00077	1155
H50BR-15	0.00082	1255
H50BR-18	0.00075	1395
H50BR-20	0.00075	1495
H50BR-21	0.00075	1135
H50BR-24	0.00075	990
H50BR-25	0.00075	1315
Mean	0.00075	1260 ± 95
Standard Deviation	-	195

TABLE 26. STRAIN-RATE DATA FROM LARGE, NO. 5-SIZE PLASTER TORSION SPECIMENS

Specimen No.	Strain-Rate in./in./min	Torsion Strength, psi
H50SR-7	0.0024	1050
H50SR-8	0.0024	1180
H50SR-10	0.0024	815
H50SR-11	0.0024	1000
H50SR-13	0.0024	1305
H50SR-14	0.0024	1125
H50SR-15	0.0024	1025
H50SR-16B	0.0024	1065
H50SR-18	0.0024	1390
H50SR-21	0.0024	1400
H50SR-22	0.0024	980
H50SR-25	0.0024	1295
Mean	0.0024	1135 ± 100
Standard Deviation	-	180

THE EFFECT OF TEMPERATURE ON MECHANICAL PROPERTIES

A study of the strength of brittle materials cannot be considered complete without consideration of the effects of temperature. It has long been known, for example, that the absolute temperature of a metallic body affects its strength. This is quite obvious when it is realized that metals all become fluid if subjected to sufficiently high temperatures. By definition, a fluid cannot withstand shear stresses and will flow readily if subjected to shear stresses. This observation can be extended to all brittle materials, metallic or otherwise.

Why, then, does a material which fractures with practically no prior deformation at so-called room temperatures behave as a fluid at some elevated temperature? In answering this question, many scientists have proposed that it is more correct to speak, not of brittle materials, but of the "brittle states" of these materials. They infer that a material may be termed "brittle" when it exists in such a state that it will fracture before it will flow under the action of shear stresses. Then a transition in the effect of shear stresses must occur suddenly or gradually, as the temperature of the body approaches the melting point.

In general, the strengths of metals have been observed to tend to increase with decreasing temperature. In addition, it has been noted that the entire stress-strain curve of a material tends to change with temperature.[35-38] None of the phenomenological or mechanistic theories mentioned in this report take into consideration the effects of temperature on strength. Because of the "softening" of materials with temperature, these effects will be quite complex.

Elevated-Temperature Torsion Tests on Titanium Carbide K151A

During the period of this report, tests were initiated at 1300 F on titanium carbide K151A torsion specimens of the same lot as those reported in Table 7 of WADC Technical Report No. 52-67. The purpose of these tests was primarily to establish the methods for torsion testing brittle materials at elevated temperatures.

In testing these specimens, temperature measurements were taken at four points along the gage length in order to determine the temperature distribution in this region. Four platinum-platinum-rhodium thermocouples were mounted along the gage length at points about 5/8 inch apart, directly in contact with the specimen surface.

In these tests, only the stress at fracture was measured; no strain measurements were taken. The applied moments were determined by means of a torsion dynamometer mounted at the fixed end of the torsion machine. This dynamometer consisted of a 1-3/4-inch-diameter steel shaft, onto

which SR-4 strain gages had been cemented. The strain of the SR-4 gages was calibrated against the applied moment.

The specimens were mounted between torsion heads or adapters of the type shown in Figure 6 of AF Technical Report No. 6512. However, the heads used in these elevated-temperature tests had cooling coils wrapped around their bases. The entire assembly of specimen, thermocouples, and torsion heads was placed in a horizontal-tube, wire-wound furnace.

The specimens were heated to the test temperature and allowed to soak at temperature for two hours. After soaking, the temperature distribution along the specimen was determined. In the specimens tested during this period, a maximum temperature variation of 30 F was noted. This variation arose from the cooling of the torsion heads. The temperature was found to decrease from the center of the specimen outward.

After the temperature distribution had been measured, the specimen was twisted to fracture. This was carried out at a predetermined rate of 0.0427 radian per minute, which corresponded to a principal strain rate of 0.0027 inch/inch/minute. The temperature in the center of the specimen and the torsion-dynamometer strain at fracture were recorded. In addition, the atmospheric pressure and the dry-bulb and wet-bulb temperatures were measured in the vicinity of the specimen. These tests were conducted in air.

The results of the tests on the four titanium carbide K151A specimens are given below:

Specimen No.	Test Temp, F	Strength, psi
2-1	1300	59,000
2-5	1300	55,000*
2-12	1290	58,000*
2-13	1300	41,300*

*A small flaw was found in the fracture surface.

The strengths of these specimens were considerably below the average strength, 97,800 psi, reported for specimens of this lot tested at room temperature (see Table 7, WADC Technical Report No. 52-67). When these data are compared qualitatively with modulus-of-rupture data obtained by the National Advisory Committee for Aeronautics[39], the two sets of data are found to be in relative agreement. These results serve to verify the statement made earlier that K151A is not a profitable material for investigation due to its tendency to contain objectionable flaws. Nevertheless, these data serve to substantiate the observation that temperature affects the strength of ceramic materials.

TESTING METHODS

Size-Effect Compression Tests

The quantities desired from the size-effect compression tests on plaster were Young's modulus, Poisson's ratio, and the compression strength. However, the values of compression strength observed were felt to be of doubtful validity because of end effects, as described earlier in this report.

In the measurement of elastic properties, the considerable size difference between the No. 1 size and the No. 5 size made it necessary to use different sizes of gage. Different types of gages were employed in an effort to cover relatively the same amount of surface area. The No. 1-size specimen was too small to mount the four gages necessary for the simultaneous measurement of Young's modulus and Poisson's ratio. As a consequence, Young's modulus was obtained from two of the small specimens in each batch and Poisson's ratio was obtained from the remaining small specimen.

In the preparation of the two No. 1 specimens used in modulus determinations, three A-7 type SR-4 strain gages were cemented at 120-degree intervals to the cylindrical surface of each specimen. These three gages were used to secure axial alignment in the test. Only two A-7-type gages were cemented to each of the small specimens used for Poisson's-ratio measurements. These two gages were mounted on the same vertical element of the specimen, one above the other, but with their axes perpendicular.

In the preparation of the large, No. 5-size specimens, it was possible to measure Young's modulus and Poisson's ratio simultaneously on the same specimen. Three A-5-type strain gages were cemented to the specimen at 120-degree intervals and a fourth "transverse" gage was mounted perpendicular to one of the three "longitudinal" gages. The mounting of the transverse gage can be seen in Figure 20.

After the strain gages had been cemented to all of the specimens of a batch, the entire batch was returned to the curing oven and kept there until about 12 hours prior to testing. At that time, the entire batch was taken from the oven and placed on the bed of the testing machine. This procedure was used in an effort to permit the specimen to adjust to the surrounding atmospheric conditions before testing.

In testing the two sizes, 3 thicknesses of paper were placed between the specimen and each of the hardened-steel compression pads. The specimen was loaded to just above the maximum load to be used in determining

the modulus of elasticity. The load was removed and the cycle repeated three times for the purpose of prestraining the SR-4 strain gages. (15)

Then the specimen was aligned and loaded in increments to a stress level of about 1500 psi, reading each strain gage at each load level. The loading was continued above 1500 psi in 2000-psi increments until fracture. The loading during these latter increments was carried out at a calculated strain rate of about 0.0045 inch/inch/minute. In the loading of the small, No. 1-size specimens used for obtaining Poisson's ratio, the alignment could not be checked accurately, since only one longitudinal gage was used. In this case, the loading was adjusted to produce the same indicated strain in the longitudinal gage as had been obtained previously in those No. 1 specimens with three gages. Alignment was a less serious problem in the case of Poisson's ratio specimens in that superposed bending should have a negligible effect on the ratio of two strains from gages on the same vertical element.

Along with the various values of load and strain, the room-temperature (dry-bulb) and the wet-bulb temperatures in the vicinity of the specimen were recorded during each test. The barometric pressure also was recorded.

Size-Effect Tension Tests

The procedure for conducting tension tests on the No. 1-size tension specimen was similar to that for testing the Hydrostone size-effect compression specimens. After a No. 1 tension specimen had been in the curing oven for 10 to 12 days, it was removed, if necessary, for mounting SR-4 strain gages. Since only one tension specimen could be cast from each batch of plaster, the specimens could be removed from the oven individually.

Two SR-4, Type A-7, gages were used on each specimen from which modulus of elasticity data were desired. These two gages were cemented to opposite sides of the gage section. In the case of those No. 1 specimens from which Poisson's-ratio data were desired, Poisson's ratio was measured using small, Type A-19, SR-4 strain gages. Two A-19 gages were cemented transversely below two A-7 gages cemented longitudinally to the gage section. Even with the use of these small A-19 gages (1/16-inch gage length), a portion of the lead section of each A-19 gage could not be cemented to the specimen. The lead end of the gage extended beyond the edge of the specimen.

Before using these gages, it was necessary to determine whether this unique mounting changed their gage factor. To do this, two A-19 gages of the same lot were mounted on the tension surface of a large No. 5-size bend specimen (see Figure 7). Both of these gages were mounted transverse to the principal tensile strain. One gage was mounted exactly as the

transverse gages on the tension specimen, that is, with part of the gage hanging freely over the edge. The second gage was mounted alongside the first, but it was turned 180 degrees, so that the entire gage could be cemented to the specimen. The specimen was loaded and the strain measured on three different Baldwin strain indicators. Five elastic runs were made with each combination of indicators. The strains from the two gages were found to agree within 1 per cent, indicating that the gage factor was not changed by cementing only the active part of the gage to a specimen.

In the case of the No. 4 tension specimen, Type A-5 gages were used for measuring strains; otherwise, the treatment of No. 1 and No. 4 tension specimens was identical.

In conducting the tension test on the No. 1-size specimen, the specimen was placed in the testing machine (Baldwin Southwark 60,000-pound-capacity Universal Testing Machine) and aligned. An initial load of 15 pounds was used to maintain alignment.

The No. 1 specimen (if it had strain gages on it) was loaded then to slightly above 40 pounds (650 psi) and unloaded to 15 pounds. This cycle was repeated three times to prestrain the gages before making a recording run. Then the load was applied at a slow continuous rate and the strains recorded. The load was then lowered to about 30 pounds and reapplied at a calculated strain rate of about 0.0045 inch/inch/minute until the specimen fractured.

Size-Effect Bend Tests

A strict procedure was employed in the testing of these bend specimens. After a large, No. 5-size specimen had been in the curing oven for 10 to 12 days, it was removed and SR-4 strain gages mounted on it. A total of four strain gages was mounted on each specimen, two gages on each of the top and bottom surfaces of the gage section. One of each pair of gages (longitudinal gage) was mounted parallel to the long axis of the specimen, and the other gage (transverse gage) was mounted perpendicular to the axis. The longitudinal gages measured the major tensile and compressive strains, while the transverse gages measured transverse strains.

In testing the No. 5 bend specimen, the specimen was placed in the bend jig (see "Bend Test Loading Apparatus") and loaded to slightly above the maximum load used in elastic determinations. The specimen was unloaded and the cycle repeated three times for the purpose of prestraining the gages. Then the specimen was loaded at a slow continuous rate to approximately 550 psi and the strain recorded at regular intervals. At least three of these runs for recording elastic data were made on each No. 5 specimen. Following the last of these runs, the specimen was loaded at a strain rate of 0.0027 inch/inch/minute (predetermined from tests on trial

specimens). The load and the maximum tensile strain at fracture were recorded.

A slightly different procedure was followed in the preparation and testing of the No. 1-size bend specimen. Due to the extremely small size of the gage section of this specimen, it was impossible to mount both a longitudinal and a transverse gage on each surface of the gage section. There was room only for the longitudinal gages. As a result, Poisson's ratio was not obtained from the tests on the No. 1-size bend specimen.

Prior to testing the No. 1 specimen of plaster, a steel specimen of similar size was placed in the No. 1 bend jig. (This jig is shown in Figure 23 and discussed in detail later in this report.) The jig was cycled four times to a load considerably above the anticipated fracture load of the plaster specimens in order to stabilize the dynamometer system of the jig. Then the steel specimen was replaced with a plaster specimen, the elastic data obtained, and the specimen loaded to fracture at a strain rate of 0.0027 inch/inch/minute (predetermined by tests on trial specimens). The dynamometer load and the machine load (as a check) were recorded at fracture, along with the fracture strains.

The dry-bulb and wet-bulb temperatures and the atmospheric pressure in the vicinity of the specimen were recorded during each bend test.

Size-Effect Torsion Tests

A special loading machine was used for loading the torsion specimens. This lathe-like machine permitted the application of a torsional moment to the size-effect specimens (see Figure 7, AF Technical Report No. 6512). This machine was described in the RAND Report R-209, dated August 31, 1950, on "Mechanical Properties of Ceramic Bodies".

The torsional moment was applied to the plaster size-effect torsion specimens by means of special torsion heads or grips. One of these heads served as a torsion dynamometer for measuring the torque applied to the specimen. A special set of heads was designed and constructed for the No. 1- and the No. 5-size torsion specimens. The operation and calibration of these torsion heads and dynamometers is described in detail later in this report.

The strain gages on each dynamometer were prestrained prior to testing to insure proper operation. Then the No. 1 or No. 5 torsion specimen was placed in the torsion heads, which had been fastened to the moving and fixed heads of the torsion machine. In those tests in which no elastic data were obtained, the specimen was twisted immediately to fracture at a rate of 0.127 radian per minute.

The twist rate, 0.127 radian per minute, was determined from experiments on trial No. 5-size specimens. On these specimens, a strain gage was placed on the gage section at an angle of 45 degrees to the axis. Hence, when the specimen was twisted, the strain gage was in a position to measure the principal tensile strain in the specimen. Then the external twist rate was adjusted to give a principal strain rate of 0.0027 inch/inch/minute. This was the principal strain rate used in all the other size-effect tests on plaster except the compression tests.

This same twist rate, 0.127 radian per minute, was used in testing both the No. 5-size and the No. 1-size torsion specimens. Since it was impossible to cement strain gages to the No. 1-size specimen, it was assumed that the principles of similitude held. By these principles, both the No. 1- and the No. 5-size specimens should have the same twist rates for any given principal strain rate.

As pointed out earlier, elastic data were obtained from the large, No. 5-size specimens only. These data consisted of determinations of the modulus of rigidity of these specimens.

Prior to testing, the No. 5-size specimens were removed from the curing oven and allowed to cool. Two small silvered mirrors were cemented to the gage section of the specimen 5 inches apart. (Figure 6 of AF Technical Report No. 6512 shows two such mirrors mounted in a similar manner on a titanium carbide specimen.) Then the specimens were returned to the dryer.

In the test, each specimen was placed in the torsion heads with the plane of the mirrors vertical. Then a high-intensity light source was placed in front of the mirrors. This light source was enclosed in a light-proof box equipped with a camera shutter and a lens system. A film holder containing a piece of 8 x 11-inch film was placed in such a position that the reflected images (one from each mirror) of the light source would fall on the film if the shutter was open.

At this point, the torsion dynamometer was loosened from the fixed head so that the specimen could be turned by the driving head without applying torque to the specimen. Then the vertical movement of each of the reflected images on the film was calibrated against a known rotation of the mirrors. The calibrations and the torsion tests for elastic data were carried out in a room that was lightproofed so that it was essentially a darkroom. In this way, the positions of the reflected images of the mirrors could be photographed.

At the beginning of the torsion test, the driving head was turned manually until the strain indicator on the torsion dynamometer indicated that torque had begun to be applied. The lights in the room were turned off and the image positions photographed. The driving head was turned then until a predetermined increment of torque had been applied. The

shutter was tripped again and the process repeated through seven increments. This entire process was repeated four times to give four elastic determinations. After the final run, the specimen was twisted to fracture at the desired strain rate. The torsional moments were measured in the same manner as in the testing of the other large torsion specimens.

Upon completion of the test, the film was developed and the distances between the pinpoint images were measured with an optical comparator. The difference in movement of the images of the two mirrors was converted into torsional strain. The modulus of rigidity was determined as the slope of the curve of shear stress versus shear strain.

The dynamometer reading was recorded at the instant of fracture in all tests on the No. 1- and No. 5- size torsion specimens of plaster. The torsional moment at fracture was determined from a calibration of the dynamometers. The dry-bulb and wet-bulb temperatures and the atmospheric pressure in the vicinity of the specimen were recorded during each test.

Combined-Stress Tests

After a biaxial specimen had been cured for 12 days, it was removed from the curing oven and SR-4 strain gages were mounted on the outside surface of the gage section. Six strain gages were mounted on each specimen, three in the direction of the axis of the cylinder and three transverse to the axis. The gages were mounted in pairs, one axial gage and one transverse gage, at 120-degree intervals around the circumference of the gage section. The orientation of these gages is illustrated in Figure 17. After the strain gages had been cemented to a specimen, it was returned to the drying oven and kept there until about 12 hours prior to testing. At that time, it was placed on the bed of the testing machine so that it would adjust to the surrounding atmospheric conditions before testing.

The first step in the testing was to determine the elastic constants, the modulus of elasticity and Poisson's ratio. To do this, the specimen was placed in a Baldwin-Southwark Universal Testing Machine and loaded axially in tension through the tension adapters of the specimen by means of tension grips made up of chain links. These chain-link adapters, one end of which fastened to the head of the machine, helped to maintain axiality of loading. The specimen was loaded to just above the maximum load to be used in the elastic determinations. Then the load was removed and the complete cycle repeated three times. This process was carried out for the purpose of prestraining the strain gages.

Following the third prestraining cycle, the specimen was loaded at a continuous rate to a stress of about 300 psi. Readings were taken on all three axial gages and on one transverse gage. Then the load was removed and the loading cycle repeated at least three times, so that four loading cycles were available for elastic determinations.

Following the last elastic run, the specimen was removed and attached to the pressure-loading system (see Figure 30). Each strain gage was connected to a separate strain indicator to permit the simultaneous reading of all six strain gages at fracture. At this point, the specimen was loaded at a continuous rate to an internal pressure of 100 psi, the pressure removed, and then the entire cycle repeated three times to prestrain the SR-4 gages. Then the specimen was loaded at a slow continuous-pressure rate and strain readings were taken simultaneously every 10 psi. At the same time, the pressure was measured by means of strain gages on the Bourdon tube of the 0-300 pressure gage. After reaching a pressure of 100 psi, the pressure was released and the complete cycle repeated at least three times. At the end of the last cycle, the pressure in the specimen was increased to 100 psi and the loading valve closed. The accumulator was pumped to 300 psi. Then the loading valve was opened to a predetermined and precalibrated setting to give a pressure rate of about 1100 psi per minute. This pressure rate was calculated from a desired principal strain rate of 0.0027 inch/inch/minute, the strain rate used in the size-effect tests on Hydrostone plaster. As the pressure increased, the strain rate on one of the transverse strain gages was measured. All the strains and pressures were measured at the instant of fracture. In addition, the dry-bulb and wet-bulb temperatures and the atmospheric pressure in the vicinity of the specimen were recorded during each test.

In the case of specimens fractured under tension loading, only three longitudinal and one transverse gages were used. These specimens were fractured following the last elastic determination, by loading in tension to fracture at a measured strain rate of 0.0027 inch/inch/minute. This strain rate was obtained by trial measurements on each specimen immediately prior to testing.

DEVELOPMENT OF TEST EQUIPMENT

One of the secondary objectives of this investigation has been the development of precise techniques for the procurements of fracture data. During the period of this report, considerable effort was directed toward the development of proper test apparatus.

Bend-Test Loading Apparatus

The effort made during this period to obtain more precise bend data was described earlier in this report. During past periods of research, a great deal of difficulty was experienced in obtaining precise bend data. The alternate bend-test specimen developed during this period for the size-effect program was a partial solution to the problem of extraneous friction forces.

A loading apparatus similar to that described by Frocht(40) was designed for the loading of each size of this specimen. By virtue of its design, this type of loading apparatus eliminated practically all the frictional forces at the points of loading. The specific jig used for loading the smallest, No. 1-size alternate bend-test specimens of Hydrostone is shown in Figure 23. With this apparatus, the load was applied through wire cables which were attached by adapters to the heads of the testing machine. The use of wire cables helped to assure axiality of loading. The links of this jig were free to rotate under the application of load. Strain gages cemented to the bottom horizontal bar were employed as a dynamometer system for the measurement of load. Such a system was necessary since the load dial of the testing machine was not sufficiently sensitive to record fracture loads with the accuracy desired.

The jig for loading the largest, No. 5-size alternate bend specimen was similar to the one used for loading the No. 1-size specimen. As in the case of the small jig, the load was applied through wire cables. Strain gages were not used for measuring the load, since the loads were large enough to obtain sufficient accuracy from the load dial of the testing machine. This loading apparatus was altered slightly for the strain-rate tests on the No. 5 bend specimens, by replacing the wire cables with chain-link adapters, so that the anticipated higher loads could be obtained.

Loading Systems for Size-Effect Torsion Specimens

In order to load the No. 1- and No. 5-size torsion specimens used in the size-effect program on plaster, it was necessary to design torsional grips for twisting these specimens. These torsion grips or heads are shown in Figure 24 and Figure 25. The flange of each head was designed to

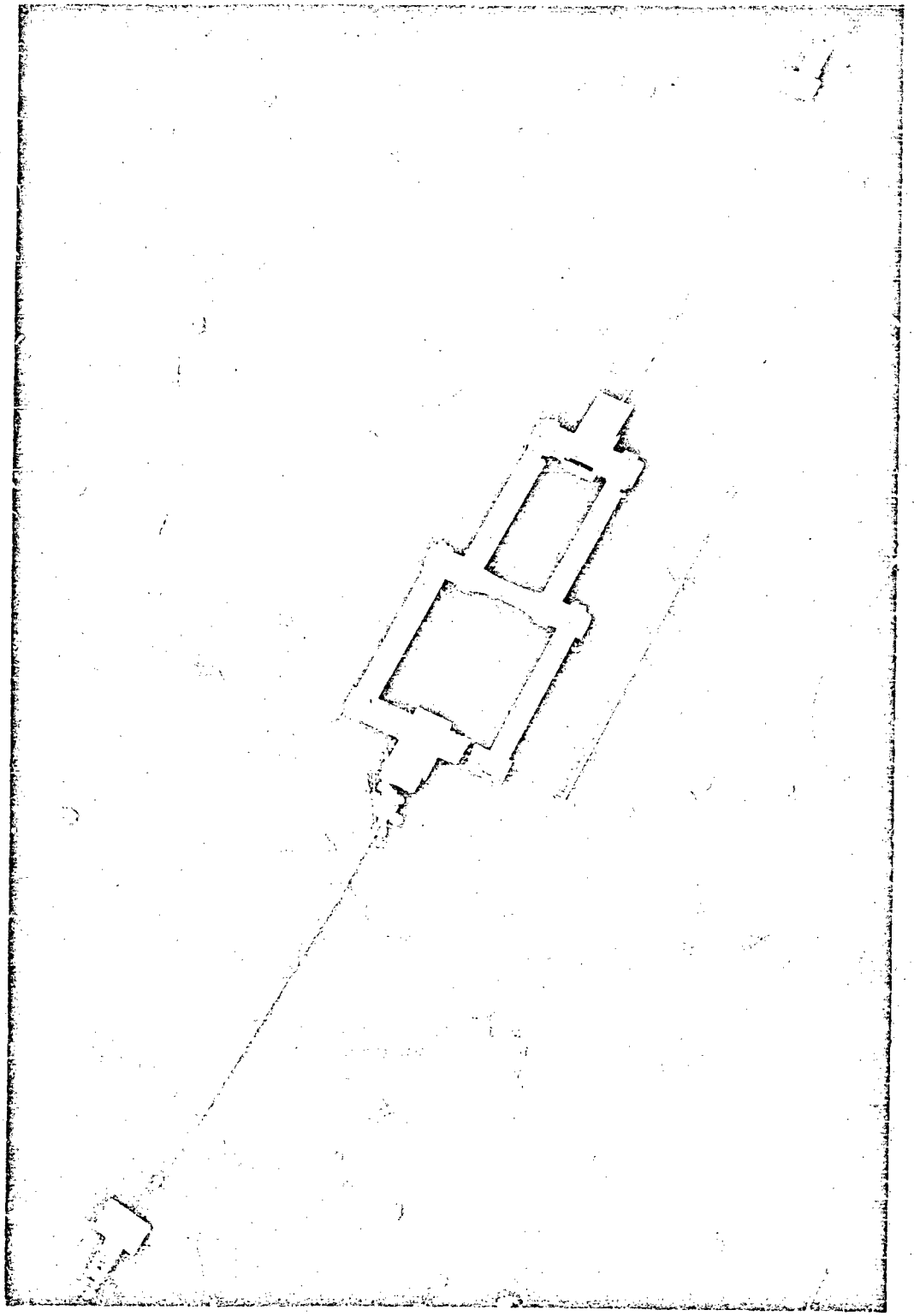

91322

FIGURE 23. LOADING APPARATUS FOR NO. 1-SIZE ALTERNATE BEND-TEST SPECIMEN

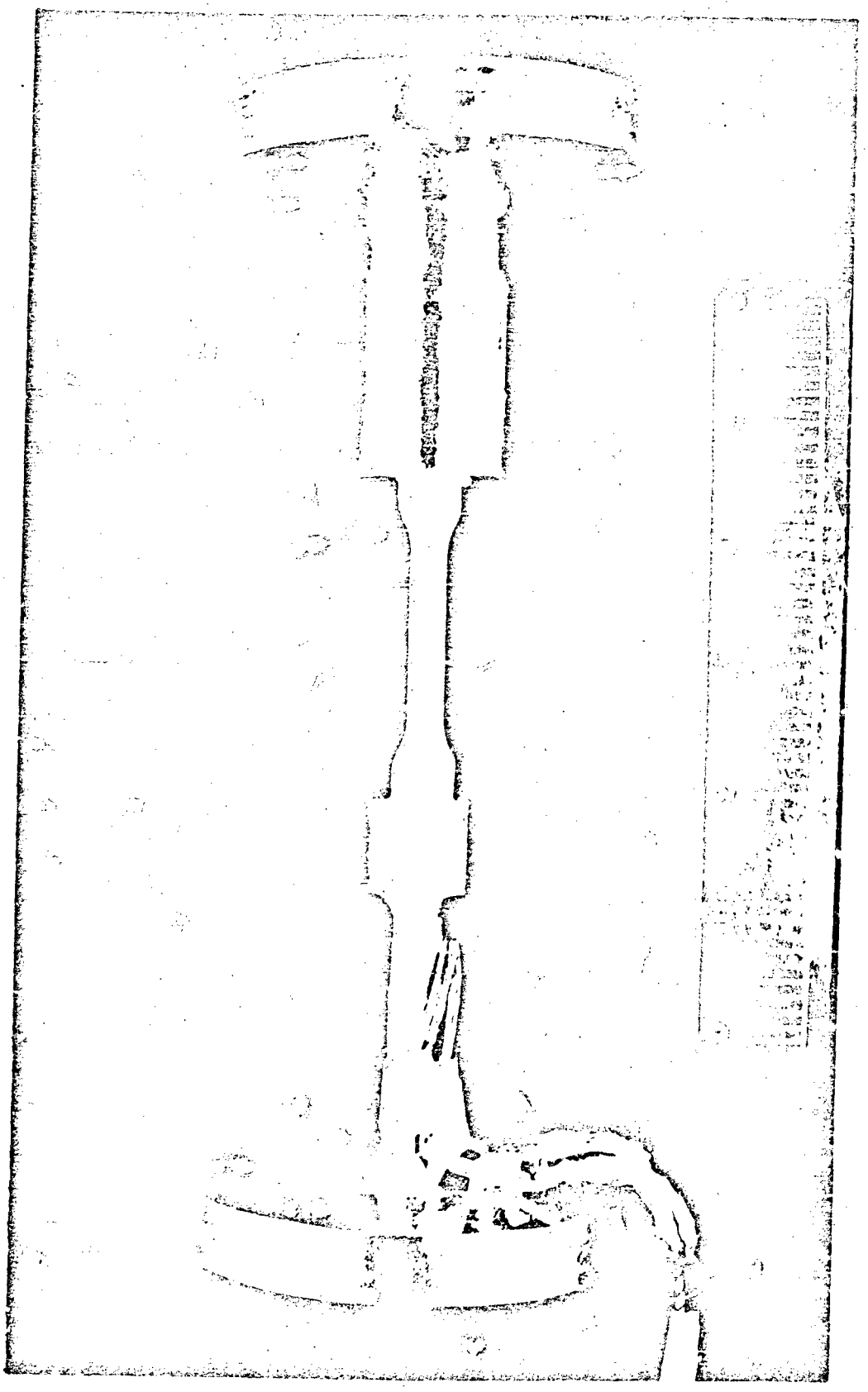

95198

FIGURE 24. LOADING SYSTEM FOR NO. 1-SIZE PLASTER TORSION SPECIMEN

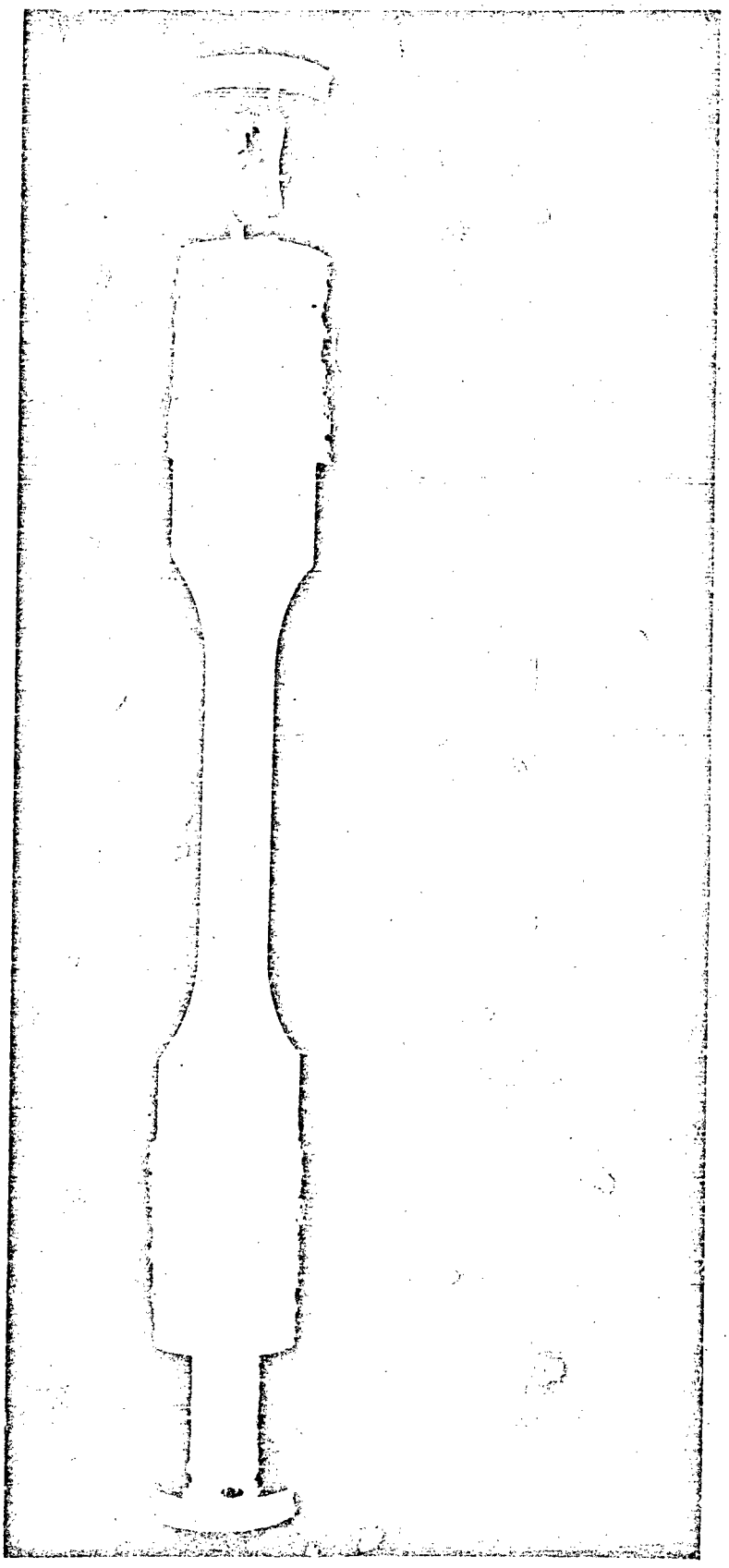

95197

FIGURE 25. LOADING SYSTEM FOR NO. 5-SIZE PLASTER TORSION SPECIMEN

fasten to the moving or fixed heads of the torsion machine. Each head was machined with a square recess into which the shoulder of the torsion specimen was fitted.

One torsion head of each pair was machined with a reduced or "necked-down" section. Four SR-4 strain gages were cemented to this reduced section with the axis of each gage at 45 degrees to the axis of the torsion head. These gages were oriented such that, when torque was applied to the head, two of the gages measured the principal tensile strain in the shank and the other two measured the principal compressive strain. The two pairs of gages were connected to opposite arms of a strain indicator. The strain from each dynamometer was calibrated against a known torque. The dynamometer for the No. 1-size specimen is at the left in Figure 24, and the dynamometer for the No. 5-size specimen is at the right in Figure 25. The torque at fracture for the No. 1- and No. 5-size specimens was determined from these dynamometers.

Biaxial Test Specimen

A biaxial specimen was developed during this period in an effort to extend the study of the effect of stress state on fracture to more complex and realistic states of stress. Essentially, this specimen, illustrated schematically in Figure 26, was a thick-walled, hollow cylinder which could be subjected simultaneously to an internal pressure and an axial tension or compression. The hollow plaster specimen was formed by casting about an internal assembly. The key part of this assembly was a metal sleeve which acted as a form for the internal surface of the gage section. This sleeve was made of a low-melting alloy which was melted out of the specimen (with warm water) after the plaster shell had hardened.

In the internal assembly, the metal sleeve was held in place by hemispherical caps of brass. These caps were split so that the rubber interlayer, a cylindrical tube of surgical rubber, could be fastened over the metal sleeve. In addition, these caps were constructed to permit the attachment of tension-loading adapters. Figure 27 shows an exploded view of this internal assembly, including the tension adapters. It should be noted that one end of the assembly has a central hole through which the metal from the sleeve could be drained, and through which the hydraulic fluid was admitted. In addition, one of the tension adapters acted as a pressure fitting. Figure 28 shows the entire internal assembly. The final product, the plaster biaxial specimen, is shown in Figure 29.

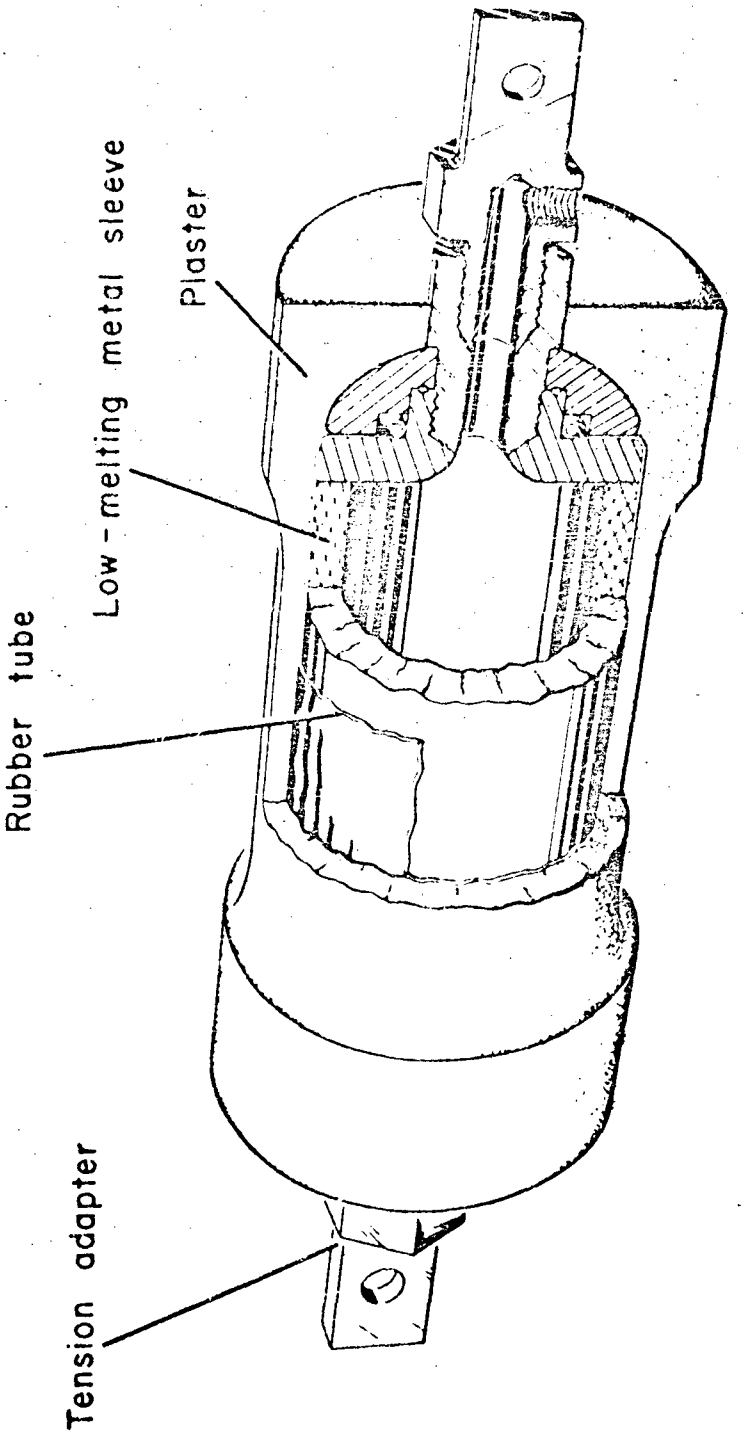

FIGURE 26. BIAXIAL-TEST SPECIMEN

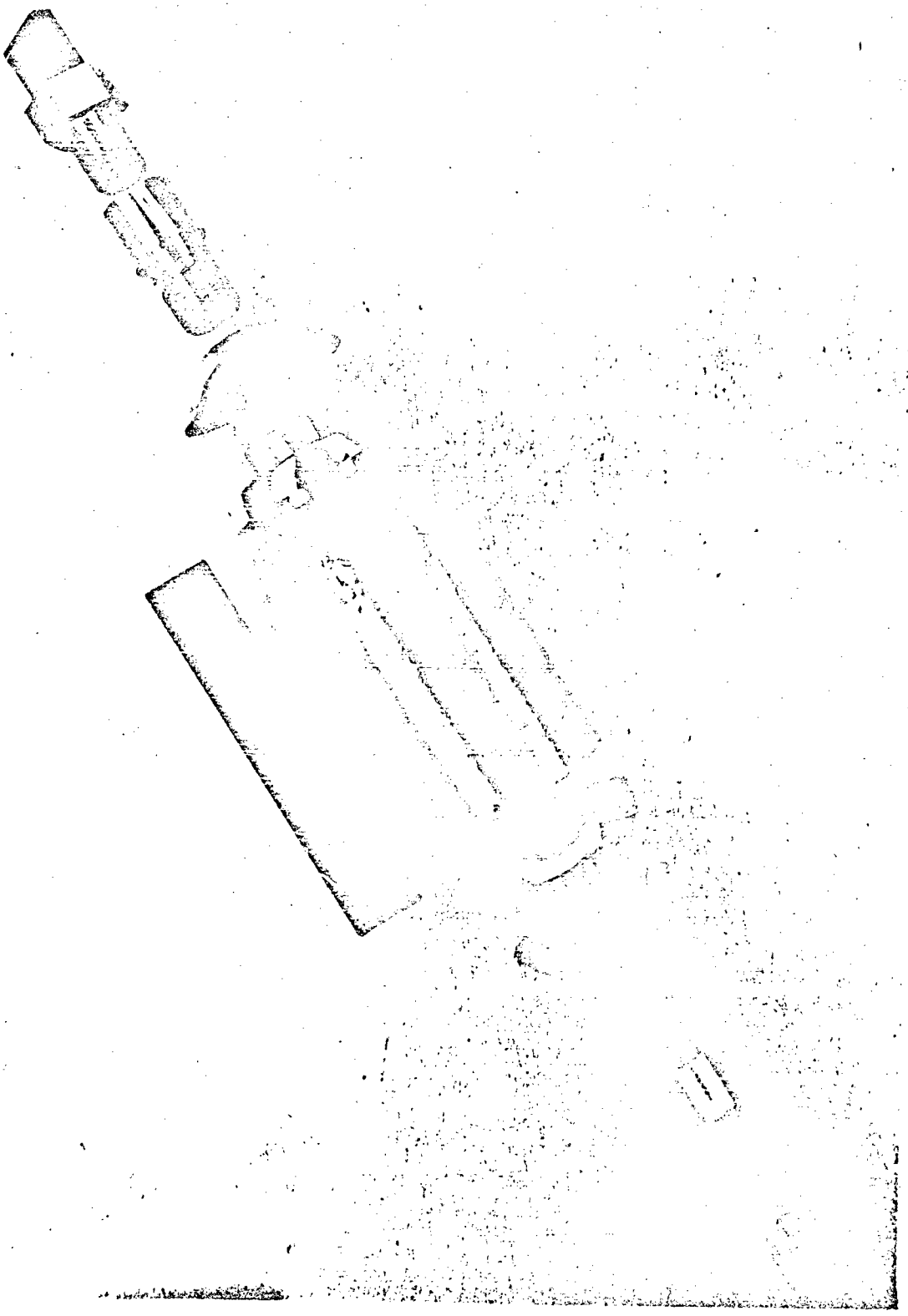

95673

FIGURE 27. EXPLODED VIEW OF INTERNAL ASSEMBLY

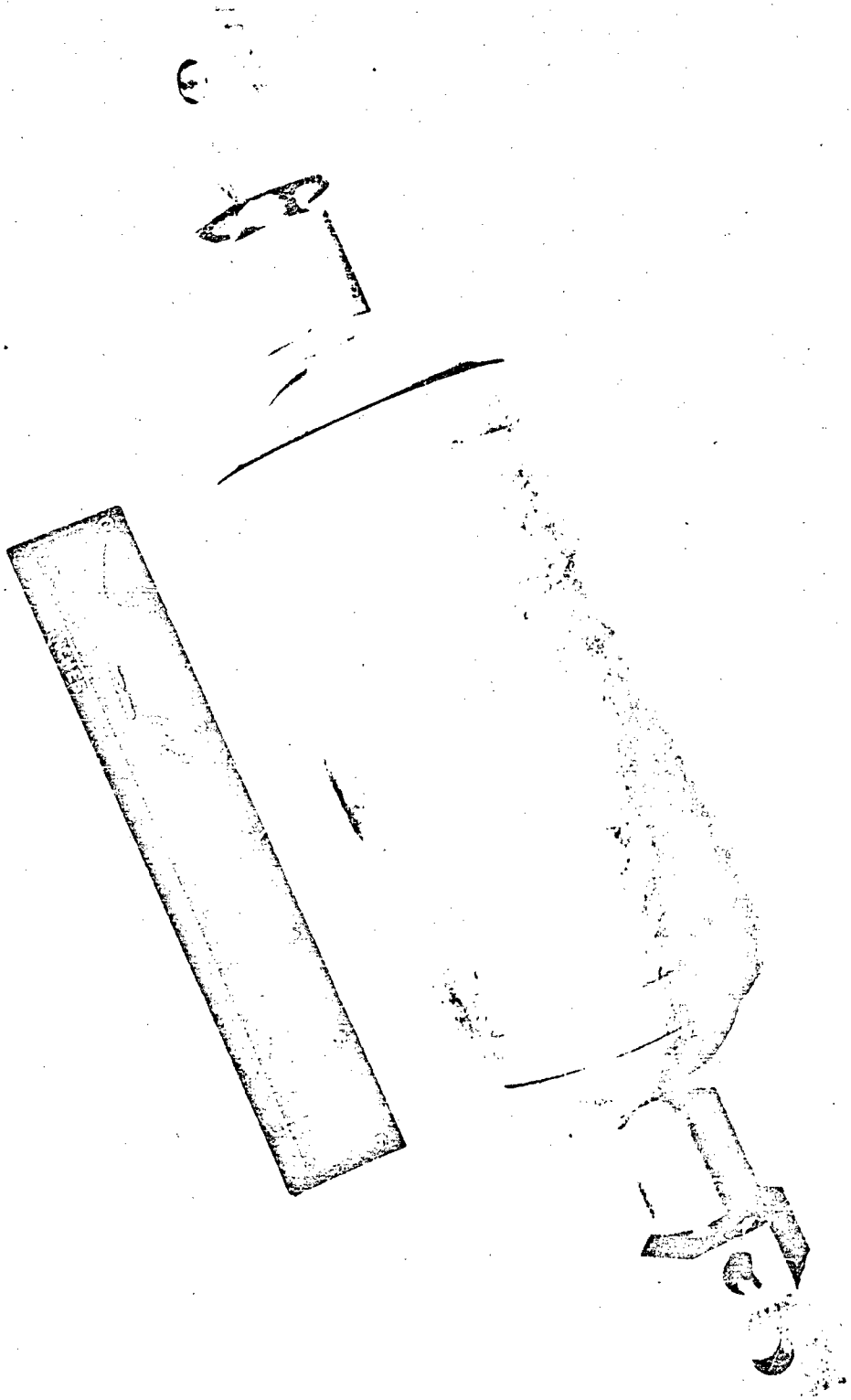

95670

FIGURE 28. INTERNAL ASSEMBLY FOR BIAXIAL SPECIMEN

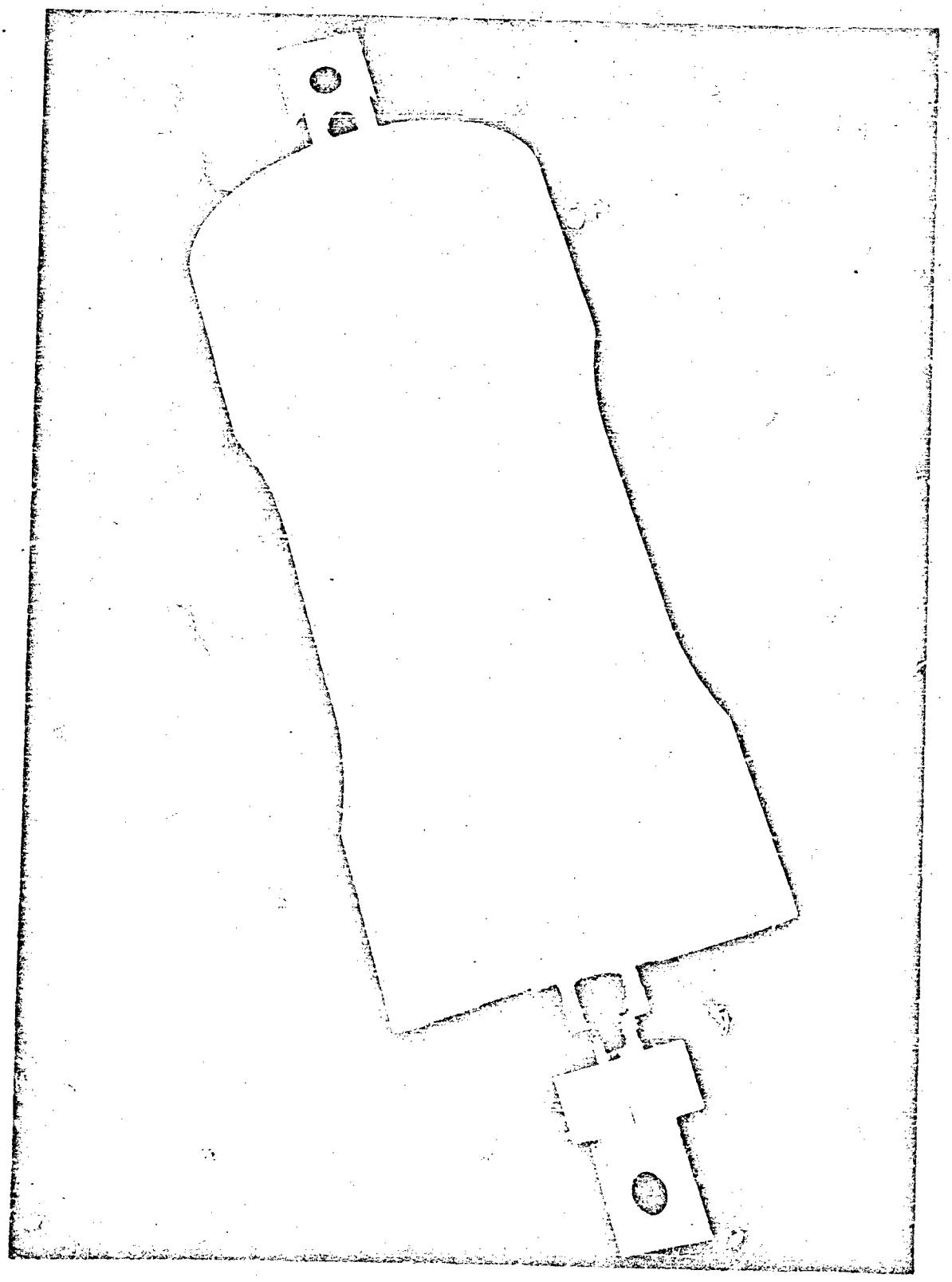

95674

FIGURE 29. HYDROSTONE PLASTER BIAXIAL SPECIMEN

Biaxial Loading System

The system used to supply hydraulic pressure to the biaxial specimen is shown in Figure 30. The specimen was loaded by the hydraulic pressure supplied from an accumulator through a valve. The pressure in the accumulator was built up by means of an aircraft hand pump. Oil was supplied to the system from a reservoir.

With the unloading valve and loading valve closed and the accumulator valve open, the pressure in the accumulator was pumped to a predetermined value and the accumulator valve closed. The specimen could be loaded at any rate then by opening the loading valve a predetermined amount. The pressure in the specimen was relieved by opening the unloading and loading valves.

In order to measure the pressure in the specimen at fracture, strain gages were mounted on the Bourdon tubes of the 0- to 300-psi pressure gage. These strain gages were calibrated with a dead-weight tester.

All the biaxial specimens tested under pressure during this period were loaded with this apparatus. Designs were completed during this period to replace the hand pump with a motor-driven pump to maintain a constant accumulator pressure.

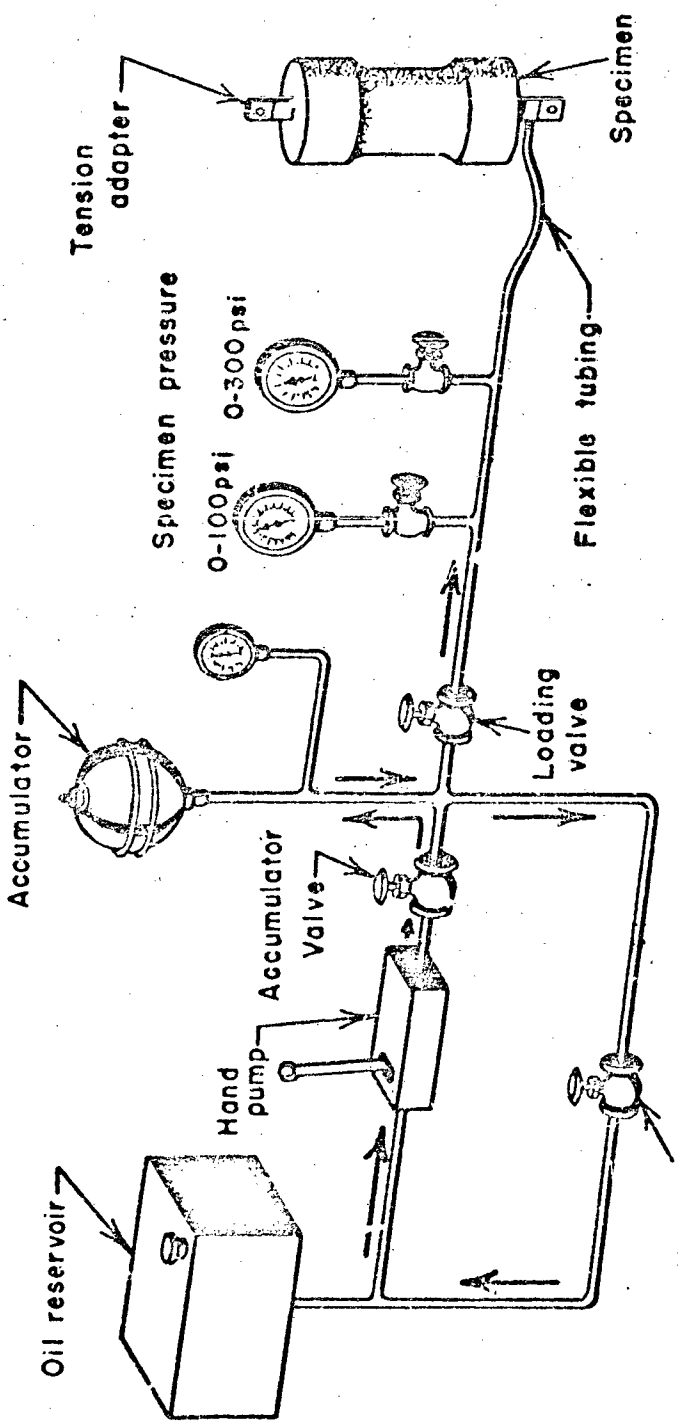

FIGURE 30. HYDRAULIC LOADING SYSTEM FOR PLASTER BIAXIAL SPECIMENS

REFERENCES

1. Griffith, A. A., "The Phenomena of Rupture and Flow in Solids", Trans. Roy. Soc. (London), A, 221, pp 163-198, 1921.

2. Auerbach, F., "Absolute Härtemessung", Ann. Phys., 43, pp 61-100, 1891.

3. Weibull, W., "Investigations Into Strength Properties of Brittle Materials", Ing. Vetenskaps Akad., Handl., No. 149, 1938.

4. Roark, R. J., Hartenberg, R. S., and Williams, R. Z., "The Influence of Form and Scale on Strength", Bull. Univ. Wis. Eng. Exp. Sta. Ser., No. 84, 1938.

5. Roark, R. J., Hartenberg, R. S., "Predicting the Strength of Structures From Tests on Plaster Models", Bull. Univ. Wis. Eng. Exp. Sta. Ser., No. 81, 1935.

6. Voigt, W., "Einige Beobachtungen Über Die Drillungsfestigkeit Von Steinsalzprismen", Ann. Phys., 48, pp 657-662, 1893.

7. Auerbach, F., "Die Härtescala in Absoluten Maasse", Ann. Phys., 58, pp 357-380, 1896.

8. Oberhoffer, P., and Poensgn, W., "Ueber Den Einfluss Des Probestabquerschnittes Auf Die Zug und Biegefestigkeit Von Gusseisen", Stahl u. Eisen, 42, pp 1189-1192, 1922.

9. Pinsl, H., "Quasiisotropie in Gusseisen, Giesserei, 20, pp 105-108, 1933.

10. Meyersberg, G., "Grösseneinfluss und Randeinfluss Auf Die Festigkeit Der Werkstoffe", Trans. Roy. Inst. Technol. Stockholm, No. 53, 1952.

11. Weibull, W., "The Phenomenon of Rupture in Solids", Ing. Vetenskaps Akad., Handl., No. 153, 1939.

12. Davidenkov, N., Shevandin, E., and Wittmann, F., "The Influence of Size on Brittle Strength of Steel", J. Appl. Mechanics, 14, No. 1, p a63, 1947.

13. Timoshenko, S., Theory of Elasticity, First Ed., pp 50-51, McGraw-Hill Book Company, New York, 1934.

14. Frocht, M. M., Photoelasticity, Vol 2, pp 30-31, John Wiley and Sons, Inc., New York, 1948.

15. Campbell, W. R., "Errors in Indicated Strain for a Typical Wire Strain Gage Caused by Prestraining, Temperature Changes, and Weathering", Nat. Advisory Comm. Aeronaut., Tech. Notes 1011, April, 1946.

16. Baumberger, R., and Field, H., "Practical Reduction Formulas for Use of Bonded Wire Strain Gages in Two-Dimensional Stress Fields", Proc. Soc. Ex. Stress Anal., 2, No. 2, 1944.

17. Reinkober, O., Physik. Z., 32, p 243, 1931; Ibid., 33, p 32, 1932.

18. Weibull, W., "A Statistical Theory of the Strength of Materials", Ing. Vetenskaps Akad., Handl., No. 151, 1939.

19. Weibull, W., "The Phenomenon of Rupture in Solids", Ing. Vetenskaps Akad., Handl., No. 153, 1939.

20. Weibull, W., "The Phenomenon of Rupture in Solids", Ing. Vetenskaps Akad., Handl., No. 153, p 22, 1939.

21. Weibull, W., "A Statistical Distribution Function of Wide Applicability", J. Appl. Mechanics, 18, pp 293-297, 1951.

22. Griffith, A. A., "The Phenomena of Rupture and Flow in Solids", Trans. Roy. Soc. (London), A, 221, p 163, 1920; "Theory of Rupture", Proc. Intern. Congr. Appl. Mechanics, p 55, 1924.

23. Timoshenko, S., Theory of Elasticity, First Ed., pp 55-58, McGraw-Hill Book Company, New York, 1934.

24. Nadai, A., Theory of Flow and Fracture of Solids, Vol 1, Second Ed., pp 334-46, 1950.

25. Siebel, E., "Grundlagen Zur Berechnung Des Krafund Arbeitsbedarfs Beim Schmieden Und Walzen", Dr. Ing. Dissertation, Berlin, 1923.

26. Nadai, A., Theory of Flow and Fracture of Solids, Vol I, Second Ed. pp 188-189, 1950.

27. Watstein, D., and Boresi, A. P., "The Effect of Loading Rate on the Compressive Strength and Elastic Properties of Plain Concrete", Nat. Bur. Standards (U.S.), Rep. No. 1523, March 20, 1952.

28. Baker, T. C., and Preston, F. W., "Fatigue of Glass Under Static Loads", J. Appl. Phys., 17, No. 3, pp 170-178, March, 1946.

29. Preston, F. W., and Glathard, J. L., "Fatigue Modulus of Glass", J. Appl. Phys., 17, No. 3, pp 189-195, 1946.

30. Murgatroyd, J. B., "The Mechanism of Brittle Rupture in Glass", J. Soc. Glass Technol., 28, p 406, 1944.

31. Preston, F. W., J. Am. Ceram. Soc., 18, p 220, 1935.

32. Poncelet, F., "A Theory of Static Fatigue for Brittle Solids", Fracturing of Metals, ASM, pp 201-227, 1948.

33. Bartenev, G. M., "Dependence of Tensile Strengths on Duration of Applied Stress for Brittle Fracture", Doklady Akad. Nauk SSSR, 71, pp 23-26, March 1, 1950; "Phenomenon of Brittle Fracture in Silicate Glass", Zhur. Tekh. Fiz., 21, 5, pp 579-588, May, 1951.

34. Hodgdon, F. B., Stuart, D. A., and Bjorklund, F. E., "The Application of Rate Process Theory to Glass — Breaking Strength", J. Appl. Physics, 21, pp 1156-1159, November, 1950.

35. Boas, W., and Schmid, E., Z. Physik, 71, p 703, 1931.

36. Schmid, E., and Siebel, E., Z. Elektrochem., 37, p 447, 1931.

37. MacGregor, C. W., and Welch, L. E., "True Stress-Strain Relations at High Temperatures by the Two Load Method", Trans. Am. Inst. Mining Met. Engrs., 154, pp 423-437, 1943.

38. Lea, F. C., "Effect of Low and High Temperatures on Materials", Proc. Inst. Mech. Engrs., Part II, pp 1053-1096, 1924.

39. Nat. Advisory Comm. Aeronaut. Research Memorandum No. E52H05, August 18, 1952 (See Figure 9).

40. Frocht, M. M., Photoelasticity, Vol 1, pp 380-381, John Wiley and Sons, Inc., New York, 1941.

41. ASTM Manual on Presentation of Data, Am. Soc. Testing Materials, Third Printing, 1940.

OKS/WHD/ADS:at:ng:pl:bep:eab

APPENDIX I

PREPARATION OF DATA

APPENDIX I

PREPARATION OF DATA

Size-Effect Compression Data on Plaster

A specific procedure was used in the calculation of the various data from the size-effect compression tests. In the case of the small, No. 1-size compression specimen, all strain data were calculated taking into consideration the effect of the transverse sensitivity of the strain gages. For those No. 1-size specimens that had only one longitudinal and one transverse strain gage, the longitudinal strain, ϵ_1, was calculated from the equation[16]:

$$\epsilon_1 = \frac{1 - \nu_o K}{1 - K^2} \left[\epsilon_{a1} - K\, \epsilon_{a2}\right], \tag{20}$$

where

ν_o = constant = 0.285,
K = constant depending on the type of gage = 0.01 (for A-7 gages),
ϵ_{a1} = value of indicator strain on the longitudinal gage (in. per in.),
ϵ_{a2} = value of indicator strain on the transverse gage (in. per in.).

The transverse strain, ϵ_2, on this specimen was calculated from:

$$\epsilon_2 = \frac{1 - \nu_o K}{1 - K^2} \left[\epsilon_{a2} - K\, \epsilon_{a1}\right]. \tag{21}$$

It is important to point out that the use of Equations (20) and (21) demands careful consideration of the sign of each term involved, particularly the sign of the indicator strains. In compression, ϵ_{a1} is negative and ϵ_{a2} is positive. In tension, ϵ_{a1} is positive and ϵ_{a2} is negative.

The nominal compression stress, σ, was calculated from:

$$\sigma = \frac{P}{A_o} \text{ (psi)}, \tag{22}$$

where:

P = axial compressive load, lb,
A_o = original cross-sectional area, sq in.

The "true" longitudinal strain, δ_1, based on the concept of "true stress and true strain", was calculated, where necessary, as:

$$\delta_1 = \ln (1 + \epsilon_1) \quad . \tag{23}$$

The transverse "true" reduction of area, q', was calculated as:

$$q' = 2 \ln (1 + \epsilon_2) \quad . \tag{24}$$

For values of ϵ_1 less than 0.001 in. per in., δ_1 and ϵ_1 are equivalent for all practical purposes. Similarly, for values of ϵ_2 less than 0.001 in. per in., q' is equivalent to 2 ϵ_2. In most instances, in the calculation of data, the difference between the "true" strain and the "ordinary" strain was too insignificant to warrant calculation of "true" strains.

In the calculation of Poisson's ratio, a plot of nominal stress, σ, versus "true" longitudinal strain, ϵ_1, was constructed and the slope, E_1, of this curve was determined. A plot of σ versus "true" reduction of area, q', was constructed also and the slope, E_q, of this curve was determined. Then Poisson's ratio, ν, was calculated from the equation:

$$\nu = \frac{1}{2} \frac{E_1}{E_q} \quad . \tag{25}$$

The validity of Equation (25) is immediately apparent for strains less than 0.001 in. per in., since

$$E_1 = \frac{\sigma}{\epsilon_1} \quad ,$$

and

$$E_q = \frac{\sigma}{q} = \frac{\sigma}{2\epsilon_2} \quad .$$

Then:

$$\nu = \frac{1}{2} \frac{\left(\frac{\sigma}{\epsilon_1}\right)}{\left(\frac{\sigma}{2\epsilon_2}\right)} = \frac{\epsilon_2}{\epsilon_1} \quad . \tag{26}$$

For values of strain greater than 0.001 in per in., Equation (25) is still valid in that:

$$\mu = \frac{\frac{1}{2}\left(\frac{\sigma}{\epsilon_1}\right)}{\left(\frac{\sigma}{q'}\right)} = \frac{1}{2}\frac{q'}{\epsilon_1} = \frac{\ln(1+\epsilon_2)}{\ln(1+\epsilon_1)} .$$

Where:

$$\ln(1+\epsilon_2) = \epsilon_2 - \frac{\epsilon_2^2}{2} + \frac{\epsilon_2^3}{3} - \frac{\epsilon_2^4}{4} + \ldots$$

$$\ln(1+\epsilon_1) = \epsilon_1 - \frac{\epsilon_1^2}{2} + \frac{\epsilon_1^3}{3} - \frac{\epsilon_1^4}{4} + \ldots ,$$

then:

$$\nu = \frac{\epsilon_2 - \frac{\epsilon_2^2}{2} + \frac{\epsilon_2^3}{3} - \frac{\epsilon_2^4}{4} + \ldots}{\epsilon_1 - \frac{\epsilon_1^2}{2} + \frac{\epsilon_1^3}{3} - \frac{\epsilon_1^4}{4} + \ldots} \doteq \frac{\epsilon_2}{\epsilon_1} ,$$

where, for values of ϵ_1 and ϵ_2 as high as 0.1 in. per in., it is within experimental accuracy to drop all terms of higher order.

The "true" stress, σ', was calculated as:

$$\sigma' = \frac{P}{A_T} \text{ (psi)} , \tag{27}$$

where: A_T = "true" area = $(1+\epsilon_2)^2 A_o$(sq in.).

For those No. 1-size compression specimens which had three longitudinal gages, the longitudinal strains, ϵ_1, ϵ_3, and ϵ_4, were calculated from the equations:

$$\epsilon_1 = \left(\frac{1-\nu_o K}{1-\nu K}\right)\epsilon_{a1} , \tag{28}$$

$$\epsilon_3 = \left(\frac{1 - \nu_0 K}{1 - \nu K}\right) \epsilon_{a3} , \tag{28a}$$

$$\epsilon_4 = \left(\frac{1 - \nu_0 K}{1 - \nu K}\right) \epsilon_{a4} , \tag{28b}$$

where ν was the value of Poisson's ratio determined from the No. 1-size compression specimen of the same batch.

The average longitudinal strain, ϵ_c, was determined and used to calculate, where desired, the average longitudinal true strain, δ_c, from the equation:

$$\delta_c = \ln (1 + \epsilon_c) \tag{29}$$

$$= \epsilon_c \qquad (\epsilon_c < 0.001) \tag{29a}$$

Stress-strain curves were drawn for these specimens with three gages by plotting stress, σ, versus average longitudinal strain, ϵ_c. The modulus of elasticity, E, was determined then as the slope of the stress-strain curve. Compression strengths were calculated, where possible, from Equation (27) above.

In the case of the larger, No. 5-size compression specimens, the data were calculated using essentially the same procedure and formulas as were used for calculating data for the No. 1-size specimen. The value of the constant, K, in Equations (20), (21), (28), (28a), and (28b), however, had a value of +0.035 (for A-5 gages).

As three longitudinal gages and a transverse gage were mounted on each of the No. 5 specimens, it was possible to obtain both Poisson's ratio and Young's modulus from each specimen. Hence, the value of ν used in Equations (28a) and (28b) was that value determined from the same specimen.

Size-Effect Tension Data on Plaster

The testing procedure for conducting tension tests on the smallest, the No. 1-size, alternate tension specimen was essentially similar to that for compression testing. The data obtained from the tension test of No. 1-size specimens of Hydrostone were calculated in a somewhat different manner from that used in the calculation of data from the size-effect compression specimens. The strains observed were so small, even at fracture (about 550 microinches per in.), that the magnitude of the

correction introduced by using strain relations similar to Equation (26) was within experimental error. In view of this fact, the indicator strains recorded during the test were used directly as final data. Also, stresses were calculated on the basis of the original cross-sectional area. Young's modulus was determined from a plot of this stress versus average indicator strain.

In the calculation of Poisson's ratio, a plot of nominal stress, σ, versus the average indicated longitudinal strain, ϵ_{a1}, was constructed and the slope, E, of this curve was determined. A plot of σ versus the average observed transverse strain, ϵ_{a2}, was constructed also and the slope, Q, of this curve was measured, then Poisson's ratio, ν, was calculated from the equation:

$$\nu = \frac{Q}{E} \quad . \tag{30}$$

A value of ν was calculated for each elastic determination and the average value reported.

The data obtained from the large, No. 4-size alternate tension specimen were calculated in the same manner as the data for the No. 1-size tension specimen.

Size-Effect Bend Data on Plaster

The strain data obtained from the No. 1-size bend specimens were calculated without consideration of the effect of transverse sensitivity. As in the tension tests, the strains observed were too small to warrant correction. In addition, since it was impractical to measure transverse strains on the No. 1-bend specimen due to its small size, no corrections could be made. In these tests, Young's modulus, E, was determined for each surface, tension and compression of the bend specimen. Here, E was calculated as the slope of the plot of the nominal bend stress, σ_b, versus the indicated longitudinal strain. The nominal bend stress, σ_b, was calculated from the expression:

$$\sigma_b = \frac{3Pc}{bd^2} \quad , \tag{31}$$

where c, b, and d are defined in Figure 7, and where P was the total axial load.

The strain data from the No. 5-size bend specimens also were calculated without consideration of the effect of transverse sensitivity. Young's modulus was determined for the No. 5 specimen in exactly the same manner as for the No. 1-size specimen. Poisson's ratio was calculated for the

No. 5 bend specimen in the same manner as for the large tension specimen; that is, using Equation (30). A value of Poisson's ratio was obtained for each surface, tension and compression. The nominal bend stress, σ_b, was used in these calculations.

Size-Effect Torsion Data on Plaster

The strain data taken from those tests on the No. 5 torsion specimen for the purpose of determining the strain rate were not corrected for transverse sensitivity. The modulus of rigidity, G, obtained from the tests on the No. 5 torsion specimen was determined as the slope of the curve of shear stress versus shear strain; that is, the slope of the plot of the shear stress, σ_T (Equation 1), versus the shear strain, γ_{xy}. The shear strain was calculated by means of the relation:

$$\gamma_{xy} = \frac{\theta_t d}{2L} \quad , \tag{32}$$

where:

d = diameter of specimen, inches,
L = distance between mirrors, inches,
θ_t = angle of relative twist between mirrors, radians.

In the tests on the No. 5 torsion specimen, a value of L = 5 inches was used. The value of G reported for each specimen was the average of the slopes of at least three such plots.

Size-Effect Compression Data on Porcelain

The elastic data determined from the size-effect compression specimens of porcelain were calculated in precisely the same manner as the data from the compression specimens of plaster.

Combined-Stress Data on Plaster

The method of calculating the data from the tests on the biaxial-stress specimen of plaster is described in detail in the body of this report. It should be pointed out again, however, that Equations (20) and (21) were used to correct all observed strains for transverse sensitivity.

Strain-Rate Data on Plaster

The method of calculating the strain data and fracture data from the strain-rate tests conducted on size-effect specimens of plaster is described in detail in the body of this report.

APPENDIX II

STATISTICAL TREATMENT OF DATA

APPENDIX II

STATISTICAL TREATMENT OF DATA

The data obtained from the tests conducted during this period were organized and treated in a specific manner. In the treatment of all these data, it was necessary to assume that the data from any one observation or test were subject to statistical treatment. Hence, the most probable value of a measured quantity was assumed to be the arithmetic mean, X_m, of the N measurements, X_1, X_2, X_3, $\cdots$ X_n $\cdots$ X_N, or the quantity:

$$X_m = \frac{X_1 + X_2 + X_3 \cdots + X_n \cdots + X_N}{N} = \frac{\Sigma X_n}{N} \quad . \tag{33}$$

After the deviations from the mean, $x_n = X_n - X_m$, were obtained, the approximate values of the standard deviation, a, of a single observation and the probable error, P_o, of the mean were determined.

In the treatment of standard-deviation data under Weibull's theory, Equation (34) was found to be appropriate as a definition of the standard deviation:

$$a^2 = \frac{\Sigma(X_n - X_m)^2}{N - 1} \quad . \tag{34}$$

All standard deviations appearing in this report were calculated according to Equation (34).

In this report, all probable errors have been computed on the basis of the principle that 9 out of every 10 observations should fall within the limits $X_m - P_o$ and $X_m + P_o$; that is, on the basis of a probability of 0.90. Then, according to this concept, the probable error, P_o, of the mean of a series of observations may be defined as:

$$P_o = \pm \beta a \quad , \tag{35}$$

where a is the standard deviation as defined by Equation (34), and β is a constant depending on N. For values of N greater than 25, β is approximately equal to

$$\beta = \frac{1.645}{\sqrt{n-3}} \text{ (approximately)} \quad . \tag{36}$$

Values of β for N less than 25 appear in Table II, Supplement A, of the "ASTM Manual on Presentation of Data".(41)

APPENDIX III

WEIBULL'S STATISTICAL THEORY OF STRENGTH

APPENDIX III

WEIBULL'S STATISTICAL THEORY OF STRENGTH

Weibull's theory is founded on the fact that no material exhibits a unique fracture strength. If 100 seemingly identical specimens were broken in identically the same way, it is quite possible that no two would fracture at the same load. Instead, they might break over a wide range of loads; however, the greater portion most probably would fracture within a narrow range of loads. Intuition would lead us to believe that the strength of a material might lend itself to statistical treatment. This is precisely what Weibull has done.

Suppose we take a chain link and pull it until it breaks. We know already that, if we break six more links from the same chain, they will not all break at the same load, but we can predict that a certain proportion of the next six will have broken by the time we reach a certain load, P. In other words, we can predict a definite 50-50 or 40-60 chance that they will be broken at the load, P.

Instead of breaking one link at a time, suppose we fasten two links together and break the combination. Now there is a greater chance that the combination will be broken at the load, P. If we had a chain, or a thousand such links, each with a 50-50 chance of being broken at the load P, at least one of these links is almost certain to have broken by the time we reach P. Thus, the longer we make the chain, the greater is the chance that it will be broken when we reach the load, P.

Now let us imagine a tension specimen to be made up of a multitude of fibers, each acting like a chain. We can see that, when a uniform load is applied to the specimen, each of these fibers will have a certain probability of breaking, depending on how long it is. If each fiber has a 50-50 chance of breaking by the time we reach P, and there are 100 fibers, then there is a greater than 50-50 probability that one of these fibers will be broken when we reach the load P. We can see now that the larger a specimen is, the greater is the chance that it will break at a certain load. We can say now that the probability that a specimen will break at a load is a function of its volume.

Suppose that we take two identical links and pull one with a force P and the other with a force 2P. If either were to break, it is obvious that the probability is much greater that the latter will be the one. This same argument would apply to two chains. Now we see that the probability or the odds that a specimen of fibers will break depends on how heavily each fiber is loaded.

We know that, if there is a 40-60 chance that a fiber will be broken by the time the load P is reached, there is also a 60-40 chance or 0.60 probability that the fiber will not break under a load P. But what is the actual probability that a certain fiber will withstand the load P, and how is this probability related to the size of the fiber? The answer to these questions is the crux of Weibull's theory. Weibull has assumed that the probability of a fiber's withstanding a load is related to the volume of the fiber by a certain function, which he calls the material function. (This is equivalent to the assumption of a distribution function.) He assumed further, quite logically, that the probability of fracture is related to the load on the fiber. The success of this theory depends on how well the assumed material function fits the actual material.

If, for example, we consider the experimental strengths obtained from a series of specimens, we will find that there is a definite relationship between the probability that a specimen will fracture and the stress to which it is subjected. This relationship is often called the distribution function of the strength. The No. 1 tension specimen, the No. 4 tension specimen, the No. 5 bend specimen, and the No. 1 bend specimen each has a unique distribution function. In other words, the distribution function is dependent upon the size and design of the specimen. A typical distribution curve of strength is shown in Figure 31.

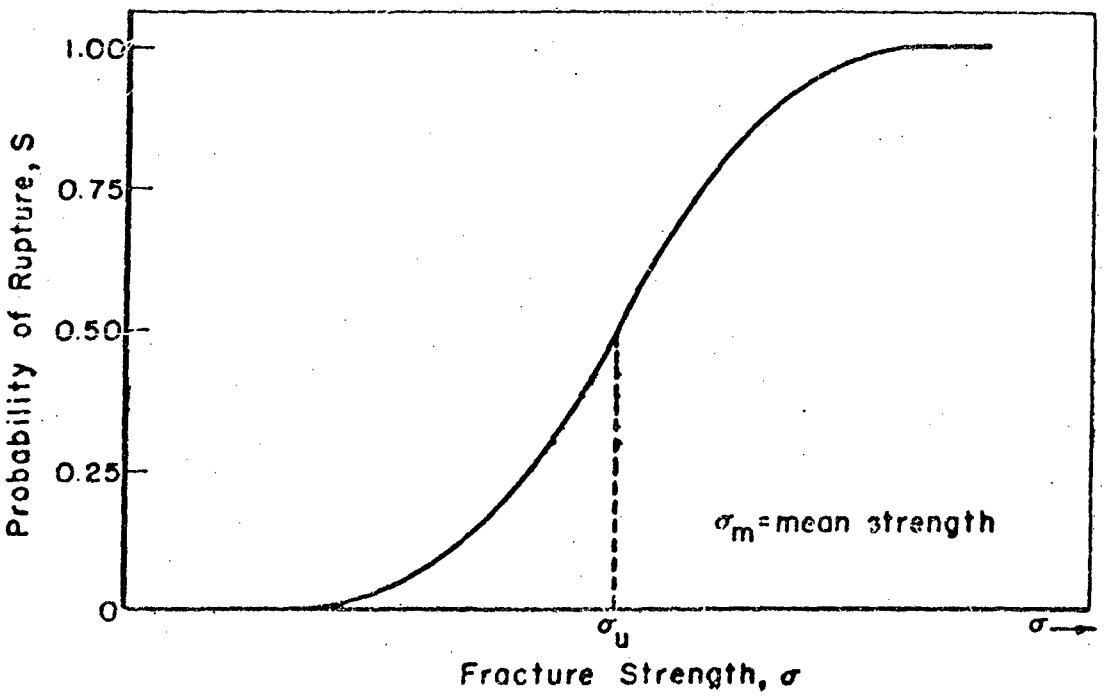

FIGURE 31. TYPICAL DISTRIBUTION CURVE OF STRENGTH

A-4581

These concepts can be used to show that the mean strength of a set of specimens (σ_m in Figure 31) is equivalent to the first moment of the distribution about $\sigma = 0$.

Using this concept of probability, Weibull has defined the fracture strength of a brittle material as:

$$\sigma_m = \int_0^{\infty} \sigma dS \ , \tag{37}$$

where σ denotes the stress state in a body and S is the probability of fracture's having occurred when the stress state, σ, is reached.

As we have pointed out above, a specimen may be considered to be made up of many fibers. Each of these fibers can be considered to have its own probability of withstanding a load, but the probability for the entire specimen will be the result of considering the individual probabilities of all the fibers. For example, if we bend a specimen, one-half of the fibers in the gage section will be in tension, and the remaining fibers will be in compression. Weibull has assumed that fibers in compression have a zero probability of fracture (that they will not break under compression). As a result, these compression fibers do not contribute to the probability for the entire specimen. Therefore, an entire half of the specimen is neglected in Weibull's consideration of the probability of a specimen's withstanding a bending load. The important point here is that, in considering the probability of a specimen's withstanding a load, every fiber must be considered.

Using this concept, Equation (37) defining the fracture strength of a body can be rewritten in the form:

$$\sigma_m = \int_0^{\infty} e^{-B} d\sigma \ , \tag{38}$$

where B is defined as the "risk" of fracture of the entire body, and B is a function of the probability of fracture of the entire body, and hence, at the same time, a function of the probability of fracture at every point in the body. The risk of fracture, B, is a logarithmic function of the probability of fracture, S, of the body; that is,

$$B = - \log (1 - S) \ . \tag{39}$$

Weibull proposes that the risk of fracture, B, is related to the volume of a body, V, and the stress state, σ, by the relation:

$$B = \int_V n(\sigma)\, dV \quad . \tag{40}$$

The function $n(\sigma)$ is the material function. He also assumes that the material function may take the form

$$n(\sigma) = K\sigma^m \quad , \tag{41}$$

where K is a constant and m is a constant designated as the material constant.

The risk of fracture, B, of the entire body, in turn, may be defined in terms of B', the risk of fracture at a particular point in the body; that is,

$$B = \int_V B'\, dV \quad . \tag{42}$$

In principle, B' represents the total risk of fracture's occurring at a point in a body subjected to stress. Since a probability of fracture exists for every plane through a point on which the normal stress is tensile, the total probability of fracture, B', at a point must consider the probability associated with every plane on which the normal stress is tensile. Then B' can be shown to be of the form

$$B' = \iint n_1(\sigma) \cos\phi\, d\phi\, d\psi \, , \tag{43}$$

where ϕ and ψ are defined in Figure 2 of WADC Technical Report No. 52-67.

Then Equations (43), (42) and (38) can be used to determine the fracture strength of a body under any state of stress.

The Effects of Size and Stress State on Strength

It can be seen from the above discussion that the strength of a body in the concept of Weibull's theory is the composite result of the stress state at every point in a body, as well as of the gross size of the body.

When the concepts outlined above are combined with this definition of strength, Equation (38), the following fracture strengths are obtained for the following simple stress states:

Tension (For any cross section):

$$\sigma_d = \frac{I_m}{[KV]^{\frac{1}{m}}} \quad , \tag{44}$$

where:

σ_d = fracture strength in tension,
K = a constant,
V = volume of the gage section,
m = a constant depending on the material,

$$I_m = \int_0^\infty e^{-Z^m} dZ, \text{ a constant depending on the value of m.}$$

Bending (Rectangular cross section):

$$\sigma_b = \frac{I_m}{\left[\frac{KV}{2m+2}\right]^{\frac{1}{m}}} \quad , \tag{45}$$

where σ_b = fracture strength in pure bending.

Torsion (Circular cross section):

$$\sigma_T = \int_0^{\infty} e^{-B}\, dr_p \,, \tag{46}$$

where:

σ_T = fracture strength in torsion,
r_p = maximum shear stress in the gage section,

$$B = 2\pi L \int_0^r \rho B' d\rho \,,$$

where:

L = length of the gage section,
r = radius of the gage section,

$$B' = 2k_1 r_p^m \int_0^{\pi/2} \cos^{2m+1}\phi\, d\phi \int_0^{\pi/2} \sin^m 2\psi\, d\psi \,,$$

ρ = radius to the point where B' is evaluated,

and where:

k_1 = a constant.

It can be seen from Equations (44), (45), and (46) that the strengths of tension, bending, and torsion specimens are functions of the volume of the specimen. In theory, every point in a body at which there is a probability of fracture, regardless of how small, should be considered as contributing to the fracture characteristics of the entire body. This means that the volume associated with all of these points should be used. In this study, however, only the points in the gage section have been considered and, hence, the volume used in these expressions for strengths has been the volume of the gage section. This simplification seemed justified in the light of the relatively small probability of fracture's occurring at points outside the gage section. This simplification was substantiated by the size-effect tests on Hydrostone in tension, bending, and torsion, in which the great majority of the specimens fractured in the gage section.

It can be seen now, if we apply Equation (44) to two similar tension specimens of different sizes but of the same material, that the volume, V, is the only factor that changes. Let us compare, for example, the No. 1- and the No. 4-size alternate tension specimens. From Equation (44), the ratio of the fracture strengths of the two specimens becomes:

$$\frac{\sigma_{d1}}{\sigma_{d4}} = \left[\frac{V_{d4}}{V_{d1}}\right]^{\frac{1}{m}} , \qquad (47)$$

where:

σ_{d1} = strength of No. 1-size tension specimen,
σ_{d4} = strength of No. 4-size tension specimen,
V_{d1} = volume of No. 1-size tension specimen,
V_{d4} = volume of No. 4-size tension specimen.

If we compare the No. 1- and the No. 5-size alternate bend specimens, the ratio of the fracture strengths from Equation (45) becomes:

$$\frac{\sigma_{b1}}{\sigma_{b5}} = \left[\frac{V_{b5}}{V_{b1}}\right]^{\frac{1}{m}} , \qquad (48)$$

where:

σ_{b1} = strength of No. 1-size bend specimen,
σ_{b5} = strength of No. 5-size bend specimen,
V_{b1} = volume of No. 1-size bend specimen,
V_{b5} = volume of No. 5-size bend specimen.

Although it is not immediately obvious from Equation (46), the same form of equation can be derived for the No. 1- and the No. 5-size torsion specimens; that is:

$$\frac{\sigma_{T1}}{\sigma_{T5}} = \left[\frac{V_{T5}}{V_{T1}}\right]^{\frac{1}{m}} , \qquad (49)$$

where:

σ_{T1} = strength of No. 1-size torsion specimen,
σ_{T5} = strength of No. 5-size torsion specimen,
V_{T1} = volume of No. 1-size torsion specimen,
V_{T5} = volume of No. 5-size torsion specimen.

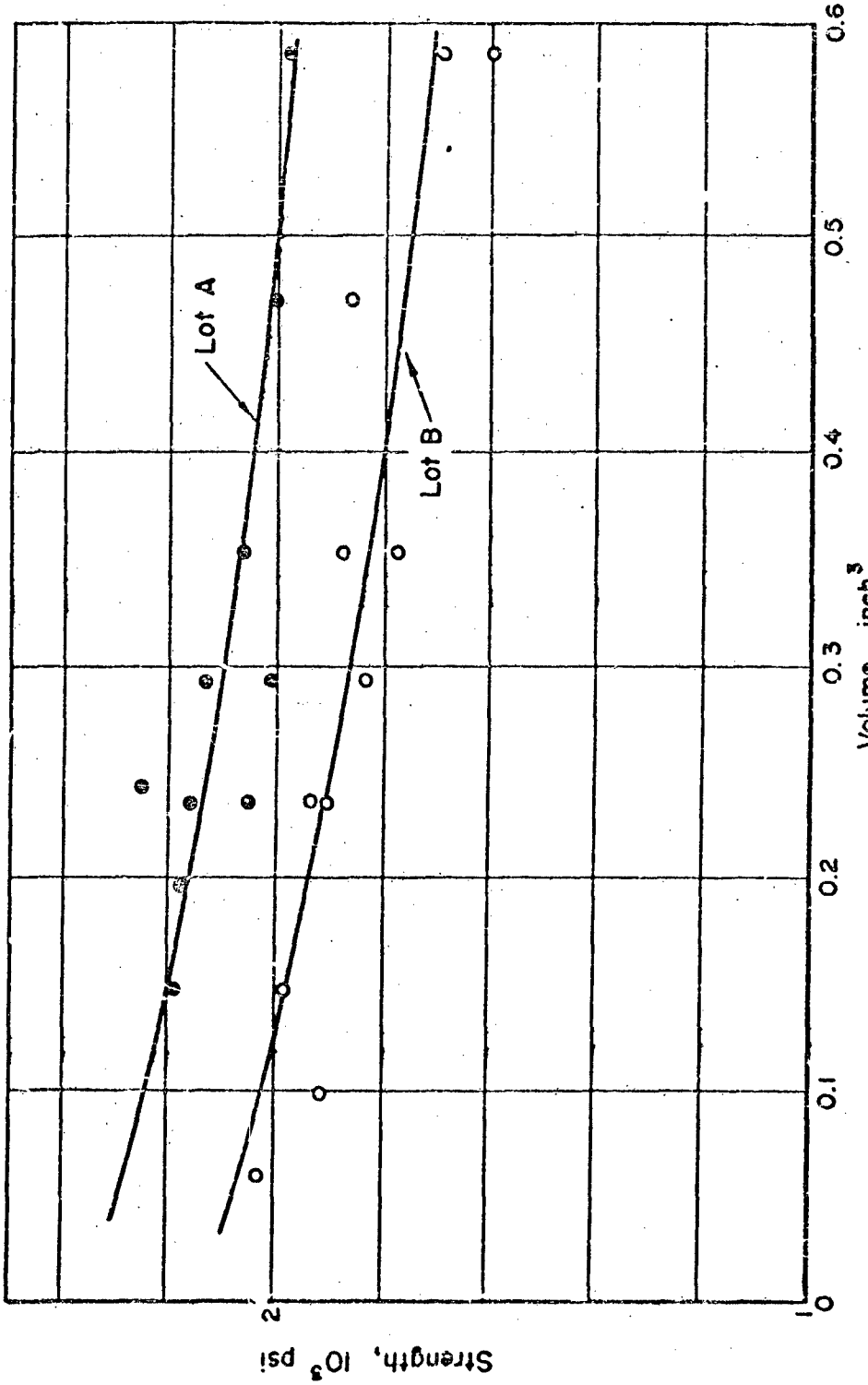

FIGURE 32. VARIATION OF STRENGTH WITH GAGE-SECTION VOLUME OF HYDROSTONE SIZE-EFFECT BEND SPECIMENS

The values of the material constant, m, in Table 12 of this report were obtained from Equations (47), (48), and (49).

The bend data reported in Table 4 of WADC Technical Report No. 52-67 also were analyzed to determine the material constant, m, for Hydrostone plaster. An average value of m = 12 was determined from these data. This determination was accomplished by use of the curves in Figure 32, where each point represents the mean of a series of tests. Equation (48) of this report was used in these determinations.

The values of m determined from size-effect data and reported in Table 12 indicate that, for Hydrostone plaster, m has a value of the order of 12 to 14. When a value of m = 12 is used, it can be shown that, for Hydrostone, the ratio of the strength of a tension specimen to that of a torsion specimen becomes:

$$\frac{\sigma_d}{\sigma_T} = \left[\frac{V_T}{10\,V_d}\right]^{\frac{1}{12}} \quad . \tag{50}$$

Similarly, the ratio of the strength of a bend specimen to the strength of a torsion specimen becomes:

$$\frac{\sigma_b}{\sigma_T} = \left[\frac{2.6\,V_T}{V_b}\right]^{\frac{1}{12}} \quad . \tag{51}$$

Also, the ratio of the strength of a bend specimen to that of a tension specimen of Hydrostone becomes:

$$\frac{\sigma_b}{\sigma_d} = \left[\frac{26\,V_d}{V_b}\right]^{\frac{1}{12}} \quad . \tag{52}$$

Equations (50) and (51) were used in calculating the predicted strengths reported in Table 16 of this report.

Effects of Stress State and Size on the Standard Deviation of the Strength

It has been pointed out that the mean strength, σ_m, of a set of specimens has been defined by Weibull as equivalent to the first moment of the distribution about $\sigma = 0$. In general, the nth moment, u_n', of the distribution is defined by the integral

$$\mu_n' = \int_0^1 \sigma^n \, dS \ , \tag{53}$$

and, hence, the first moment, μ_1', becomes

$$\mu_1' = \int_0^1 \sigma \, dS = \sigma_m \ .$$

Similarly, the nth moment, μ_n, of the distribution about the mean $\sigma = \sigma_m$ is defined by the integral

$$\mu_n = \int_0^1 (\sigma - \sigma_m)^n \, dS \ . \tag{54}$$

From this definition, it can be shown that the square of the standard deviation, a, is equivalent to the second moment of the distribution about the mean, σ_m; that is:

$$a^2 = \mu_2 = \int_0^1 (\sigma - \sigma_m)^2 \, dS \ , \tag{55}$$

where σ is the strength of a particular specimen of the series (which may vary from one to infinity), S is the probability of fracture corresponding to σ, and σ_m is the ultimate strength of the series as defined by Equation (37). Weibull points out that

$$a^2 = \int_0^1 \sigma^2 \, dS - \int_0^1 2\sigma_m \sigma \, dS + \int_0^1 \sigma_m^2 \, dS = \int_0^1 \sigma^2 \, dS - \sigma_m^2 \tag{56}$$

and that

$$\int_0^1 \sigma^2 \, dS = 0 \ . \tag{57}$$

Hence, the square of the standard deviation can be defined as

$$a^2 = \int_0^\infty e^{-B} d(\sigma^2) - \sigma_m^2 \quad , \tag{58}$$

where

$$B = \int_V n(\sigma)\, dV \quad . \tag{40}$$

If we let $n(\sigma) = k\sigma^m$, for a tension specimen with an ultimate strength, σ_d,

$$B = \int_V n(\sigma)\, dV = \int_{-h}^{h} k\sigma^m (bL)\, dX = Vk\sigma^m; \tag{59}$$

then

$$a^2 = \int_0^\infty e^{-Vk\sigma^m} d(\sigma^2) - \sigma_d^2 \quad . \tag{60}$$

If we let

$$Z = (Vk)^{\frac{2}{m}} (\sigma^2) \quad , \tag{61}$$

then

$$a^2 = \frac{1}{[Vk]^{\frac{2}{m}}} \int_0^\infty e^{-Z^{\frac{m}{2}}} dZ - \sigma_d^2 \quad . \tag{62}$$

Then the standard deviation, a_d, in tension can be determined from

$$a_d^2 = \frac{I_{m/2}}{[Vk]^{2/m}} - \sigma_d^2 \quad . \tag{63}$$

Substituting from Equation (44)

$$a_d^2 = \frac{I_{m/2}}{[Vk]^{2/m}} - \frac{I_m^2}{[Vk]^{2/m}} , \tag{64}$$

$$a_d^2 = \frac{1}{[Vk]^{2/m}} [I_{m/2} - I_m^2] . \tag{65}$$

Then for the No. 1- and the No. 4-size tension specimens with volumes, V_{d1} and V_{d4},

$$\frac{a_{d1}}{a_{d4}} = \left[\frac{V_{d4}}{V_{d1}}\right]^{1/m} . \tag{66}$$

For the case of a specimen loaded in pure bending, it can be shown that

$$B = \frac{Vk\sigma^m}{2m + 2} , \tag{67}$$

and, hence, that the standard deviation, a_b, of the mean bend strength, σ_b, is

$$a_b^2 = \int_0^\infty e^{-\frac{Vk\sigma^m}{2m + 2}} d(\sigma^2) - \sigma_b^2 . \tag{68}$$

Letting

$$Z = \left[\frac{Vk}{2m + 2}\right]^{2/m} \sigma^2 , \tag{69}$$

and substituting from Equation (45),

$$a_b^2 = \frac{1}{\left[\frac{Vk}{2m+2}\right]^{2/m}} \left[I_{m/2} - I_{nf}^2\right] \quad . \tag{70}$$

Then for the No. 1- and the No. 5-size bend specimens with volumes, V_{b1} and V_{b5},

$$\frac{a_{b1}}{a_{b5}} = \left[\frac{V_{b5}}{V_{b1}}\right]^{1/m} \quad . \tag{71}$$

In addition, it can be shown that, for $n(\sigma) = k\sigma^m$ and for $m = 12$ (for Hydrostone plaster), for a torsion specimen,

$$B = \frac{0.112\pi k_1 V_r^{12}}{14} \quad . \tag{72}$$

Then the standard deviation, a_T, of the strength, σ_T, of a set of torsion specimens becomes:

$$a_T^2 = \int_0^\infty e^{-\frac{0.112\pi k_1 V_r^{12}}{14}} d(r^2) - \sigma_T^2 \quad , \tag{73}$$

where $k_1 = \frac{.75k}{2\pi}$. Then it can be shown that, for $m = 12$,

$$a_T^2 = \frac{I_6}{[0.100\ Vk]^{1/6}} - \sigma_T^2 \quad . \tag{74}$$

It can also be shown that, for Hydrostone plaster ($m = 12$),

$$\sigma_T = \frac{I_{12}}{[0.100\ Vk]^{1/12}} \quad . \tag{75}$$

Hence, a_T^2 becomes

$$a_T^2 = \frac{1}{[0.100\ V_k]^{1/12}} [I_6 - I_{12}] \quad (76)$$

Then for the No. 1- and the No. 5-size torsion specimens with volumes, V_{T1} and V_{T5},

$$\frac{a_{T1}}{a_{T5}} = \left[\frac{V_{T5}}{V_{T1}}\right]^{1/12} . \quad (77)$$

From Equations (65), (70), and (74), it can be shown that, for Hydrostone plaster,

$$\frac{a_b}{a_d} = \left[\frac{2.6\ V_d}{V_b}\right]^{1/12} , \quad (78)$$

$$\frac{a_d}{a_T} = \left[\frac{V_T}{10\ V_d}\right]^{1/12} , \quad (79)$$

and

$$\frac{a_b}{a_T} = \left[\frac{2.6\ V_T}{V_b}\right]^{1/12} . \quad (80)$$

Equations (78) and (79) were used to calculate the theoretical standard deviations appearing in Table 17. It should be noted that Equations (78), (79), and (80) and Equations (50), (51), and (52) lead to the following:

$$\frac{a_b}{a_d} = \frac{\sigma_b}{\sigma_d} , \quad (81)$$

and

$$\frac{a_T}{a_d} = \frac{\sigma_T}{\sigma_d} . \quad (82)$$

Effect of Biaxial Stresses on Strength

It was pointed out that the fracture strength of a body is a function of the stress state at every point in that body. It was also pointed out that the fracture strength of a body can be defined in terms of B', the risk of fracture at each point in the body, and that B' can be of the form

$$B' = \iiint n_1(\sigma)\cos\phi\, d\phi\, d\psi, \tag{43}$$

where σ denotes the stress state at the point at which B' is to be evaluated. If each point in a body is subjected to a system of biaxial stresses, the normal stress, σ, in a particular direction may be defined in terms of the principal stresses, σ_1 and σ_2, by the relation

$$\sigma = \cos^2\beta(\sigma_1\cos^2\psi + \sigma_2\sin^2\psi) \ . \tag{83}$$

Furthermore, if $n_1(\sigma)$ is assumed to be of the form

$$n_1(\sigma) = k_1\sigma^m \ , \tag{84}$$

then the risk of fracture, B', becomes

$$B' = 2k_1 \int_c^{\pi/2} \cos^{2m+1}\phi\, d\phi \int_{-\psi_o}^{\psi_o} (\sigma_1\cos^2\psi + \sigma_2\sin^2\psi)^m d\psi. \tag{85}$$

If the ratio of the principal stresses is defined as

$$\frac{\sigma_2}{\sigma_1} = c^2 \ , \tag{86}$$

then Equation (85) becomes

$$B' = 2k_1\sigma_1^m \int_0^{\pi/2} \cos^{2m+1}\phi\, d\phi \int_{-\psi_o}^{\psi_o} (\cos^2\psi + c^2\sin^2\psi)^m d\psi. \qquad (87)$$

If σ_1 and σ_2 are both tensile stresses,

$$B' = 4k_1\sigma_1^m \int_0^{\pi/2} \cos^{2m+1}\phi\, d\phi \int_0^{\pi/2} (\cos^2\psi + c^2\sin^2\psi)^m d\psi. \qquad (88)$$

If one of the principal stresses is negative or compressive,

$$\tan\psi_0 = \sqrt{\frac{\sigma_1}{-\sigma_2}}. \qquad (89)$$

It can be seen that B' cannot be evaluated from (72) or (73) for a state of biaxial stress until the value of the material constant, m, is known for the material. Once B' has been determined, then the fracture strength of a body can be determined from Equations (22) and (26).

It is important to note here that B' is a function of σ_1 and σ_2 and, as such, may vary from point to point in a body as the principal stresses vary. For this reason, the functional relation between B' and the principal stresses must be considered in the evaluation of the risk of rupture, B, of the entire body and, hence, in the evaluation of the fracture strength.

If we consider the case of a body of a volume, V, which is subjected to a uniform biaxial stress such that the principal stresses are constant throughout the body, then the total risk of rupture, B, becomes

$$B = \int_V B'\,dV = B'V, \qquad (90)$$

and the fracture strength becomes

$$\sigma_m = \int_0^{\infty} e^{-B' V} d\sigma \quad . \tag{91}$$

Table 27 contains values for Hydrostone plaster of B and σ_m determined for various principal stress ratios where the volume, V, of the material is assumed to be uniformly stressed.

Effect of Eccentricity on Tension Strength

According to the concept of Weibull's theory, the tension strength, σ_d, of a body may be defined as:

$$\sigma_d = \int_0^{\infty} e^{-B_d} d\sigma \quad , \tag{92}$$

where:

$$B_d = \int_V n(\sigma) dV \quad , \tag{93}$$

and where $n(\sigma)$ may be of the form:

$$n(\sigma) = k\sigma^m \quad . \tag{41}$$

Now let us consider a body of rectangular cross section, loaded eccentrically in tension as shown in Figure 33. Here, the eccentricity, e, of the load causes the nonuniformity of tensile stress on the gage section shown in Figure 33(c). It can be seen from Figure 33(c), that the resulting stress in the gage section (of length, L) is the sum of a uniform tension stress, σ_d, and a bending stress. Then, for this state of stress, it can be shown that the stress, σ, at any distance, x, from the neutral axis can be expressed as:

$$\sigma = \sigma_d \left(1 + \frac{3ex}{h^2} \right) . \tag{94}$$

TABLE 27. RISKS OF FRACTURE AND FRACTURE STRENGTHS FOR HYDROSTONE PLASTER SUBJECTED TO BIAXIAL STRESSES

Principal Stress Ratio, σ_2/σ_1	Risk of Rupture, B	Fracture Strength, σ_m
1	$0.496\pi k_1 V\sigma_1^{12}$	$\frac{I_{12}}{[0.496\pi k_1 V]^{1/12}}$
0.8	$0.1875\pi k_1 V\sigma_1^{12}$	$\frac{I_{12}}{[0.1875\pi k_1 V]^{1/12}}$
2/3	$0.147\pi k_1 V\sigma_1^{12}$	$\frac{I_{12}}{[0.147\pi k_1 V]^{1/12}}$
1/2	$0.118\pi k_1 V\sigma_1^{12}$	$\frac{I_{12}}{[0.118\pi k_1 V]^{1/12}}$
1/3	$0.0972\pi k_1 V\sigma_1^{12}$	$\frac{I_{12}}{[0.0972\pi k_1 V]^{1/12}}$
0	$0.0800\pi k_1 V\sigma_1^{12}$	$\frac{I_{12}}{[0.0800\pi k_1 V]^{1/12}}$
- 1/3	$0.0688\pi k_1 V\sigma_1^{12}$	$\frac{I_{12}}{[0.0688\pi k_1 V]^{1/12}}$
- 1/2	$0.0648\pi k_1 V\sigma_1^{12}$	$\frac{I_{12}}{[0.0648\pi k_1 V]^{1/12}}$
- 1	$0.0559\pi k_1 V\sigma_1^{12}$	$\frac{I_{12}}{[0.0559\pi k_1 V]^{1/12}}$
- 2	$0.0448\pi k_1 V\sigma_1^{12}$	$\frac{I_{12}}{[0.0448\pi k_1 V]^{1/12}}$
- 3	$0.0363\pi k_1 V\sigma_1^{12}$	$\frac{I_{12}}{[0.0363\pi k_1 V]^{1/12}}$
- 4	$0.0293\pi k_1 V\sigma_1^{12}$	$\frac{I_{12}}{[0.0293\pi k_1 V]^{1/12}}$

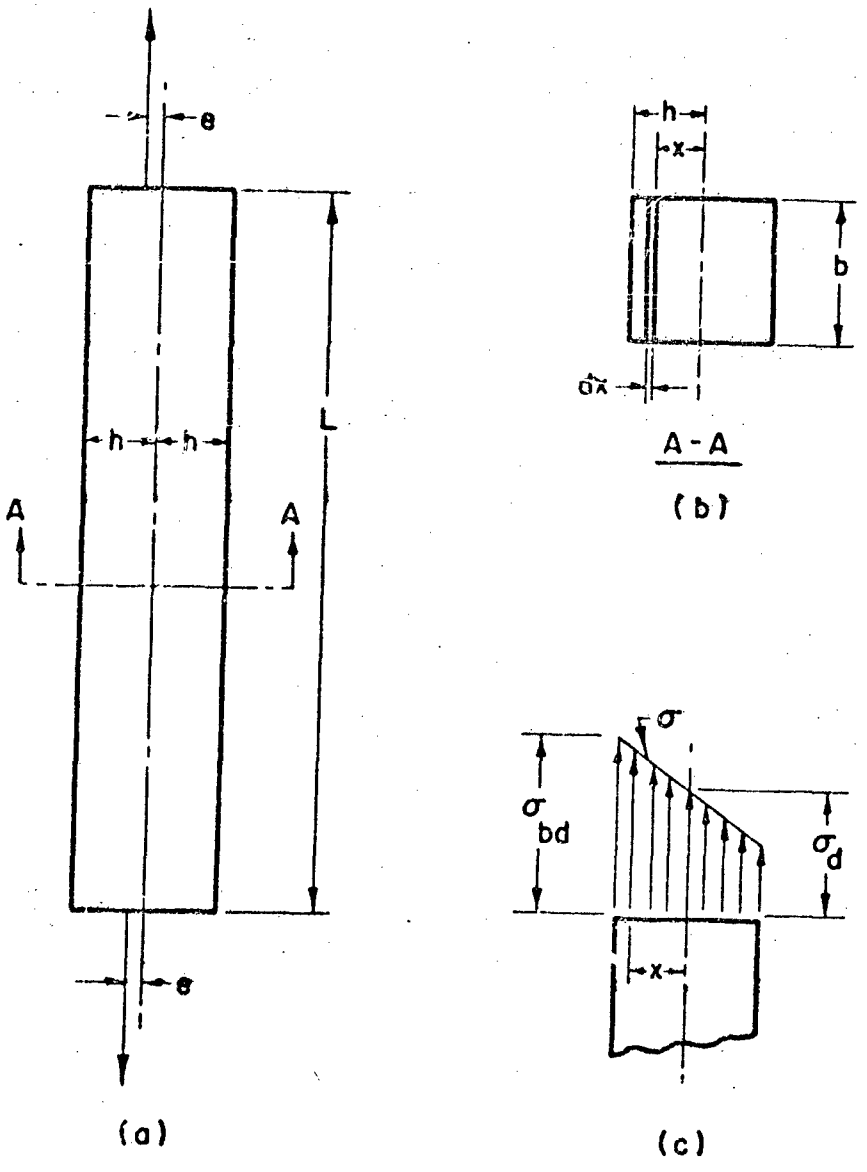

FIGURE 33. RECTANGULAR SPECIMEN LOADED ECCENTRICALLY IN TENSION

A-3858

Then, the risk of fracture, B_{bd}, in bending plus tension becomes:

$$B_{bd} = \int_V n(\sigma) dV \ , \tag{95}$$

where

$$n(\sigma) = k\sigma^m \ . \tag{41}$$

Then

$$n(\sigma) = k\sigma_d{}^m \left(1 + \frac{3ex}{h^2}\right)^m \ , \tag{96}$$

and

$$dV = bLdx \ .$$

Then

$$B_{bd} = bLk\sigma_d{}^m \int_{-h}^{h} \left(1 + \frac{3ex}{h^2}\right)^m dx \ . \tag{97}$$

Then (97) can be written:

$$B_{bd} = \frac{bh^2 k\sigma_d{}^m}{3e} \int_{1-\frac{3e}{h}}^{1+\frac{3e}{h}} z^m dz \ . \tag{98}$$

For $V = 2bhL$,

$$B_{bd} = \frac{Vhk\sigma_d{}^m}{6e(m+1)} \left[\left(1 + \frac{3e}{h}\right)^{m+1} \left(1 - \frac{3e}{h}\right)^{m+1}\right] \ . \tag{99}$$

Equation (99) can be rewritten as:

$$B_{bd} = Vk\sigma_d{}^m S_m \ , \tag{100}$$

where

$$S_m = \sum_{r=0}^{r=\frac{m}{2}} \frac{m!\left(\frac{3e}{h}\right)^{2r}}{(m-2r)!(2r+1)!} \quad . \tag{101}$$

For pure tension, the risk of fracture, B_d, similarly can be shown to be:

$$B_d = kV\sigma_{d'}^{m} \quad . \tag{102}$$

Then the ratio of the risks of fracture, B_{bd} and B_d, becomes:

$$\frac{B_{bd}}{B_d} = \frac{\sigma_d^m S_m}{\sigma_{d'}} \quad . \tag{103}$$

It can be seen from Equation (103) that the value of B_{bd}/B_d will depend on the magnitude of σ_d and $\sigma_{d'}$. It is very important to note at this point that, if we are to calculate the fracture strengths in bending plus tension and in tension, we must set up the risks of fracture in terms of the desired stresses. B_{bd} is desired in terms of the maximum stress, σ_{bd}, in the cross section; then:

$$\sigma_d = \frac{\sigma_{bd}}{\left(1 + \frac{3e}{h}\right)} \tag{104}$$

Then

$$B_{bd} = VkS_m \left[\frac{\sigma_{bd}}{1 + \frac{3e}{h}}\right]^m \quad . \tag{105}$$

The ultimate strength, σ_{bd}, in bending plus tension then becomes:

$$\sigma_{bd} = \int_0^\infty e^{-B_{bd}} d\sigma_{bd} = \int_0^\infty e^{-VkS_m\left[\frac{\sigma_{bd}}{1+\frac{3e}{h}}\right]^m} d\sigma_{bd} \quad , \tag{106}$$

and for

$$I_m = \int_0^\infty e^{-z^m} dz \quad ,$$

$$\sigma_{bd} = \frac{\left(1 + \frac{3e}{h}\right) I_m}{\left[VkS_m\right]^{1/m}} \quad . \tag{107}$$

Similarly, the strength in tension is:

$$\sigma_{d'} = \int_0^{\infty} e^{-B_d} \, d\sigma_{d'} = \int_0^{\infty} e^{-V_k \sigma_{d'}^m} \, d\sigma_{d'} \quad ,$$

$$\sigma_{d'} = \frac{I_m}{\left[V_k\right]^{1/m}} \quad . \tag{108}$$

Then the ratio of the strength of a specimen loaded eccentrically in tension, $\sigma_{bd'}$ to the strength of a similar specimen loaded uniformly in tension, $\sigma_{d'}$, according to Weibull's theory, becomes:

$$\frac{\sigma_{bd}}{\sigma_{d'}} = \left(1 + \frac{3e}{h}\right) \left[\frac{V_{d'}}{V_{bd}\, S_m}\right]^{1/m} \quad , \tag{109}$$

where

σ_{bd} = fracture strength of a rectangular specimen subjected to combined bending and tension, psi,

$\sigma_{d'}$ = fracture strength of a specimen subjected to pure tension, psi,

e = eccentricity of load, inches,

h = half the width of the specimen, inches,

V_{bd} = volume of the gage-section of the specimen loaded in combined bending and tension, cubic inches,

$V_{d'}$ = volume of the gage section of the specimen loaded in pure tension,

m = material constant from Weibull's theory,

$$S_m = \sum_{r=0}^{r=\frac{m}{2}} \frac{m\,!\left(\frac{3e}{h}\right)^{2r}}{(m-2r)\,!\,(2r+1)!} \quad . \tag{101}$$

For Hydrostone plaster (m = 12) and for $V_{bd} = V_{d'}$,

$$\frac{\sigma_{bd}}{\sigma_{d'}} = \frac{\left(1 + \frac{3e}{h}\right)}{S_{12}^{1/12}} \quad , \tag{110}$$

where

$$S_{12} = \sum_{r=0}^{r=6} \frac{12!\left(\frac{3e}{h}\right)^{2r}}{(12-2r)!\,(2r+1)!} \quad . \qquad (111)$$

APPENDIX IV

BASIC TEST DATA FROM COMBINED-STRESS TESTS

This appendix has been attached in order to present all the raw data taken in the combined-stress tests on plaster, the results of which are discussed in this report.

TABLE 28. BASIC ELASTIC AND FRACTURE DATA FROM TENSILE TESTS ON BIAXIAL SPECIMENS OF HYDROSTONE PLASTER[1][2]

Specimen Number	Poisson's Ratio	Modulus of Elasticity, 10^6 psi	Fracture Stress, psi		Fracture Strains, in./in. x 10^{-6}				Specimen Dimensions, in.		Temperature, F		Relative Humidity, %	Remarks
					Longitudinal			Transverse						
			σ_{2o}	σ_{1o}	ϵ_b	ϵ_d	ϵ_f	ϵ_e	D_o	D_i	Dry Bulb	Wet Bulb		
HOP-2	0.185	2.37	500	1000	—	—	239	41	3.503	3.005	76.7	68.9	66	Fracture occurred in shoulder of specimen
HOP-3	0.255	2.42	650	1300	327	328	308	87	3.502	3.004	79.4	68.5	57	Fracture occurred in shoulder of specimen
HOP-10	0.198	2.39	845	1690	352	397	444	93	3.502	3.050	77.2	66.2	56	
HOP-18	0.237	2.43	565	1130	268	271	269	67	3.502	3.046	81.3	69.0	53	
HOP-19	0.243	2.32	740	1480	375	402	352	81	3.503	3.053	75.2	63.4	51	
HOP-20	0.255	2.38	930	1860	461	465	451	111	3.503	3.053	79.8	70.0	60	Fracture occurred in shoulder of specimen
HOP-21	0.250	2.39	700	1400	338	365	292	85	3.503	3.053	77.8	66.4	53	Bubble in fracture surface
HOP-22	0.225	2.34	925	1850	421	442	453	101	3.503	3.049	79.4	67.3	52	
HOP-23	0.259	2.38	925	1850	443	435	427	104	3.502	3.055	79.4	67.7	53	Fracture occurred in shoulder of specimen
HOP-24	0.271	2.49	1235	2470	527	525	505	137	3.503	3.049	76.2	65.6	56	

(1) Strain rate for fracture of all specimens = 0.0027 in./in./min.

(2) For definition of symbols, see text, "Combined-Stress Tests on Plaster".

TABLE 29. BASIC ELASTIC AND FRACTURE
HYDROSTONE PLASTER SUBJECTED

Specimen No.	Poisson's Ratio	Modulus of Elasticity, 10^6 psi	$\frac{\Delta\sigma_{1o}}{\Delta\epsilon_{1o}}$, 10^6 psi	$\frac{\sigma_{1o}}{\epsilon_{1o}}$, 10^6 psi	$\frac{\Delta\sigma_{1o}}{\Delta\epsilon_{2o}}$, 10^6 psi	$\frac{\sigma_{1o}}{\epsilon_{2o}}$, 10^6 psi	Fracture Pressure, psi	Fracture Stresses,(2) psi σ_{2o}	σ_{1o} $(?\sigma_{2o})$	σ_{11}
HOP-4	--	--	2.48	2.73	9.42	9.23	175	525	1050	1225
HOP-5	0.243	2.48	2.57	2.82	9.34	9.65	117	370(I)	740	860
HOP-6	0.258	2.40	2.57	2.76	9.68	9.92	177	540	1080	1255
HOP-7	0.266	2.37	2.53	2.73	8.73	10.13	137	420(B)	840	980
HOP-8	0.206	2.48	2.48	2.76	9.50	8.44	163	495	990	1155
HOP-9(4)	0.245	1.60	1.73	2.74(2)	6.29	9.41	118	380(B)	760	875
HOP-11	0.234	2.48	2.48	2.81	9.09	9.32	144	445	890	1035
HOP-12	0.238	2.49	2.29	2.54	8.99	9.50	133	420	840	970
HOP-13	--	--	--	--	--	--	175	550	1100	1270
HOP-14	0.240	2.32	2.97	2.64	8.43	9.67	126	395(B)	790	915
HOP-15	0.227	2.42	2.57	2.73	8.92	9.20	120	395	790	915
HOP-16	0.263	2.40	2.79	2.76	9.38	10.13	139	450	900	1040
HOP-17	0.248	2.43	--	--	--	--	--	--	--	--

(1) For definition of symbols, see text, "Combined-Stress Tests on Plaster".

(2) All specimens were loaded to give a major principal strain rate ($\dot{\epsilon}_{11}$) of 0.0027 in./in./minute.

(3) Ratio was calculated using experimental strains.

(4) All theoretical calculations for Specimen 9 were made using E = 2.40.

(I) Inclusion present in fracture surface of specimen.

(B) Bubble present in fracture surface of specimen.

DATA FROM BIAXIAL SPECIMENS OF
TO PRESSURE LOADING[1]

σ_{2o}[3]	Fracture Strains, in./in. $\times 10^{-6}$								Specimen Dimensions, in.		Temperature, F		Relative Humidity,
	Transverse				Longitudinal								
σ_{1o}	ϵ_a	ϵ_c	ϵ_e	Avg	ϵ_b	ϵ_d	ϵ_f	Avg	D_o	D_i	Dry Bulb	Wet Bulb	%
0.496	--	399	--	--	--	116	--	--	3.507	3.037	77.9	67.0	56
0.495	--	--	307	--	--	--	89	--	3.502	3.054	--	--	--
0.475	--	--	443	--	--	--	110	--	3.503	3.037	78.0	70.0	67
0.487	--	--	351	--	--	--	89	--	3.503	3.043	77.8	67.0	57
0.444	380	421	414	405	104	111	103	106	3.503	3.037	72.0	65.0	68
0.476	455	372	--	414	123	94	--	109	3.502	3.054	78.8	67.1	53
0.470	376	344	341	354	98	91	93	94	3.502	3.044	80.2	71.8	65
0.467	373	390	328	364	96	98	87	94	3.502	3.050	78.0	66.4	54
--	--	--	--	--	--	--	--	--	3.502	3.048	69.3	59.7	57
0.564	221	265	291	259	102	84	101	96	3.502	3.048	75.0	64.0	53
0.477	333	327	281	314	85	91	87	88	3.503	3.069	75.0	64.3	55
0.521	366	282	325	324	91	104	92	96	3.503	3.059	76.0	66.0	58
--	--	--	--	--	--	--	--	--	3.503	3.047	77.0	67.0	58